ESTABLISHING ZEBRAFISH, *DANIO RERIO*, AS A GENETIC MODEL FOR GLAUCOMA

by

©Jurgienne Arizza Gomez Umali, B.Sc. (Hons)

A thesis submitted to the

School of Graduate Studies

in partial fulfillment of the

requirements for the degree of

Master of Science in Medicine

Faculty of Medicine

Memorial University of Newfoundland

Date: May 2020

St. John's Newfoundland and Labrador

Abstract

Glaucoma is characterized by retinal ganglion cell (RGC) death, leading to vision loss. The leading risk factor for glaucoma is elevated intraocular pressure (IOP), however 30 percent of patients have IOP within the reference range, suggesting IOP-independent mechanisms underlying disease pathogenesis. Mutations in the forkhead transcription factor *FOXC1* cause Axenfeld-Rieger Syndrome with early-onset or congenital glaucoma, however the mechanism by which this occurs is not fully understood. We assessed RGC number and optic nerve width in embryonic zebrafish with inhibition of *foxc1a* and *foxc1b* via antisense morpholinos and CRISPR-mediated mutation. At 5 days post fertilization, *foxc1b*$^{-/-}$ embryos injected with *foxc1a* morpholinos have decreased cells in the RGC layer and thinner optic nerves. *In situ* hybridization shows loss of *foxc1* results in dysregulation of *atonal homolog 7 (atoh7),* a gene involved in RGC differentiation. Overall, we propose that altered RGC differentiation interacts with other risk factors to influence *FOXC1*-associated glaucoma pathogenesis.

Acknowledgements

First and foremost, I would like to thank my supervisor, Dr. Curtis French, for giving me this opportunity, and for his guidance and patience as my mentor during my graduate training. I also thank Dr. French for encouraging me to attend and present my research in conferences to further my learning and academic career, and for helping me navigate academia and build confidence in my abilities as a researcher. I highly appreciate Dr. French's support, especially as I continued to work on my graduate studies while simultaneously being enrolled in the Doctorate of Medicine program.

I also thank my supervisory committee, Dr. Ann Dorward and Dr. Michael Woods. I highly appreciate their valuable comments, encouragement, and perspective on research, academia, and approach to life. I also thank Dr. Jacqueline Vanderluit for her incredible generosity with her equipment, words of encouragement and time. I would also like to extend my gratitude to the Discipline of Genetics at the Faculty of Medicine, Memorial University of Newfoundland.

I am grateful to the current and past members of the French lab for technical and emotional support: Gerissa Fowler, Alexia Hawkey-Noble, and Danielle French. These women are brilliant and hardworking researchers, and I am lucky to know them.

I would also like to acknowledge the Canadian Glaucoma Research Society and Memorial University of Newfoundland for financially supporting me and this project. Thank you to the Faculty of Medicine's Office of Research and Graduate Studies for

being so supportive of their graduate students, and for helping me navigate dual enrollment in graduate school and medical school as well.

Finally, I am indebted to my family, friends, and loved ones for being with me throughout my studies. I especially would like to extend my love and gratitude to my parents, Anna Georgina and Jacinto Jr., my aunt, Amabellee Gomez, my grandparents, Anita and Ricardo Gomez, and my partner, Matthew Nelder. Thank you for being my pillars of strength and for believing in me, even on days when I myself did not. Words cannot express how grateful I am for their care, unwavering support, and for cheering me on as I continue to pursue my dreams and ambitions, no matter how challenging the road may be.

Table of Contents

List of Tables

List of Figures

List of Abbreviations

ARS Axenfeld-Rieger Syndrome

ASD Anterior Segment Dysgenesis

Atoh *Atona*l homolog

bHLH Basic helix-loop-helix

cDNA Complementary Deoxyribonucleic Acid

CRISPR Clustered regularly interspaced short palindromic repeats

Cas9 CRISPR-associated protein 9

CNV Copy Number Variation

Dpf Days post fertilization

DNA Deoxyribonucleic Acid

EDTA Ethylenediaminetetraacetic acid

FGF Fibroblast growth factor

FGFR Fibroblast growth factor receptor

FOXC Forkhead box transcription factor of the Class C

FOXO Forkhead box transcription factor of the Class O

GLC Glaucoma loci

GMDS GDP-mannose 4,6-Dehydratase

GWAS Genome-wide association study

Hpf Hours post fertilization

Hsp Heat Shock protein

INL Inner Nuclear Layer

IOP Intraocular Pressure

IPL Inner plexiform layer

mRNA Messenger Ribonucleic acid

NaOH Sodium Hydroxide

OCT Optimal Cutting Temperature

ONL Outer Nuclear Layer

p53 Tumor protein p53

PACG Primary Angle-Closure Glaucoma

Pax Paired box homeobox

PBST Phosphate buffered saline with 20% Tween-20

PCR Polymerase Chain Reaction

pdgfrα platelet-derived growth factor receptor α

PFA Paraformaldehyde

PITX Paired Like Homeodomain

POAG Primary Open-Angle Glaucoma

pou4f2 pou domain, class 4, transcription factor 2

PTU 1-phenyl 2-thiourea

RGC Retinal ganglion cell

RNA Ribonucleic acid

RNAP Ribonucleic acid polymerase

RPE Retinal pigmented epithelium

RT-PCR Reverse Transcription Polymerase Chain Reaction

SNP Single Nucleotide Polymorphism

SSC Saline-sodium citrate

Tris-HCl Tris(hydroxymethyl)aminomethane Hydrochloride

VCDR Vertical Cup-to-Disc Ratio

List of Appendices

Author Statement

This thesis contains data figures and ideas that have been published in the peer-reviewed journal Vision Research (Umali, Hawkey-Noble, & French, 2019).

1 Introduction

1.1 Human Eye Anatomy

The normal adult human eye is a complex spherical organ, measuring an average of 24 mm (Riordan-Eva, 2011). Several structures can be observed externally. These include the pupil, a black-looking opening that allows light to enter the eye, and the iris, a pigmented circular muscle that controls the size of the pupil, thus effectively controlling how much light enters the eye (Kolb, 1995). The eye has a transparent external covering called the cornea, which plays a role in focusing an image at the back of the eye, and is continuous with the sclera, which forms the supporting wall of the eyeball (Willoughby et al., 2010).

A cross-section of the eye results in three distinguishable layers: an external layer formed by the cornea and sclera, a middle layer composed of the iris, the ciliary bodies and the choroid, and the inner layer consisting of the retina (**Figure 1.1**). These three layers surround three chambers of fluid. The anterior chamber is located between the cornea and the iris, while the posterior chamber is found between the iris, zonule fibres, and the lens. The vitreous chamber, containing vitreous humour, is located between the lens and the retina. In the middle layer, ciliary bodies connect to the lens via zonular fibres, which suspend the lens just behind the iris (Riordan-Eva, 2011).

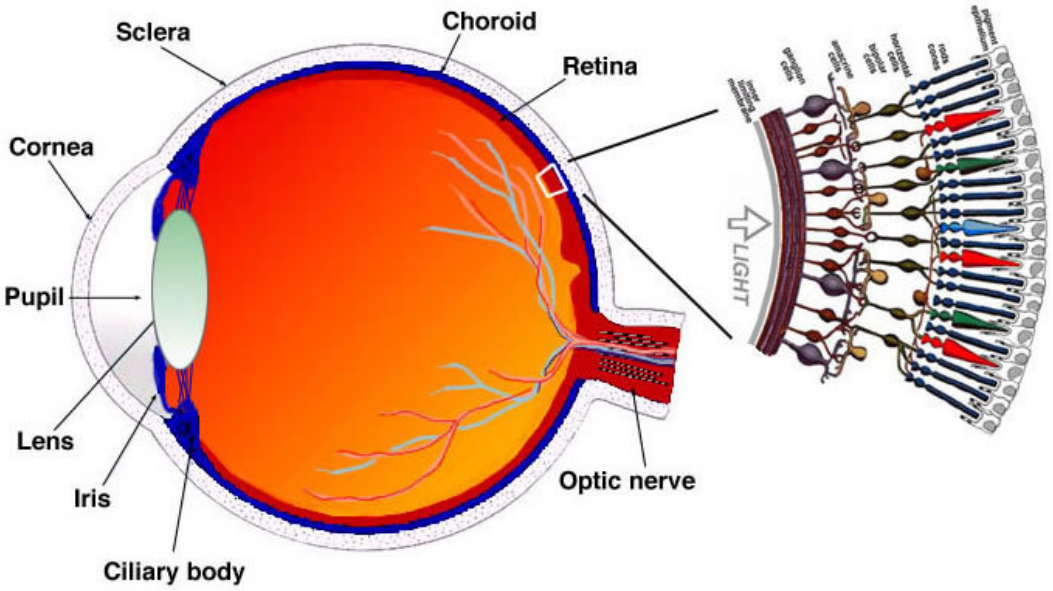

Figure 1.1 Cross-section of a human eye with a schematic enlargement of the retina.

This drawing shows the external layer of the eye composed of the cornea and sclera, the intermediate layer composed of the iris, ciliary bodies, and the choroid, and the internal layer consisting of the retina. The retina consists of layers of neurons that capture and process light.

The ciliary bodies consist of ciliary epithelium and ciliary muscles. The ciliary muscles are involved in the alteration of the shape of the lens (Riordan-Eva, 2011; Willoughby et al., 2010). This occurs to focus light onto the retina for both near and distant objects in the visual field.

1.1.1 Aqueous Humour Outflow

The anterior and posterior chambers are important sites relating to the outflow of aqueous humour, a clear fluid that provides nutrition, removes metabolic products, transports neurotransmitters, and contributes to the stabilization of the structure and homeostasis of the eye (Goel, Picciani, Lee, & Bhattacharya, 2010). Structurally, the anterior chamber angle lies at the junction of the cornea and the iris and features the trabecular meshwork, a triangular structure composed of perforated collagenous and elastic sheets that form a filter and gradually becomes smaller as it overlies Schlemm's Canal (Riordan-Eva, 2011). Schlemm's Canal is a structure comprised of endothelial cells that possess collector channels and is connected to episcleral and conjunctival veins (Goel et al., 2010). The internal portion of the meshwork facing the anterior chamber is known as the uveal meshwork, while the external portion adjacent to Schlemm's Canal is the corneoscleral meshwork.

Aqueous humour is produced by the ciliary body in the posterior chamber, which then flows into the anterior chamber to be passively drained via the anterior chamber angle (**Figure 1.2**).

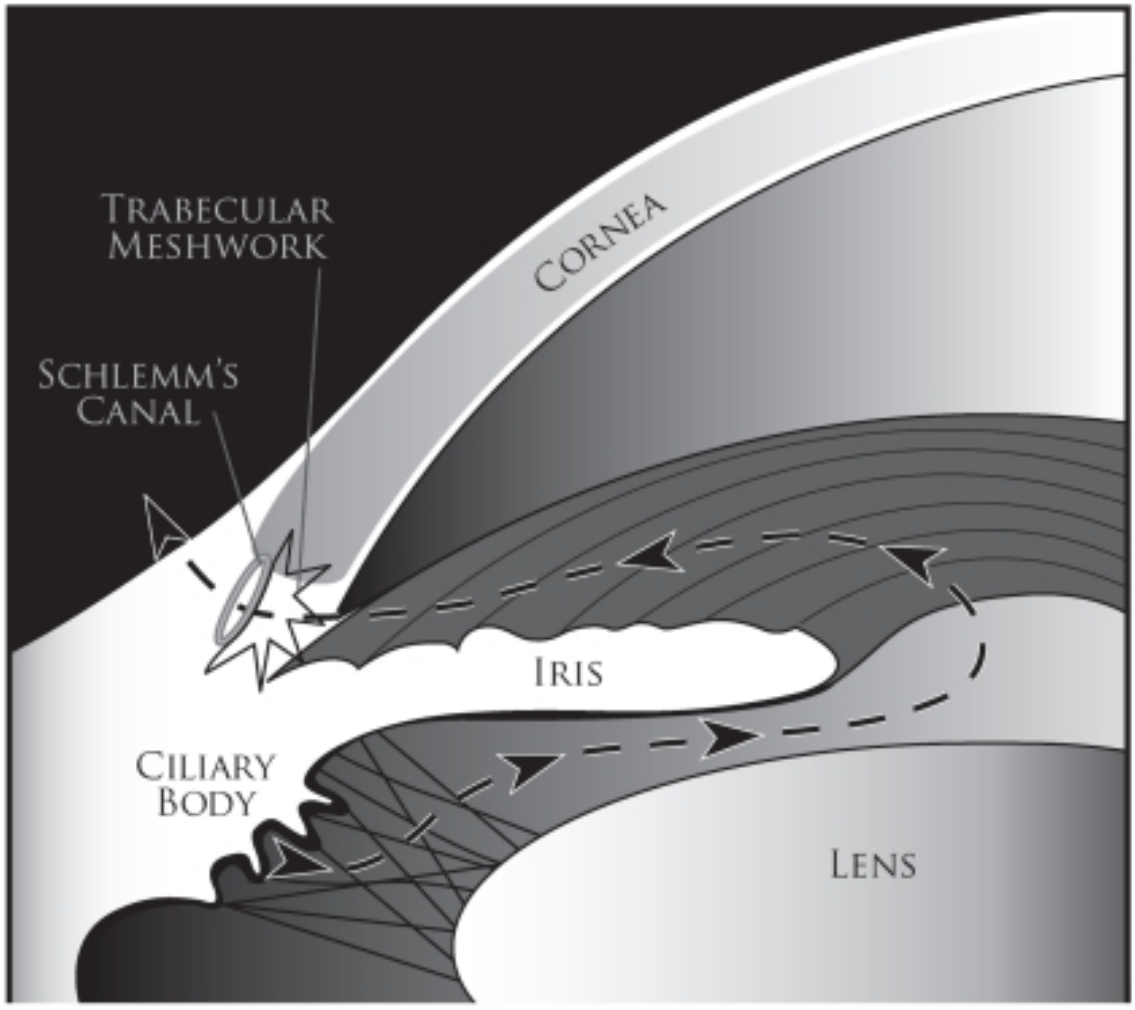

Figure 1.2 Conventional Aqueous Humour Outflow Pathway.

Aqueous humour (represented by the dashed line shown with arrowheads) is produced by the ciliary body, flows from the posterior chamber through the pupil, and into the anterior chamber. In the anterior chamber, aqueous humour drains through the trabecular meshwork into the Canal of Schlemm, both of which are present in the anterior chamber angle. Aqueous humour is then absorbed in the venous drainage through the episcleral veins. Copyright: © (Goel et al., 2010); Licensee Bentham Open, under the Creative Commons Attribution Non-Commercial License.

Aqueous humour drains through the anterior chamber angle via two pathways: the conventional pathway consisting of movement down a pressure gradient through the trabecular meshwork, across the inner wall of Schlemm's Canal, into collector channels, and venous drainage, and the non-conventional route through the uveal meshwork (Goel et al., 2010). Disruption of aqueous outflow may result in a rise in intraocular pressure (IOP), which is a major risk factor for the development of glaucoma.

1.1.2 The Human Retina

The retina comprises the inner surface of the eye and is functionally responsible for receiving light energy and converting it into an electrical signal to be transmitted through the optic nerve to the visual cortex of the brain, to be structurally and spatially perceived (Fletcher, Chong, Augsburger, & Correa, 2011). Clinically, the retina can be superficially examined using an ophthalmoscope, with the optic nerve head being centrally visible. Also known as the optic disc, a normal optic nerve head appears as a circular, orange/pink area measuring about 1.5-2mm in diameter, with the major retinal vasculature radiating from the center (**Figure 1.3**) (Chang, 2011; Kolb, 1995; Willoughby et al., 2010).

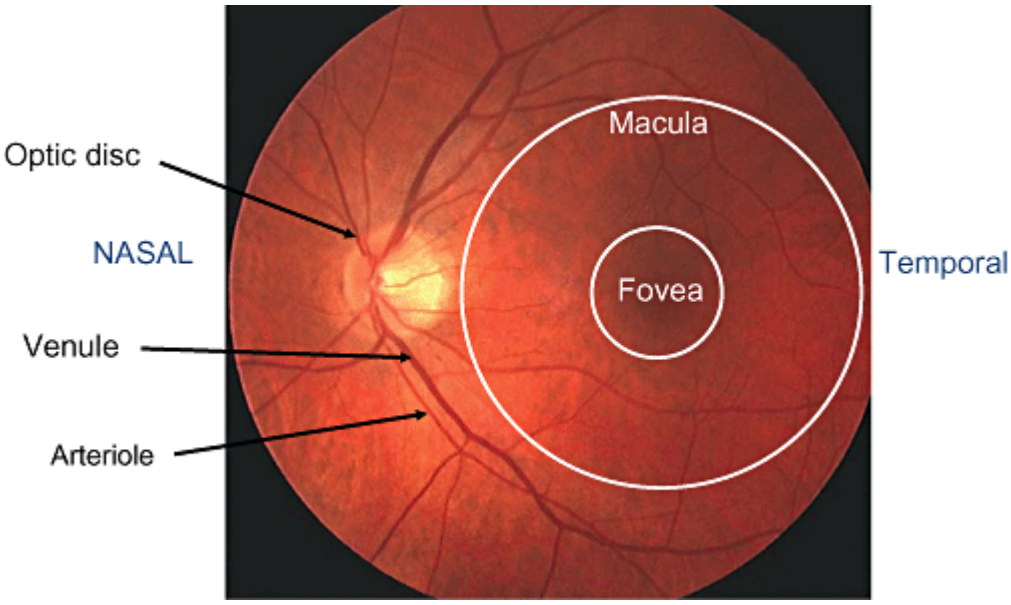

Figure 1.3 Ophthalmoscopic view of the retina.

The optic disc can be visualized as an orange circular area, with major vasculature radiating from its centre. Adjacent to the optic disc is the macula, and its central area called the fovea, which contains the largest abundance of cone photoreceptors in the eye. Thus, the fovea is responsible for sharp central vision and is the area of highest visual acuity. Reproduced from(Willoughby et al., 2010), with permission from John Wiley and Sons.

Changes to the optic disc or optic cup may be visualized using an ophthalmoscope and are indicative of ocular diseases. Adjacent to the optic disc, one can see the macula, the area considered to be the centre of the retina, which contains several layers of ganglion cells compared to the single-cell layer of ganglion cells in the periphery (Willoughby et al., 2010). Within the centre of the macula lies a slightly oval-shaped, vasculature-free spot called the fovea, the area of the retina responsible for sharp central vision and has the highest visual acuity due to its high concentration of cone photoreceptors (Kolb, 1995; Willoughby et al., 2010).

The cells of the neural retina are arranged in layers (**Figure 1.4**). These are the internal limiting membrane, nerve fibre layer, ganglion cell layer, inner plexiform layer, inner nuclear layer, outer plexiform, outer nuclear layer, photoreceptor cell layer of rods and cones, and the retinal pigment epithelium (Willoughby et al., 2010). The nerve fibre layer contains the ganglion cell axons passing to the optic nerve, while the inner plexiform layer contains bipolar cells. The inner nuclear layer consists of bipolar, amacrine, and horizontal cell bodies, whereas the outer plexiform layer contains connections of the bipolar and horizontal cells with photoreceptors (Willoughby et al., 2010). Finally, the outer nuclear layer is comprised of photoreceptor cell nuclei.

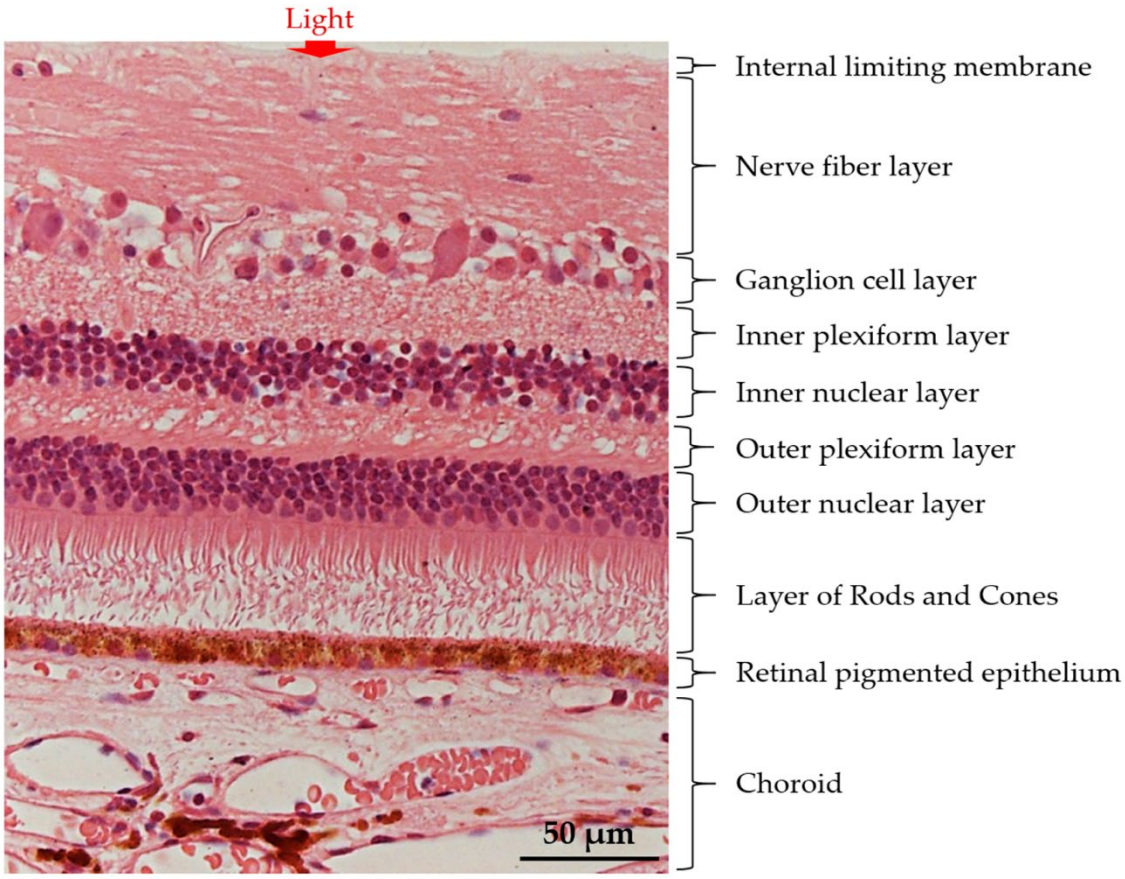

Figure 1.4 Layers of the Neural Retina.

From the innermost aspect, the layers of the neural retina are the internal limiting membrane, the nerve fibre layer, ganglion cell layer, inner plexiform layer, inner nuclear layer, outer plexiform layer, outer nuclear layer, photoreceptor layer consisting of rods and cones, and the retinal pigmented epithelium. Reused from (Ding, Kumar, & Mok, 2017) under the Creative Commons Attribution License.

Absorption of photons by the visual pigment in the photoreceptors is translated into a series of biochemical and electrical messages (Kolb, 1995). These are then transmitted to the ganglion cells, exiting the eye through the optic nerve and into the brain for interpretation in the visual cortex. Degeneration of the RGCs and subsequent damage to the optic nerve are indicative of ocular diseases such as glaucoma and may lead to vision loss if left untreated.

1.2 Glaucoma

1.2.1 Disease Prevalence

Glaucoma is a clinical condition characterized by optic nerve cupping and RGC death, and is the leading cause of irreversible blindness worldwide, and affects about 70 million people globally, with 10 million people experiencing bilateral vision loss due to the disease (Quigley & Broman, 2006; Tham et al., 2014). A Canadian study examining population-based surveys from 1994-2003 estimates that about 400,000 Canadians had glaucoma in 2002-2003 (Perruccio, Badley, & Trope, 2007). Despite the prevalence of glaucoma worldwide and the impact of vision loss on quality of life and health expenditures (Buys, 2011; Cruess, Gordon, Bellan, Mitchell, & Pezzullo, 2011), research on the prevalence of glaucoma in Canada is sparse. The only two population-based glaucoma clinical screening studies that have been performed were in Ontario in 1965 in 17,968 individuals, and the second evaluating 291 high-risk individuals in Quebec in 2005 (Buys, 2013). Most data have been obtained from health surveys, with self-reported prevalence ranging from 2.7%-11%, depending on the age group (Perruccio et al., 2007).

However, no assessments of Canadian population-based surveys have been published since then.

Glaucoma is mostly asymptomatic and progresses at varying rates among individuals, with vision loss slowly occurring in a peripheral to central manner over a long period of time. Health surveys may be limited by self-report bias, as proven by the Toronto epidemiology glaucoma survey, in which 3.9% of the negative respondents to self-reports of glaucoma were found to have glaucoma after presenting for clinical examination (Anraku et al., 2011). This overall prevalence of undetected glaucoma amongst negative respondents (3.9%) was comparable to the rate of self-reported glaucoma among Canadians aged 50 years and over (3.9%). Thus, it is likely that the number of affected individuals is higher, as significant ganglion cell degeneration may progress before defects in visual function are detected for the individual to seek medical care. Vision loss due to glaucoma is irreversible, with management through medication and surgery being the only methods of slowing the progression of the disease as, at present, there is no cure for glaucoma.

1.2.2 Clinical Diagnosis and Subtypes

Glaucoma is recognized to be an optic neuropathy, with diagnosis being reserved for patients who present with both structural damage to the optic disc and associated functional defects of at least one eye (Quigley, 2011). Diagnosis is based on measuring damage to the optic disc, sometimes also referred to as the optic nerve head. The optic disc is the point at which nerve fibres of RGCs exit the eye, and marks the beginning of the formation of the optic nerve (Quigley, 2011). The formation of the optic nerve leaves a central depression, often referred to as the optic cup, that visually looks paler than the rim containing the nerve fibres (**Figure 1.5)**. An increasing optic cup-to-optic disc ratio is indicative of a widening and excavation of the cup (Quigley, 2011). This points to degeneration of RGCs and their axons, and the deformation of connective tissues that support the optic disc.

Assessment of functional loss is performed by measuring light sensitivity through a visual field test. A patient is diagnosed with glaucoma if, along with the structural damages mentioned above, they also present with significant loss of their visual field. However, up to 30%-50% of RGCs may be lost before visual field tests may detect functional defects (Harwerth, Wheat, Fredette, & Anderson, 2010; Weinreb, Aung, & Medeiros, 2014). Therefore, a deeper understanding of the etiology and mechanisms underlying glaucomatous RGC loss may aid in early diagnosis and management to avoid significant optic disc damage and irreversible vision loss.

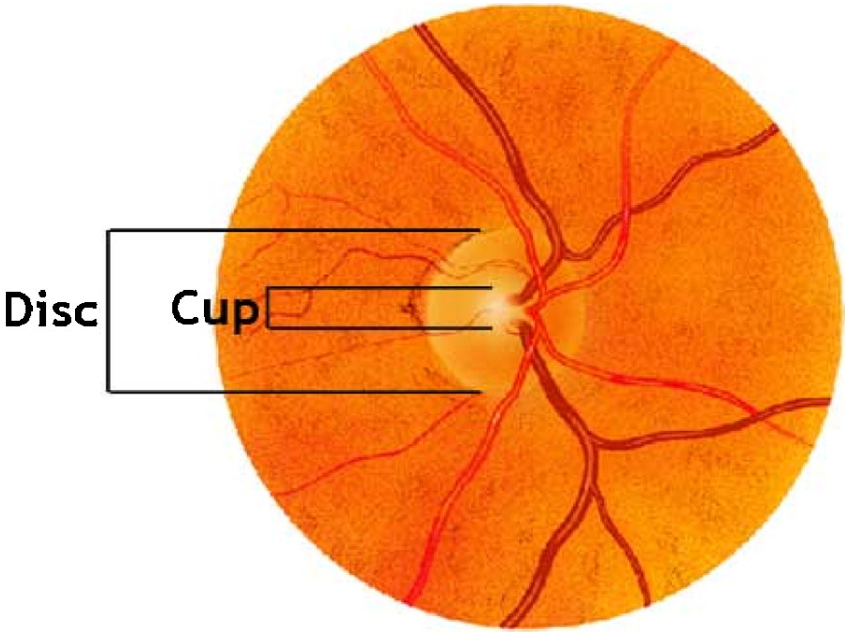

Figure 1.5 Optic disc and optic cup viewed through an ophthalmoscope.

The optic disc marks the beginning of the formation of the optic nerve. Within the optic disc is a central depression called the optic cup, that visually looks paler than the rim. An increasing optic cup-to-optic disc ratio is indicative of a widening and excavation of the cup, pointing to degeneration of RGCs and their axons. Reprinted with permission from (Haleem, Han, Van Hemert, & Li, 2013). Copyright ©2013 Elsevier.

Clinically, glaucoma is classified as either primary or secondary, with primary glaucoma often being idiopathic and affecting both eyes, whereas secondary glaucoma is incited through other factors such as mechanical injury, infection, or disease. Glaucomatous phenotypes are usually characterized based on the morphology of the anterior chamber angle, the main outflow facility of aqueous humour (Stamper, 2009; Weinreb et al., 2014). The two subtypes based on anterior chamber angle morphology are open-angle and angle-closure glaucoma (**Figure 1.6**). A brief overview of glaucoma clinical subtypes is outlined in **Table 1.1.**

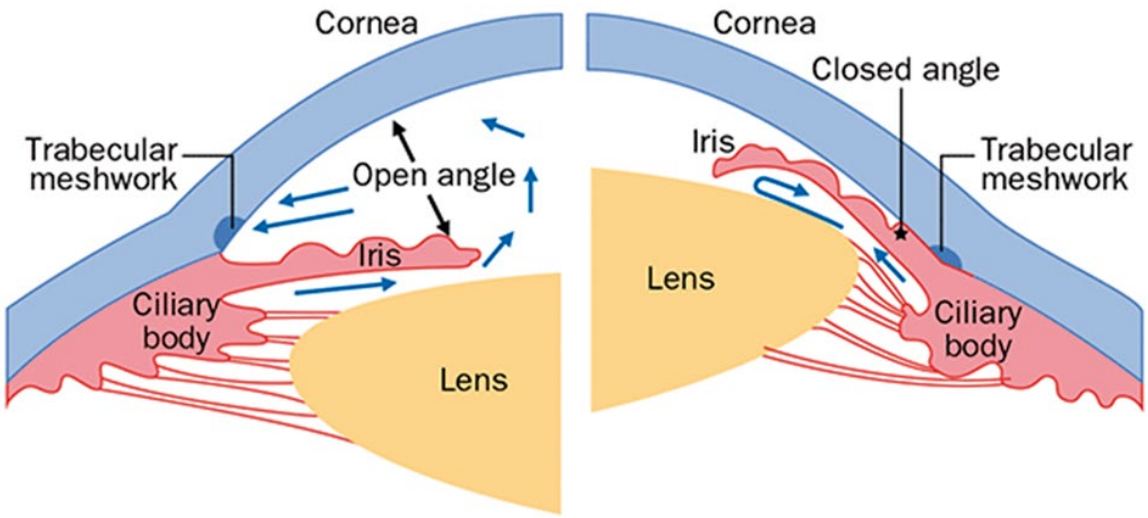

Figure 1.6 Anterior Chamber Angle Morphology observed in Open-Angle Glaucoma and Angle-Closure glaucoma.

The two subtypes based on anterior chamber angle morphology are open-angle and angle-closure glaucoma. In open-angle glaucoma, there is increased resistance to aqueous outflow through the trabecular meshwork despite an open anterior angle (left), as opposed to physical obstruction of the outflow, as seen in angle-closure glaucoma (right). Reused with permission from (Wiggs & Pasquale, 2017), with permission of Oxford University Press.

Table 1.1 Clinical subtypes of glaucoma

Clinical Subtype	Epidemiology	Features	Theories on Pathogenesis	References
Primary Open-Angle Glaucoma (POAG)	Global prevalence of 3.05% in 2013, with 52 million people projected to have POAG in 2020, and 79 million in 2040.	Increased resistance to aqueous outflow through the trabecular meshwork despite an open anterior angle. Elevated IOP is a leading risk factor, however normal-tension glaucoma (IOP <21 mmHg) constitutes a large proportion of POAG cases.	Mechanical stress, deformation and remodelling of other eye structures such as the sclera and the lamina cribrosa that results from the increase in ocular pressure, leading to axonal damage. Vascular dysregulation and autoimmunity are two IOP-independent mechanisms theorized to contribute to glaucoma.	(Burgoyne, Downs, Bellezza, Suh, & Hart, 2005; Downs, Roberts, & Sigal, 2011; Kim & Park, 2016; Stamper, 2009; Tham et al., 2014)
Primary Angle-Closure Glaucoma (PACG)	Global prevalence of 0.50% in 2013, with 23 million people projected to have PACG in 2020, and 32	Obstruction of the anterior chamber angle between the iris and the cornea.	Obstruction often occurs due to high resistance in aqueous outflow through the angle, leading to accumulation of aqueous humour behind the iris, causing the iris to bulge forward and close off access to the trabecular	(Quigley, 2011; Tham et al., 2014)

	million in 2040.		meshwork. This decreases aqueous outflow, leading to elevated IOP and RGC death.	
Primary Congenital Glaucoma	Birth prevalence varies world-wide, ranging from 1:1250 in the Rom population in Slovakia to 1:5,000-22,000 in Western countries. It is the most common pediatric glaucoma.	Eyes present with an isolated maldevelopment of aqueous outlflow system without other developmental ocular anomalies or syndromes that could result in elevated IOP.	Primary congenital glaucoma phenotypes are attributed to trabeculodysgenesis, in which bundles of trabecular meshwork are enlarged due to maldevelopment of the anterior chamber.	(Abu-Amero & Edward, 2017; Cascella et al., 2015; Faiq et al., 2013)
Secondary and Syndromic Glaucoma	Variable depending on primary disorder or syndrome.	Glaucoma presents as a characteristic phenotype of various syndromes, notably Anterior Segment	ASD disorders primarily result from defects in migration or differentiation of mesenchymal cells. Exfoliation syndrome and pigmentary glaucoma both	(Gould & John, 2002; Stamper, 2009)

		Dysgenesis (ASD) disorders, exfoliation syndrome and pigmentary glaucoma.	result in the production and accumulation of fibrillar material or pigment in the anterior segment, particularly on the surface of the lens and margins of the pupil. This debris accumulates within the trabecular meshwork and reduce aqueous outflow, leading to increased IOP.	

1.2.3 Molecular Genetics of Glaucoma

Glaucoma is understood to have a hereditary component, with family history having been established as a risk factor for glaucoma going as far back as 1869 (Leske, Connell, Wu, Hyman, & Schachat, 1995; Wolfs et al., 1998). However, due to its genetic and phenotypic heterogeneity, it is difficult to determine glaucoma's genetic etiology.

Early-onset forms of glaucoma affect children and young adults, typically manifesting between the ages 5-40 years (Vincent et al., 2002). They typically present with a Mendelian autosomal dominant or recessive inheritance pattern. Late-onset forms are typically multifactorial, and are a result of the interaction between genetic and environmental risk factors (Cascella et al., 2015; Wang, R. & Wiggs, 2014).

Glaucoma genes mapped through familial studies

Several chromosomal regions and genes linked to glaucoma have been successfully identified through family-based genetic linkage analysis (Liu & Allingham, 2017). Glaucoma loci (GLC) are grouped into three categories according to each clinical subtype – GLC1, GLC2, and GLC3 for POAG, PACG, and congenital glaucomas, respectively (Friedman & Walter, 1999). Each progressive locus mapped for each glaucoma type are then designated with as "A, B, C…" and so on. Candidate genes for glaucoma mapped to their respective loci are summarized in **Table 1.2.**

Table 1.2 Primary Glaucoma Genes and Loci Identified Through Familial Studies

Glaucoma Clinical Subtype and Phenotype	Locus	Candidate Gene & Chromosomal Location	Likely Mechanism of Glaucoma Pathogenesis / Functional Roles impacted	References
POAG; Juvenile and adult-onset	GLC1A	Myocilin *(MYOC)* (1q24.3)	Gain of function mutations cause intracellular accumulation of abnormal myocilin, possibly impacting trabecular meshwork integrity and being associated with the degeneration of the optic nerve	(Chou, Tomarev, & Porciatti, 2014; Stone et al., 1997; Zhou, Grinchuk, Wawrousek, & Tomarev, 2007)
POAG; Adult-onset and normal-tension glaucoma	GLC1E	Optineurin (*OPTN)* (10p13)	Disruption of inflammatory signalling pathways, increased susceptibility to oxidative stress due to impaired mitophagy, increased induction of cell death, aberrant Golgi organization and post-Golgi membrane trafficking, and protein secretion.	(Kachaner, Genin, Laplantine, & Weil, 2012; Rezaie et al., 2002; Slowicka, Vereecke, & van Loo, 2016; Slowicka & van Loo, 2018)
POAG; Adult-onset	GLC1G	WD repeat-containing protein 36 *(WDR36)*	Disruption of 18s rRNA maturation, increased apoptotic cell death in RGCs	(Chi et al., 2010; Gallenberger et

		(5q22.1)		al., 2010; Monemi et al., 2005; Skarie & Link, 2008)
POAG; Adult-onset and normal-tension glaucoma	GLC1P	Tank-binding kinase 1 (*TBK1)* (12q14)	Dysregulation of the inflammatory response, aberrant autophagy of damaged mitochondria.	(Liu & Allingham, 2017; Tucker et al., 2014)
Primary congenital glaucoma	GLC3A	Cytochrome p450, Subfamily 1, polypeptide 1 *(CYP1B1*) (2p21)	Metabolic dysregulation, increased oxidative damage, and decreased periostin contributing to the loss of structural integrity in the trabecular meshwork	(Choudhary et al., 2007; Zhao, Sorenson, & Sheibani, 2015; Zhao et al., 2013)
Primary congenital glaucoma	GLC3D	Latent transforming growth factor binding protein 2 *(LTBP2)* (14q24)	Decrease in cell adhesion within the ciliary body, resulting in increased elasticity and changes in the ability to support surrounding structures, disrupting aqueous outflow.	(Ali et al., 2009; Cascella et al., 2015).

Glaucoma-associated loci and genes identified through genome-wide association studies (GWAS)

The advent of GWAS allows for the identification of large numbers of genomic regions associated with a specific disease or phenotype through high throughput DNA genotyping technology (Liu & Allingham, 2017). Though linkage analysis can detect rare loci that are strongly causative to a disease, it has limited ability to investigate common genetic variants with a modest impact on complex diseases. Compared to family-based methods, GWAS is performed in large populations, with subject numbers ranging from hundreds to thousands of individuals. Given that phenotypes may not result solely from the mutation of one gene but may arise from disruption of a whole genetic network to which the mutated gene belongs, along with environmental risk factors, GWAS allows for the expansion of our understanding of diseases by looking at common genetic variants associated with certain diseases across large populations (Cascella et al., 2015). These variants may act as modifiers or may each be low-risk variants that interact together to result in a spectrum of phenotypes, which is especially true for complex diseases. Clinically, an example of how GWAS has been useful at the bedside is genetic testing for HLA-B27, a genetic marker discovered to have an association with ankylosing spondylitis, to diagnose patients suspected to have the disease due to their clinical signs and symptoms (Choosing Wisely NL, 2017). Information gathered from GWAS may be clinically useful in identifying individuals and their families who have multiple variants that are associated with risk factors for glaucoma.

Given the prevalence of POAG compared to the other subtypes, most GWAS have been conducted on patient populations with the disease. Major POAG loci discovered are summarized in **Table 1.3.**

With regards to the adult-onset form of PACG, eight genes have been identified to date, although they only account for <2% of the genetic variance in PACG. These genes are pleckstrin-homology-domain-containing family A member 7 (*PLEKHA7),* collagen type 11 alpha 1 chain (*COL11A1),* protein-L-isoaspartate (D-aspartate) O-methyltransferase domain containing 1 *(PCMTD1-ST18),* ependymin-related 1 (*EPDR1),* choline O-acetyltransferase (*CHAT),* Gli-similar family zinc finger 3 (*GLIS3),* fermitin family homolog 2 (*FERMT2),* and Dolichyl-Phosphate Mannosyltransferase Subunit 2 (*DPM2-FAM102)* (Wiggs & Pasquale, 2017)**.** Though some studies suggest a genetic etiological overlap between Primary Congenital glaucoma, POAG, and ASD disorders (Kaur et al., 2005; Micheal et al., 2016; Nishimura et al., 1998; Vincent et al., 2002), there seems to be little etiological overlap between PACG and other clinical subtypes of glaucoma, with 2 POAG loci being nominally associated with PACG (Khor et al., 2016)**.** This may suggest that PACG may exist outside of the spectrum involving POAG, Primary Congenital Glaucoma, and ASD, and has a distinct genetic etiology and pathogenesis.

Table 1.3 Major POAG candidate genes identified using GWAS

Candidate Gene and Chromosomal Location	Expression patterns	Theorized functional roles and/or pathogenesis	References
caveolin 1 and 2 *(CAV1/CAV2)* (7q31)	Expressed in human trabecular meshwork cells and Schlemm canal endothelial cells.	encode calveolins, integral membrane proteins involved in a variety of biological processes such as transcellular transport, endocytosis, cell proliferation, and signal transduction. *CAV1* and/or *CAV2* may influence risk of POAG through effects on IOP.	(Liu & Allingham, 2017; Surgucheva & Surguchov, 2011)
cyclin-dependent kinase inhibitor 2B antisense RNA 1 *(CDKN2B-AS1)* (9p21)	Expressed in human inner retinal nuclear and ganglion cell layers, corneal epithelium, and trabecular meshwork cells.	Loss of *CDKN2B* in mice have been found to result in lens opacity and malformation, a deeper anterior chamber, and susceptibility to RGC loss and axonal degeneration in response to increased IOP.	(Gao & Jakobs, 2016; Liu & Allingham, 2017)
sine oculis homeobox 1 and 6 *(SIX1/SIX6)* (14q23)	Expressed in the murine developing retina, optic nerve, cornea and trabecular meshwork.	Mutations in *SIX6* have been shown to cause anopthalmia in humans and mice. Knockdown of *six6a* using translation-blocking morpholinos resulted in a	(Carnes et al., 2014; Iglesias et al., 2013; Liu & Allingham, 2017)

		reduction in eye size and optic nerve volume in the zebrafish model. *six6b* zebrafish embryos also presented with a small eye phenotype, with histological analysis showing retinal lamination, thinner optic nerves and immature, cellularized lens, indicating a delay in ocular development.	
forkhead box c 1 (*FOXC1)* (6p25)	Expressed broadly in adult human tissue, including the eye and the kidney. Expressed in murine periocular mesenchyme and trabecular meshwork. In zebrafish embryos, it is expressed in the periocular mesenchyme and neural crest cells.	Mutations in *FOXC1* are linked to ASD disorders. Theories on *FOXC1*-associated glaucoma pathogenesis include haploinsufficiency, disruption of downstream targets, and susceptibility to oxidative stress.	(Bailey et al., 2016; Berry et al., 2008; Ito, Goping, Berry, & Walter, 2014; Kume et al., 1998; Nishimura et al., 1998; Smith et al., 2000; Umali et al., 2019)
guanosine diphosphate mannose 4,6-Dehydratase *(GMDS)* (6p25.3)	Expressed in the human retina, optic nerve, and trabecular meshwork.	Certain variants may alter the sequence of regulatory motifs for binding of *SIX6,* a gene linked to glaucoma. In addition, *GMDS* encodes a	(Bailey et al., 2016; Gharahkhani et al., 2014; Liu & Allingham, 2017)

		protein required for synthesis of fucose, which is required for diverse biological functions, including growth factor receptor signalling.	
Atonal homolog 7 (*ATOH7)* (10q21.3)	Expressed in the developing murine and zebrafish retina.	In the murine and zebrafish model, *atoh7* has been shown to be crucial to neuronal differentiation of retinal progenitor cells, with complete loss of *Atoh7* resulting in complete absence of ganglion cells, optic nerves, and chiasmata in mice, and loss of visual function, significant loss of cells in the ganglion cell layer and a barely visible optic nerve in the zebrafish model.	(Brown, Patel, Brzezinski, & Glaser, 2001; Kay, Finger-Baier, Roeser, Staub, & Baier, 2001; Mabuchi et al., 2012; Ramdas et al., 2011)

In addition, researchers have conducted GWAS to look at the heritability and genetic determinants of glaucoma-associated traits, such as elevated IOP and optic disc morphology. These are known as endophenotypes, and are typically hereditary, quantitative traits that may be related to a disease, although are not necessarily dependent on the presence of the disease to exist (Liu & Allingham, 2017). Given the inconsistency of diagnostic criteria and classifications of glaucoma subtypes across studies, endophenotype analysis may be a useful approach in providing insight into how variants affect early glaucoma risk factors, and aid in facilitating early diagnosis. Some risk factors for glaucoma have been found to have high heritability, with heritability studies finding h^2 estimates (the proportion of genetic variation due to additive allelic effects) ranging from 0.35-0.50 for IOP, 0.52-0.83 for optic disc area, and 0.48-0.66 for VCDR (Asefa, Neustaeter, Jansonius, & Snieder, 2018; Levene, Workman, Broder, & Hirschhorn, 1970; Sanfilippo, Hewitt, Hammond, & Mackey, 2010; van Koolwijk et al., 2007; Wray & Visscher, 2008). Genetic determinants for glaucoma endophenotypes are summarized in **Table 1.4.**

Furthermore, gene-gene interaction analysis identified interactions between *ATOH7-SIX6, SIX6-CDKN2B, SIX6-CARD10, SIX6-CDC7,* and *ATOH7-CDC7*, suggesting a putative, additive role of the genes and their pathways in POAG (Philomenadin et al., 2015). Identification of gene networks involved in pathogenesis of complex diseases such as glaucoma would give us more insight on how the disease develops and would potentially allow for the development of better glaucoma treatments to minimize irreversible vision loss.

Table 1.4 Candidate genes associated with glaucoma endophenotypes

Gene	Single nucleotide polymorphisms (SNPs)	Glaucoma endophenotypes	References
ATOH7	rs3858145, rs1900004	Mean optic disc area, VCDR, IOP	(Macgregor et al., 2010; Philomenadin et al., 2015; Ramdas et al., 2010)
Cell division cycle 7 (*CDC7)*	rs1192415	Mean optic disc area, VCDR, central corneal thickness	(Philomenadin et al., 2015; Ramdas et al., 2010)
cyclin-dependent kinase inhibitor 2B *(CDKN2B)*	rs1063192	VCDR, Axial length	(Philomenadin et al., 2015; Ramdas et al., 2010)
SIX1/SIX6	rs10483727	VCDR	(Philomenadin et al., 2015; Ramdas et al., 2010)
Caspase recruitment domain-containing protein 10 *(CARD10)*	rs9607469	VCDR	(Philomenadin et al., 2015)

1.2.4 The Anterior Segment and Glaucoma

The cornea, iris, lens, ciliary body, and ocular drainage structures, such as the trabecular meshwork and the Schlemm's canal, form the anterior segment of the eye. These structures arise from three main types of tissue: the surface ectoderm, neural ectoderm, and periocular mesenchyme (Gould, Smith, & John, 2004). The periocular mesenchyme, consisting of neural crest cells and cranial mesoderm derived cells, contribute extensively to the anterior segment, giving rise to the corneal endothelium, sclera, iris stroma, ciliary muscle, and trabecular meshwork (Gould et al., 2004).. Meanwhile the surface ectoderm forms the corneal epithelium and lens, while the neural ectoderm develops into the retina and epithelium of the iris and ciliary body.

Dysgenesis of the anterior segment results in malformations of these structures, particularly in tissues required for aqueous humour outflow and maintenance of IOP (Gould et al., 2004). Thus, glaucoma is a characteristic feature of ASD disorders, such as Peters Anomaly (OMIM: #261540), and Axenfeld-Rieger Syndrome (ARS) (OMIM: #180500) (OMIM®, 2019). However, developmental abnormalities of ocular drainage structures may not always be detectable clinically, and thus may affect the functionality and metabolism of aqueous outflow structures without apparent disruptions in morphology IOP (Gould et al., 2004). It is possible that developmental genes and pathways involved in anterior segment formation contribute to more common forms of glaucoma which present with no observable developmental abnormalities. Major developmental genes that mediate anterior segment development and speculated gene interactions are outlined in **Fig. 1.7.**

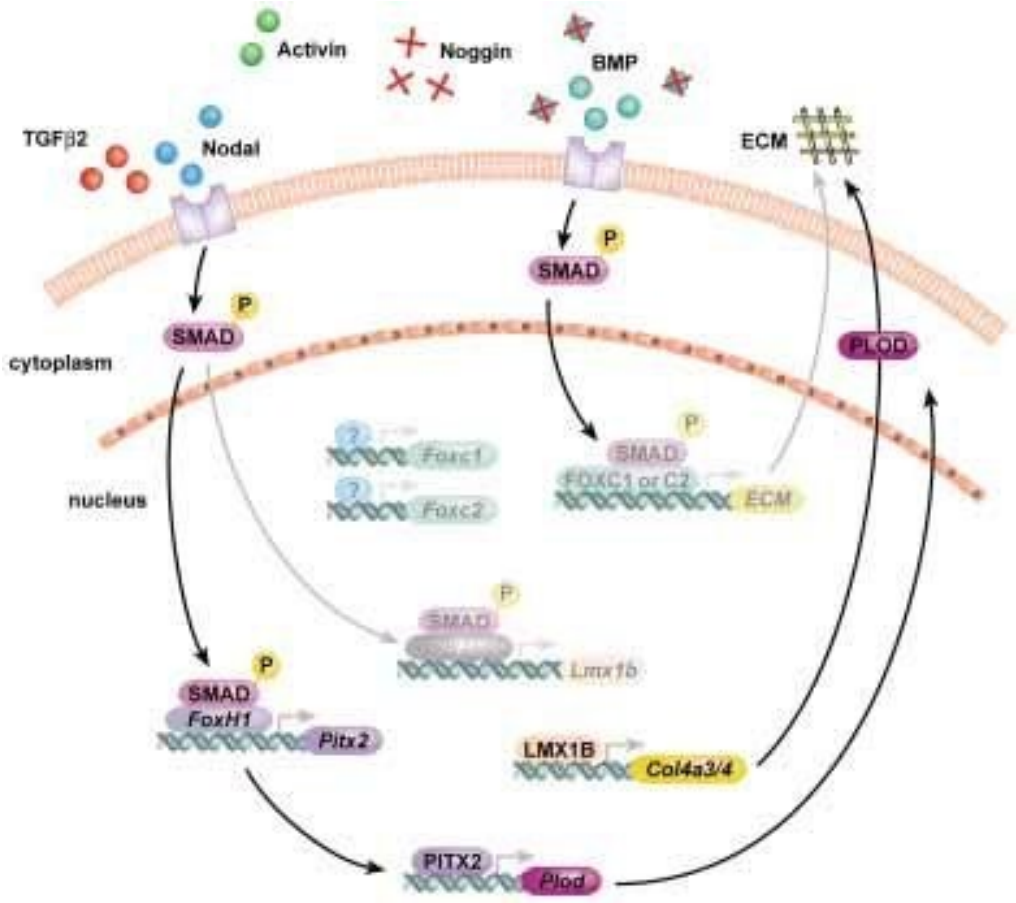

Figure 1.7 Anterior Segment Developmental Genes.

The development of the anterior segment is mediated by an intricate network of genes. This figure illustrates a possible gene network centering the *TGFβ*-superfamily/BMP signalling as the main regulating pathway in anterior segment development, as described by Gould et. al (2004). Reused with permission from (Gould et al., 2004) with permission of The International Journal of Developmental Biology.

1.3 FOXC1

The gene *FOXC1,* located on chr. 6p25, is a member of the forkhead box transcription factor family. Forkhead box transcription factors, named after the *Drosophila forkhead* gene that piloted their discovery, are characterized by a forkhead domain, a highly conserved amino acid sequence that binds to DNA and activates downstream targets. The DNA-binding motif encodes a variant of helix-turn-helix class of proteins, consisting of three α helices, two β sheets, and two large loops that give rise to two wing-like structures, thus their alternative name of 'winged-helix' transcription factors (Saleem, Banerjee-Basu, Murphy, Baxevanis, & Walter, 2004). Structurally, *FOXC1* contains N- and C-terminal transactivation domains which enable it to act as a transcriptional activator, along with a transcriptional inhibitory domain C-terminal to the forkhead domain (Berry, Saleem, & Walter, 2002).

Like other forkhead genes, *FOXC1* is a key regulator of developmental processes, particularly through transcriptional activation of its downstream targets. Most notably, it plays a significant role in the formation of the anterior segment of the eye. Expression studies of *FOXC1* have demonstrated that the gene is widely expressed in adult and fetal human tissue, with Nishimura and colleagues confirming the broad expression of *FOXC1* in adult human tissues such as the brain, heart, kidney, spleen, liver and colon (Nishimura et al., 1998). *FOXC1* expression is abundant during embryogenesis and in the adult eyes and the kidney. In the murine model, *Foxc1* is expressed in the periocular mesenchyme and later, in the trabecular meshwork of the eye, whereas this thesis concurs with previous studies showing that in the zebrafish, *foxc1* transcripts are expressed in the

periocular mesenchyme and the neural crest (French et al., 2014; Gage, Rhoades, Prucka, & Hjalt, 2005; Kidson, Kume, Deng, Winfrey, & Hogan, 1999; Topczewska, Topczewski, Solnica-Krezel, & Hogan, 2001).

Anterior segment disorders with the presence of early-onset glaucoma, particularly ARS, have been mapped to human chr. 6p25 (Gould, Mears, Pearce, & Walter, 1997; Mears et al., 1998; Mirzayans et al., 2000). Nishimura and colleagues demonstrated that mutations in the *FOXC1* gene cause a spectrum of glaucoma phenotypes, with mutations within the conserved forkhead domain being identified in glaucoma patients, suggesting that the disruption of the DNA-binding ability of the protein causes glaucoma phenotypes (Nishimura et al., 1998). Additional studies have identified more pathogenic variants in the *FOXC1* gene in association with glaucoma and anterior segment disorders, particularly with Axenfeld-Rieger Syndrome, with most of the mutations reported being heterozygous (Du et al., 2016; Mears et al., 1998; Mirzayans et al., 2000). Thus, the disease is known to be autosomal dominant. However, a homozygous in-frame deletion has been recently reported to cause ARS with congenital glaucoma (Micheal et al., 2016).. This presents the possibility that homozygous mutations in the *FOXC1* gene may cause ARS with congenital glaucoma and may be transmitted through an autosomal recessive pattern. This indicates that a loss of *foxc1* function model may be useful in understanding the mechanisms underlying *FOXC1*-associated glaucoma.

Investigations of how *FOXC1* missense mutations affect the ability of the forkhead binding domain to bind to an *in vitro*-derived oligonucleotide revealed that despite their different functional implications, all the mutations resulted in decreased transactivation

activity as measured by luciferase activity compared to wild-type levels (Saleem, Banerjee-Basu, Berry, Baxevanis, & Walter, 2001). This decrease in transactivation may result in phenotypic variability depending on gene interactions disrupted or environmental factors. Subsequent studies examining missense mutations in *FOXC1* that cause ARS have identified essential structural determinants within the forkhead domain that correspond with specific functions such as protein stability, DNA-binding specificity, nuclear localization (Saleem et al., 2004). These alterations in structure due to point mutations may result in disruption of *FOXC1's* overall regulatory function, affecting a multitude of downstream targets.

It is not only missense mutations that have been found to cause ocular abnormalities and glaucoma, as ASD is attributed to aberrant *FOXC1* gene dosage. A number of unrelated families who displayed ocular developmental abnormalities and glaucoma were identified to possess both duplications and deletions of 6p25 (Lehmann et al., 2002; Nishimura et al., 2001), providing evidence that supports the idea of stringent *FOXC1* gene dosage being crucial to normal eye development. Previous murine studies show that homozygous *Foxc1* mutations are perinatally lethal, while *Foxc1* heterozygotes exhibited multiple, clinically identifiable ocular anomalies such as irregularly shaped pupils, iris tears and iris strands attached to the cornea, and misplaced pupils starting at 11 months of age, with the penetrance of these abnormalities depending on genetic background (Kume et al., 1998; Smith et al., 2000).

Histological studies on the eyes of *Foxc1* heterozygote mice showed abnormalities regardless of genetic background, with abnormalities including small or absent

Schlemm's canal, large blood vessels and iris strands, and absent or compressed trabecular meshwork (Smith et al., 2000). However, researchers found no significant increase in IOP in *Foxc1* heterozygote mice, with only one 17-month old *Foxc1* heterozygote out of 119 mice exhibiting elevated IOP compared to normal (18.6 mmHg, >2 SDs above the normal mouse IOP range of 11.2 ± 0.7 mmHg) (Smith et al., 2000). However, no further testing apart from the measurement of IOPs were performed to identify glaucoma in the *Foxc1* heterozygote murine model. A lack of abnormalities in the optic nerve and retina were noted. However, these were not elaborated on, and no additional tests to assess vision loss, cupping of the optic disc, or ganglion cell loss were performed. Therefore, we cannot rule out the possibility that abnormalities in *Foxc1*in mice cause glaucoma.

FOXC1 has been shown to regulate genes involved in various biological functions such as apoptosis, cell growth, differentiation, transcription, and oxidative stress response. Nickel Agarose-Based Chromatin Enrichment has been used to identify *FOXC1* downstream targets, twenty of which are expressed in the eye (Tamimi, Lines, Coca-Prados, & Walter, 2004). The identified *FOXC1* targets implicate *FOXC1* in various processes such as oncogenesis (*FVT-1, BMP7, SMAD2)*, the regulation of IOP (*PTGER)*, and ocular development and cell identity (*DACH1, SIX1, WNT6)*. Furthermore, Berry and colleagues identified and validated additional *FOXC1* target genes, with genes selected based on expression within the eye, in similar non-ocular tissues as *FOXC1,* and the presence of a core *FOXC1* DNA-binding sequence (Berry et al., 2008). *FOXC1* upregulates another transcription factor, forkhead box O1 A (*FOXO1A),* which is required for cell survival

and resistance to oxidative stress in the trabecular meshwork (Berry et al., 2008). Genes expressed in the human trabecular meshwork have also been shown to be impacted by loss of *FOXC1* function, such as *CLOCK, CKL6, PLEKHG5, ITGβ1,* and the miR-204 – *MEIS2* regulatory pathway, the latter of which is essential to normal development of the lens and optic cup in other fish models (Conte et al., 2010; Paylakhi et al., 2013). These highlight the involvement of *FOXC1* in a vast array of gene pathways and is important to consider when trying to understand the underlying mechanisms of glaucoma pathogenesis.

1.3.1 FOXC1 and Oxidative Stress

The trabecular meshwork, due to its function, is constantly exposed to aqueous humour. The aqueous humour is composed of several chemicals, including glutathione, ascorbate, and hydrogen peroxide, the latter of which is a significant source of oxidative stress (Green, 2001; Ramachandran, Morris, Devamanoharan, Henein, & Varma, 1991). Susceptibility to oxidative damage in the trabecular meshwork and the retinal cells is suspected to play a key role in glaucoma pathogenesis and may be a mechanism through which *FOXC1* mutations cause degeneration of RGCs and the optic nerve.

A reduction in *FOXC1* has been shown to lead to a decrease in *FOXO1A* expression *in vitro*, effectively increasing rates of apoptosis in trabecular meshwork cells in response to oxidative stress (Berry et al., 2008). This finding is significant since trabecular meshwork cell death affects the trabecular meshwork's ability to drain aqueous humour and causes elevated IOP, a well-known risk factor for glaucoma. Reduction of *FOXO1A* expression

and increased cell death was also observed in vivo, through the use of the zebrafish eye model (Berry et al., 2008).

Furthermore, *HSPA6,* a heat-shock protein identified as a *FOXC1* target, has also been shown to be reduced when *FOXC1* is knocked-down in human trabecular meshwork cells (Berry et al., 2008; Ito et al., 2014). *HSPA6* was also shown to have a protective role in human trabecular meshwork cells upon exposure to severe doses of hydrogen peroxide, with an increased rate of apoptosis being observed when *HSPA6* was knocked down (Ito et al., 2014). This suggests that HSPA6 has a protective role against apoptosis in severe stress conditions. Ito and colleagues also examine the protective role of FOXC1 in human trabecular meshwork cells exposed to various severities of oxidative stress. Compared to human trabecular meshwork cells with normal *FOXC1* levels, a reduction of viable cells was observed in *FOXC1* knockdown cells in untreated, low H_2O_2, and high H_2O_2 conditions (Ito et al., 2014). These show that *FOXC1* may have an anti-apoptotic role under both normal and oxidative stress conditions. However, no further investigations were done to confirm whether this anti-apoptotic role is accomplished solely through FOXC1's transactivation of downstream targets or whether FOXC1 has independent mechanisms that are also protective against oxidative damage. Given *FOXC1* is a transcriptional regulator involved in multiple, parallel pathways underlying normal eye development and eye cell survival. we need to widely examine *FOXC1*'s various roles through its gene targets and their respective biological functions to gain insight into its role in glaucoma pathogenesis.

1.4 Zebrafish as a Model for Eye Genetics

1.4.1 The Zebrafish Genome

The zebrafish, *Danio rerio*, is a popular animal model frequently used to study the genetics underlying vertebrate development and disease. The use of zebrafish as a model in genetic studies was pioneered by George Streisinger and his colleagues at the University of Oregon in the 1980's, noting their many qualities that made them an ideal genetic model system such as their easy and cost-efficient maintenance, high fecundity, and rapid development (Fadool & Dowling, 2008). Zebrafish have a short generation time of 2-4 months, with a single mating pair producing large clutches of fertilized eggs (Richardson, Tracey-White, Webster, & Moosajee, 2017). Fertilization takes place *ex utero*, and their virtually transparent embryos allow for visualization and manipulation, giving researchers the ability to study early organogenesis in real-time. By 24 hours post-fertilization (hpf), some major organ systems would have formed, and spontaneous muscle flexures soon begin, while behavioural responses being observed 48 hpf.

The zebrafish genome-sequencing project was initiated at the Wellcome Trust Sanger institute in 2001, using the Tubingen zebrafish reference strain as it had been extensively used to identify mutations affecting embryogenesis through large-scale forward genetic screens. Zebrafish are chromosomally diploid, with a genome estimated at 1700 Mb, comprising of 25 pairs of mapped chromosomes, and 26,206 protein-coding genes (Howe et al., 2013). Being a member of the Teleostei infraclass, the zebrafish genome features representation in duplicate of 30% of homologous tetrapod genes compared to other vertebrate species, due to an ancient additional round of genome duplication in the

teleosts' common ancestor called the teleost-specific genome duplication (TSD) (Howe et al., 2013). Gene duplicates resulting from this process are referred to as ohnologues and are thought to contribute to the higher number of species-specific genes in the zebrafish genome compared to the human, mouse or chicken.

FOXC1 exists in duplicate in zebrafish, with a homology of 83% and 84% for *foxc1a* (located on Chr. 2) and *foxc1b* (located on Chr. 20), respectively (Zerbino et al., 2017). We need to keep the aforementioned genomic duplication in zebrafish in mind as we use them as genetic models. Studies on these duplicated genes have led to the observation that the duplicates tend to diverge over time, with the idea that functionally equivalent genes are expressed in complementary sub-domains of their tetrapod homologues (McMahon, Semina, & Link, 2004). This phenomenon can be an advantage in forward genetic screens as phenotypes that arise may be unique to a specific gene duplicate (McMahon et al., 2004). On the other hand, when both duplicates are expressed in the same domain, genetic compensation may occur. Complex traits such as glaucoma rely heavily on gene dosage, and thus mutations in gene duplicates within the same domain may result in phenotypes that may be more informative than a complete loss of activity. Thus, gene duplication might be advantageous for mutational analysis.

1.4.2 The Anterior Segment of the Zebrafish Eye

Similar to humans, the zebrafish eye develops from three distinct embryological tissues (Schmitt & Dowling, 1994). The neuroectoderm gives rise to the neural retina, retinal pigment epithelium, the optic stalk, iris dilator and sphincter muscles, and the ciliary body (Richardson et al., 2017). The surface ectoderm develops into the lens, and cornea, while

the mesenchyme forms the corneal endothelium and stroma, iris stroma, ciliary muscles, trabecular meshwork, Schlemm's canal, vasculature, and sclera.

The periocular mesenchyme is crucial to eye development as the origin of various cells that form eye structures. Once thought to be a loose array of cells solely of mesodermal origin, the cells of the periocular mesenchyme have been found to be comprised of specific cellular contributions from both the neural crest and the mesoderm, which co-mingle in the anterior segment (Gage et al., 2005). Structures of neural crest lineage include smooth muscles, pericytes, most cells within the corneal endothelium, stroma, and trabecular meshwork, while cells originating from the mesoderm gives rise to extraocular muscle fibers, endothelium of ocular vasculature, and a small population of cells within the neural crest-derived structures. Another significant function of the periocular mesenchyme is to provide signals for patterning of the optic vesicle into the RPE and neural retina, induction of ocular gland morphogenesis, and patterning and differentiation of the retinal pigmented epithelium from the optic cup (Fuhrmann, Levine, & Reh, 2000; Gage, Suh, & Camper, 1999; Govindarajan, Ito, Makarenkova, Lang, & Overbeek, 2000). Various genes such as *pitx2* and *foxc1* implicated in the proper formation of the anterior segment are expressed in the periocular mesenchyme, albeit in different amounts in cells of mesodermal lineage (Gage et al., 1999). Given the periocular mesenchyme's importance in cell fates and signalling to the development of eye structures, disruptions of genes expressed in the POM may result in ocular defects.

The development of the anterior segment of the zebrafish has been described extensively, and is composed of the cornea, lens, iris, ciliary body, and the iridocorneal angle(Soules

& Link, 2005). Lens establishment begins at 16 hpf, with contact between the evaginating optic vesicle and surface ectoderm resulting in a visible thickening of the lens placode (Soules & Link, 2005). Unlike mammalian lens development, the zebrafish lens forms by delamination of the lens placode and not through invagination (Hay, 1980), resulting in a large solid spherical lens compared to the ellipsoidal mammalian hollow lens vesicle. At 24-26 hpf, the lens vesicle detaches from the surface ectoderm place partly by apoptosis, which also marks the establishment of the anterior chamber (Glass & Dahm, 2004; Soules & Link, 2005). At 36 hpf, a transition zone appears in the lens, with the formation of a thin extracellular capsule being achieved by 72 hpf. Lens cells then continue to develop and differentiate into either epithelial or fiber cells, similar to the mammalian lens.

While the anterior chamber is being established as marked by the detachment of the lens vesicle from the surface ectoderm, undifferentiated periocular mesenchymal cells migrate and accumulate within the anterior chamber (Soules & Link, 2005). The surface ectoderm and periocular mesenchyme then develop into the cornea, with the periocular mesenchymal cells migrating from peripheral regions of the optic cup. The posterior portion of the cornea can be detected as a single layer of flattened mesenchymal cells by 36hpf, while undifferentiated mesenchymal cells continue to accumulate within the anterior chamber (Soules & Link, 2005). Differentiation of these mesenchymal cells can be detected around 48 hpf, particularly within prospective iridocorneal angle, and by 72hpf, multiple types of pigment cells and less differentiated non-pigment cells can be observed, and the rudimentary anterior segment structures are established. An additional wave of immigrating periocular mesenchymal cells forms the corneal stroma (Hay, 1980).

The corneal stroma then undergoes differentiation and deposition of collagen fibrils and other extracellular matrix components, resulting in further stratification. Both the zebrafish corneal stroma and corneal endothelium are thinner compared to mammals. Meanwhile, the corneal epithelium loses its scalloped appearance and ceases to be continuous with the outer epidermis and is thicker compared to the mammalian epithelium.

Like the iris, the ciliary zone and anterior segment angle are all formed through a series of dramatic differentiation that occurs across the embryonic stages. The ciliary zone is a term used to refer to the region underlying the base of the iris, and although zebrafish do not show ciliary processes, the ciliary zone provides a site for the attachment of lens zonules. Like mammalian and avian ciliary tissue, it is also the site of aqueous humour production (Gray, Smith, Soules, John, & Link, 2009). A significant feature differentiating the angle of embryonic and adult zebrafish with that of mammals is the presence of the annular ligament, a meshwork that fills the iridocorneal angle and covers the anterior segment in a ring-like manner and is thought to be functionally analogous to the trabecular meshwork in the human eye (Gray et al., 2009). The annular ligament appears to also be of periocular mesenchymal origin, with its shape varying between the dorsal region and the ventral region of the eye from a U-shape to a funnel shape (Soules & Link, 2005). This causes the iris to project slightly forward in the dorsal region, while bending posteriorly in the ventral region.

Extensive growth and morphogenesis which involves local proliferation, stratification and differentiation within the cornea, specialization of angle structures, and differentiation of

the iris stroma and ciliary epithelial zones, continue until the zebrafish is a month old, when the eye reaches its full maturity (Soules & Link, 2005). The lens retains its spherical shape and thick extracellular capsule in one-month old zebrafish and is suspended by zonules attaching the lens capsule to the non-pigmented epithelium of the ciliary zone. Eye growth and refinement of the zebrafish anterior segment has also been found to persist past 3 months, which is past sexual maturity.

1.4.3 The Zebrafish Retina

The development and structure of the retina are highly conserved among vertebrates. Like humans, zebrafish are diurnal and possess the seven major retinal cells types derived from the neuroectoderm – horizontal cells, bipolar cells, amacrine cells, ganglion cells, rod cells, cone cells, and Muller cells (Fadool & Dowling, 2008) (**Figure 1.8**). These major cell classes are arranged in a similarly layered pattern in humans and zebrafish, with photoreceptor rod and cones occupying the outermost layer, and ganglion cells residing closest to the lens in the innermost layer. Amacrine, bipolar, and horizontal cells function as interneurons that localize between the photoreceptor and the ganglion cell layers.

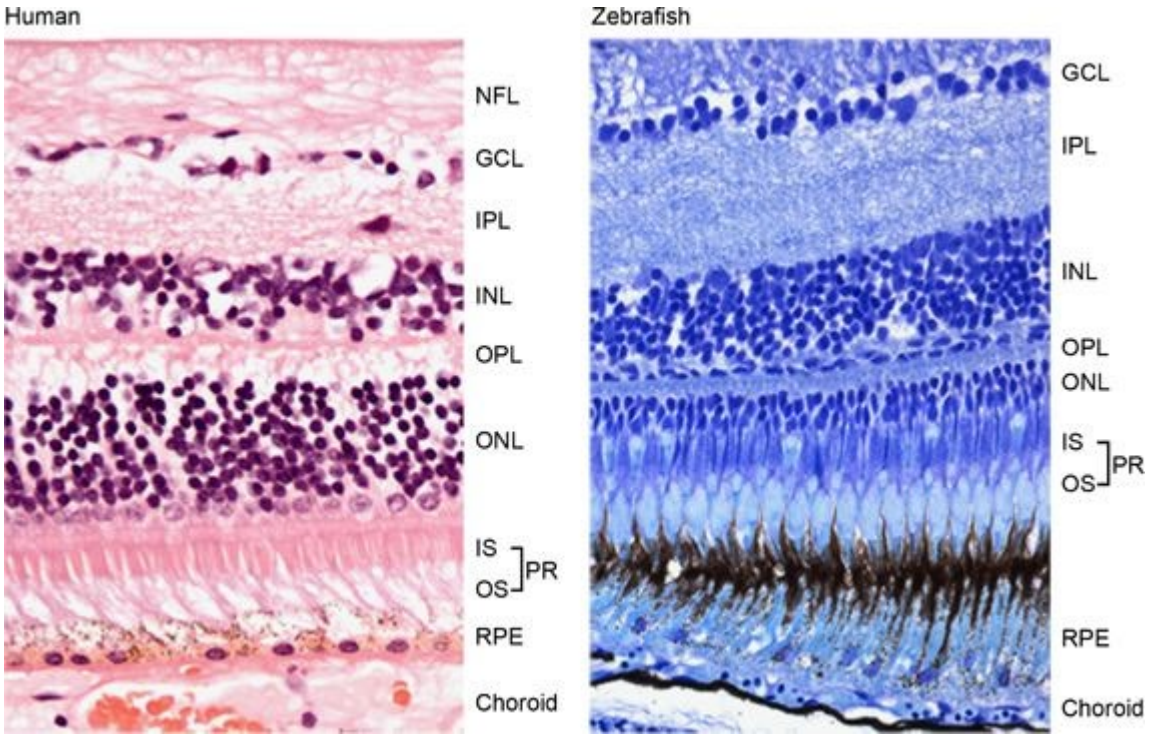

Figure 1.8 Retinal laminar structures of the human and zebrafish eye.

A high degree of similarity is observed in the retinal layers of Homo sapiens and Danio rerio. Pictured here are the retinal nerve fiber layer (NFL), ganglion cell layer (GCL), inner plexiform layer (IPL), inner nuclear layer (INL), outer plexiform layer (OPL), outer nuclear layer (ONL), the inner and outer segments (IS and OS) of photoreceptors (PR), RPE, and the choroid. Reprinted by permission from Springer Nature: Macmillan Publishers Limited. Eye. (Richardson et al., 2017). Copyright © 2017.

In this section, we will describe the development of the vertebrate neural retina, as observed in the zebrafish model. Retinal development starts with the formation of the optic cup through a series of morphogenic reorientations of the optic primordia. By 24 hpf, the optic cup is well-formed, which develops into the neuroepithelium and the retinal pigmented epithelium (Schmitt & Dowling, 1994). Retinal neurogenesis takes place shortly after the optic cup forms, with the neuroepithelium being comprised of multipotent progenitor cells that become postmitotic and migrate to the proper cellular layer to differentiate into their cell fates.

Retinal cells are generated in sequence, with the RGCs being first to be born across species (Cepko, Austin, Yang, Alexiades, & Ezzeddine, 1996; Young, 1985). Across vertebrates, retinal neurogenesis has been found to commence with the formation of an initial central patch of postmitotic cells, which then grows towards the periphery (Brown et al., 1998; McCabe, Gunther, & Reh, 1999; Straznicky & Gaze, 1971). The same is true for zebrafish, with Atoh7 expression and initiation of mitosis of progenitor cells coinciding at around 25-28 hpf in the ventronasal retina, with progenitors differentiating into ganglion cells (Hu & Easter Jr, 1999; Masai, Stemple, Okamoto, & Wilson, 2000).

Over the next 48 hours, progenitors continue to become postmitotic, with new ganglion cells differentiating next to pre-existing ones in a fan-like wave around the retina. In zebrafish, retinal neurogenesis occurs in three separate but temporarily overlapping waves, with the first wave taking place at around 25-28 hpf in the ventronasal domain, resulting in ganglion cell production (Hu & Easter Jr, 1999; Kay et al., 2001). At around 38 hpf, postmitotic cells arise to form the amacrine, bipolar, and horizontal cells that

comprise the inner nuclear layer (INL), followed by a wave of photoreceptor production to form the ONL at around 48 hpf (**Figure 1.9**).

Both intrinsic and extrinsic cues contribute to the cell fate determination in retinal progenitor cells. The most widely accepted model for retinal cell fate determination proposes that retinal progenitors undergo a series of competence states to produce a particular cell type as development progresses (Cepko et al., 1996) (**Figure 1.10**). The states of competence of these progenitors are intrinsically defined by a hierarchy of transcription factors and translational differences, which determine how each cell responds to a particular set of environmental cues to produce a certain cell type.

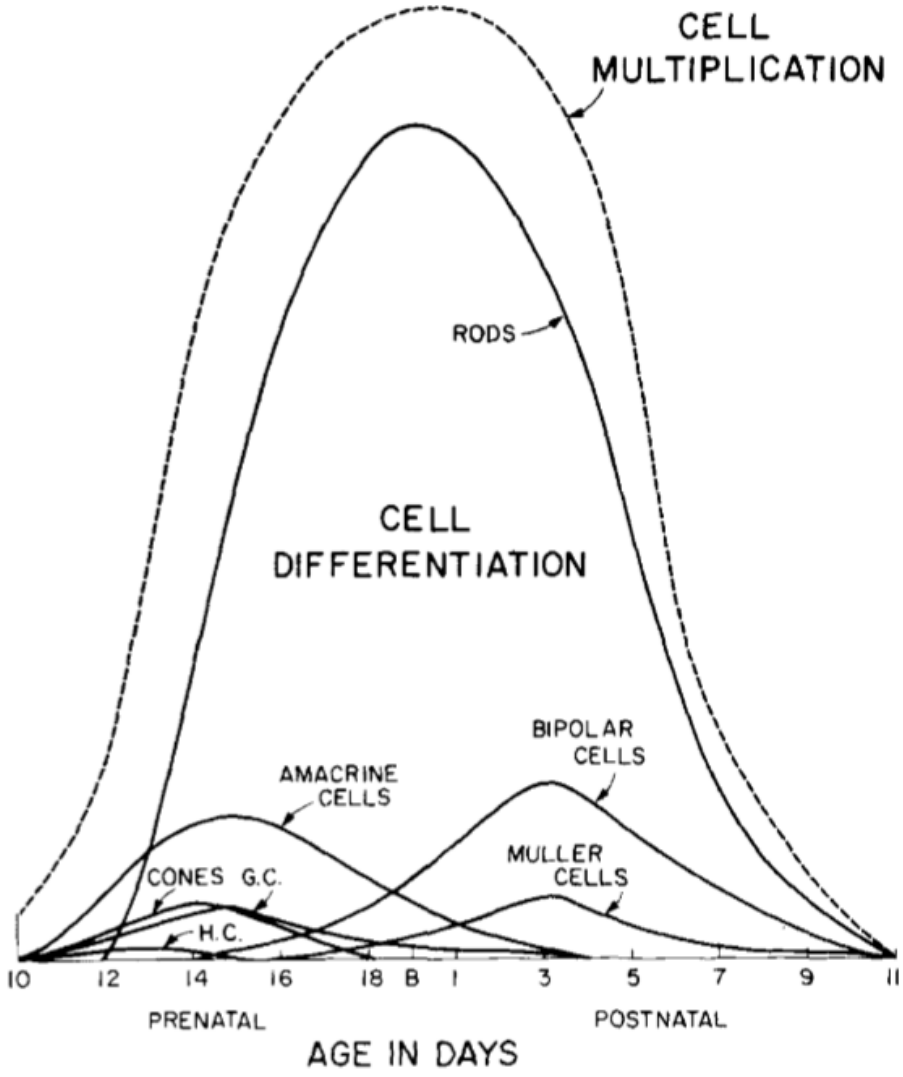

Figure 1.9 Retinal neurogenesis is initiated by differentiation of RGCs.

Reprinted from (Young, 1985), with permission from John Wiley and Sons. Copyright ©1985 John Wiley & Sons, Inc.

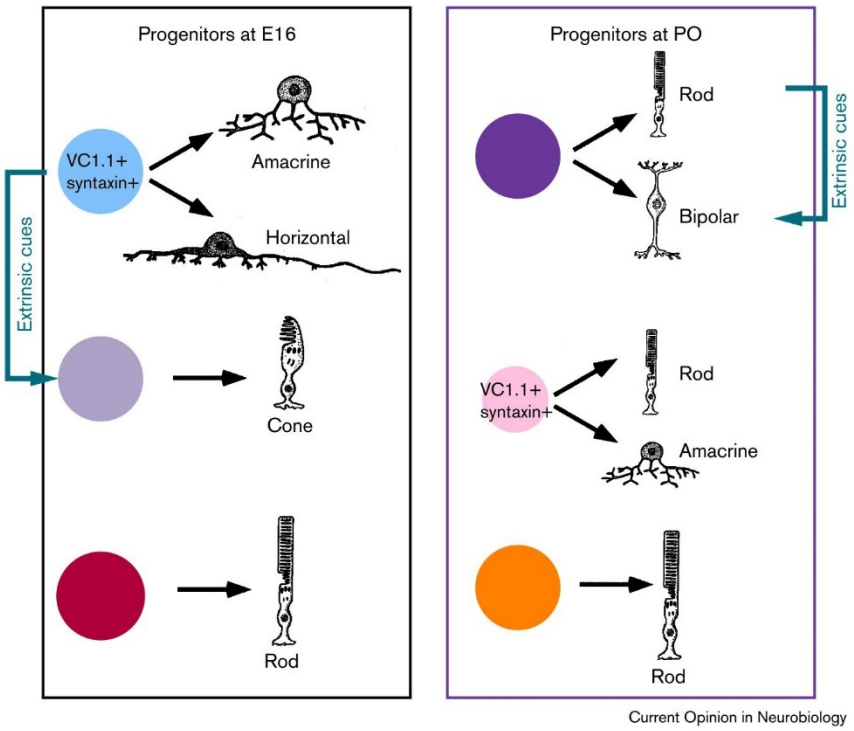

Figure 1.10 Intrinsic and extrinsic cues both contribute to the cell fate determination in retinal progenitor cells.

In this model of retinal cell fate determination, distinct progenitor cells exist at different times, with intrinsic cues defining how each cell responds to extrinsic cues to produce different ratios of cell types. While each progenitor may be intrinsically more likely to produce one or a few cell types, its progeny is not restricted. For example, at E16 in the rat, a progenitor that normally produces amacrine cells can receive feedback inhibition (an extrinsic cue) to produce photoreceptor cells instead (Cepko, 1999). At P0, a progenitor cell that normally makes rods and bipolar cells may receive extrinsic cues to make more of one than the other, or amacrine cells (Cepko, 1999). Reprinted from (Cepko, 1999), with permission from Elsevier. Copyright ©1999 Elsevier.

Extrinsic cues are crucial contributors to cell fate through the production of signals that provide feedback to both progenitors and postmitotic cells to acquire cell fate choices. Several factors have been shown to influence postmitotic cell fates extrinsically. The addition of ciliary neurotrophic factor to rat retinal explants before the intrinsic cellular expression of opsin results in inhibition of rod photoreceptor production and respecification of progenitors from a rod to bipolar cell fate in vitro (Ezzeddine, Yang, DeChiara, Yancopoulos, & Cepko, 1997). The addition of amino acid taurine to rat retinal cultures has also been shown to promote differentiation of progenitors into rods (Altshuler, Lo Turco, Rush, & Cepko, 1993). However, the increase in rod production could only be partially attributed to taurine, as retinal cell-conditioned media and extracts also promoted rod production. This further signifies the role that environmental cues play in cell fate determination.

The transcriptional hierarchies and networks underlying cell fate determination in retinal progenitors still have much to be understood. In Drosophila, neural progenitor cells express the basic helix-loop-helix (bHLH) transcription factor *atonal*, which has been identified to be essential in photoreceptor development in the fruitfly (Jarman, Sun, Jan, & Jan, 1995). Vertebrate homologs of atonal, from the murine *Atoh7* to the zebrafish *atoh7* are required for RGC differentiation from retinal progenitors, and are expressed in early stages of development (Brown et al., 1998; Kay et al., 2001).

Atoh7 regulates genes that facilitate ganglion cell production through either the establishment of progenitor cells that differentiate and commit to a ganglion cell fate or through regulation of mechanisms that underlie RGC specification and differentiation. An

identified target of *Atoh7* is class IV POU-domain transcription factor 2 (*Pou4f2*) required for differentiation, axon outgrowth and pathfinding, and survival (Wang, S. W., Gan, Martin, & Klein, 2000; Wang, S. W. et al., 2001). However, loss of *Pou4f2* has no significant effect on many other genes underlying ganglion cell production, indicating that other regulatory genetic pathways under transcriptional control of *Atoh7* that simultaneously contribute to ganglion cell genesis.

Furthermore, as a transcription factor, Atoh7 is part of a complex transcriptional network that regulates retinal neurogenesis and cell fate determination (**Figure 1.11**) (Boije, MacDonald, & Harris, 2014) . *Atoh7* is a direct target of the transcription factor *Pax6* in the murine model, with loss of *Pax6* resulting in a reduction of ATOH7 expression (Brown et al., 1998). It is also directly inhibited by another bHLH gene *PTF1A*, with overexpression studies of PTF1A in the chick demonstrating inhibition of ATOH7, thus resulting in a reduction of ganglion cell and photoreceptor production, and an increase of horizontal and amacrine (Lelievre et al., 2011). The opposite is observed when *Ptf1a* is lost, resulting in a conversion of murine horizontal and amacrine precursors to a ganglion cell fate (Fujitani et al., 2006).

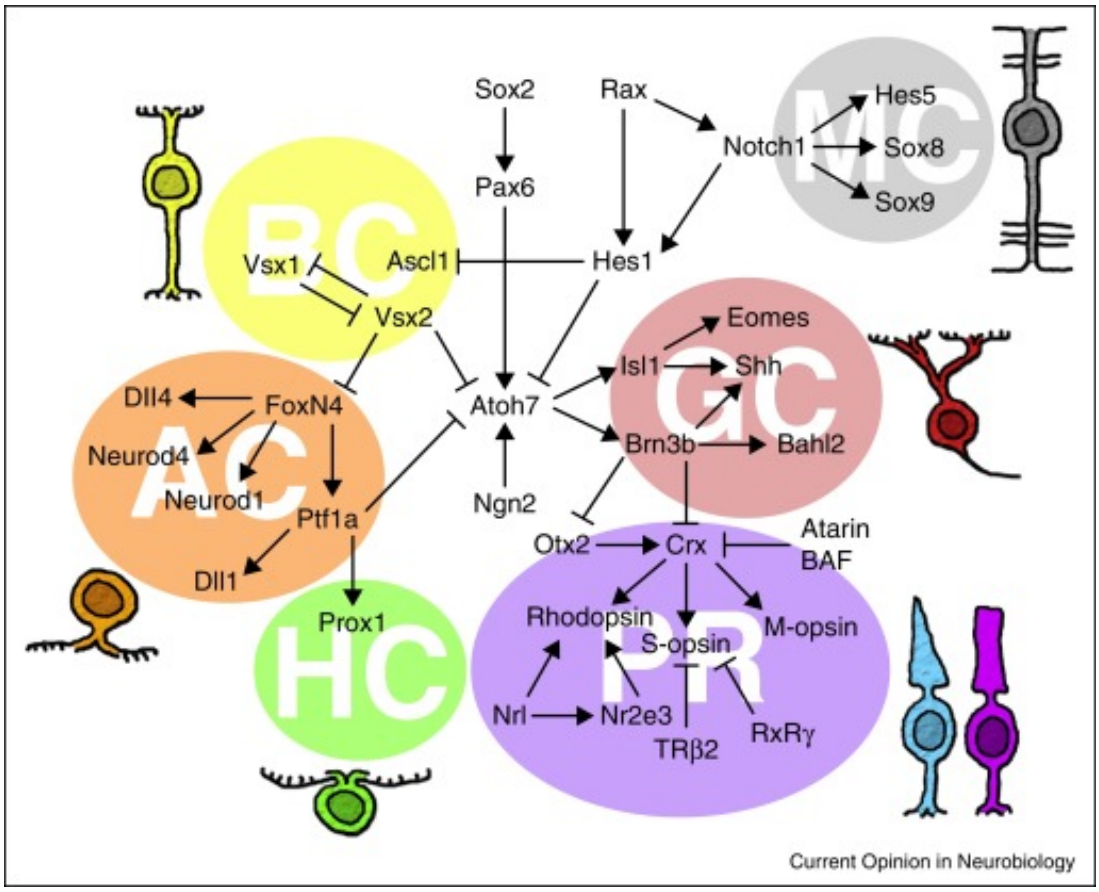

Figure 1.11Transcriptional regulation of the retina.

A complex genetic network of transcription factors underlies cell fate determination of all types of retinal cells. Reproduced with permission from (Boije et al., 2014) under the terms of the Creative Commons Attribution License.

In zebrafish, *atoh7* has also been shown to be repressed by Vsx2, another transcription factor downregulated in progenitors except those that would take a bipolar or Muller glial cell fate (Vitorino et al., 2009). As a downstream target of Ptf1a and Vsx2, Atoh7 is part of a complex network that involves FoxN4, an upstream regulator of Ptf1a, and Vsx1, which interacts with Vsx2, and their respective gene targets. This shows that Atoh7 plays a significant role not solely confined to ganglion cell production, but cell fate determination of all types of retinal cells.

In zebrafish *atoh7* mutants, the first neurogenic wave is disrupted, and undifferentiated progenitors accumulate until the second wave of neurogenesis, resulting in progenitors taking on amacrine cell fates (Kay et al., 2001). This results in the ganglion cell layer of these mutants mostly consisting of displaced amacrine cells. Furthermore, *atoh7* mutants also present with an increase in bipolar and muller glial cell numbers in the inner nuclear layer (Kay et al., 2001). This further highlights *atoh7*'s interactions with genes regulating the specification of cells in the inner nuclear layer. Loss of *atoh7* did not appear to disrupt the neurogenic waves required for INL and ONL, as both waves appeared to initiate in the expected time seen in wild type (Kay et al., 2001). *atoh7*, through its downstream target *Pou4f2*, is also involved in photoreceptor production (Boije et al., 2014). However, no change in cone photoreceptor production was observed in *atoh7* mutants, although rod production was not examined (Kay et al., 2001).

By 60 hpf, over 90% of neurons in the central retina of the zebrafish have exited the cell cycle and differentiated into the six retinal cell types, with the three distinct major neuronal layers being observable at this time (Avanesov & Malicki, 2010). *atoh7* is

downregulated in neurons at 72 hpf but remains expressed in retinoblast cells (Masai et al., 2000). Photoreceptor development continues past the 60hpf time point, with the differentiation of distinct photoreceptor types becoming apparent by 4 dpf (Branchek & Bremiller, 1984). All photoreceptor classes are morphologically distinct by 12 dpf.

As diurnal animals, the zebrafish retina contains a large number of diverse cone subtypes based on spectral sensitivity and morphology in addition to rods, which are arranged in a highly organized heterotypical photoreceptor mosaic (Fadool & Dowling, 2008; Richardson et al., 2017). The five photoreceptor classes are rods, short single cones, long single cones, and short and long double cone pairs (Avanesov & Malicki, 2010). The four cone subtypes described so far are the paired long red and short green double cones, the long single blue-sensitive cones, and short single UV-sensitive cones. These four cone subtypes provide zebrafish with colour vision similar to humans.

The high amount of conservation in morphology and developmental mechanisms in vertebrates, along with the fast generation times, high fecundity, and optic clarity of the zebrafish model, make the zebrafish retina an excellent model for understanding retinal neurogenesis, and retinal neuropathies such as glaucoma.

1.4.4 Genetic Techniques in Zebrafish

Reverse genetics or genotype-based analysis has witnessed a boom in terms of the variety, sophistication, and specificity of tools available that can be utilized in zebrafish. Morpholino oligonucleotides are used as a tool to reduce maternal and zygotic gene function and have been used to accelerate gene discovery through large-scale screens, investigating the function of candidate genes, and to confirm mutant phenotypes in

zebrafish (Bill, Petzold, Clark, Schimmenti, & Ekker, 2009). Typically composed of oligomers of 25 bases, morpholinos are targeted to the genome via complementary base pairing to the specific mRNAs of interest (Bill et al., 2009). Through injection of these anti-sense morpholino oligonucleotides, mRNAs can be knocked down in fertilized eggs through two modes of action: blocking translation or inhibition of binding to splice sites (**Figure 1.12**). Translation-blocking morpholinos bind complementary mRNA sequences within the 5' untranslated region near the start site, hindering assembly of the ribosome and blocking translation of the mRNA to its respective protein (Bill et al., 2009). Splice-site morpholinos bind and inhibit pre-mRNA processing via inhibition of the splicesome components, thus resulting in inclusion of the intron in the transcript (Bill et al., 2009). This often leads to premature stops and nonsense-mediated decay of the transcript.

In zebrafish, morpholinos are injected into the yolks of zebrafish embryos in the 1-8 cell-stage, with the cytoplasmic bridging connecting these cells allowing for ubiquitous diffusion of the hydrophilic oligonucleotides (Bill et al., 2009). Although the transient activity of morpholinos has been shown to rarely persist beyond 5 dpf, it is sufficient for the timeframe of zebrafish ocular development (Richardson et al., 2017).

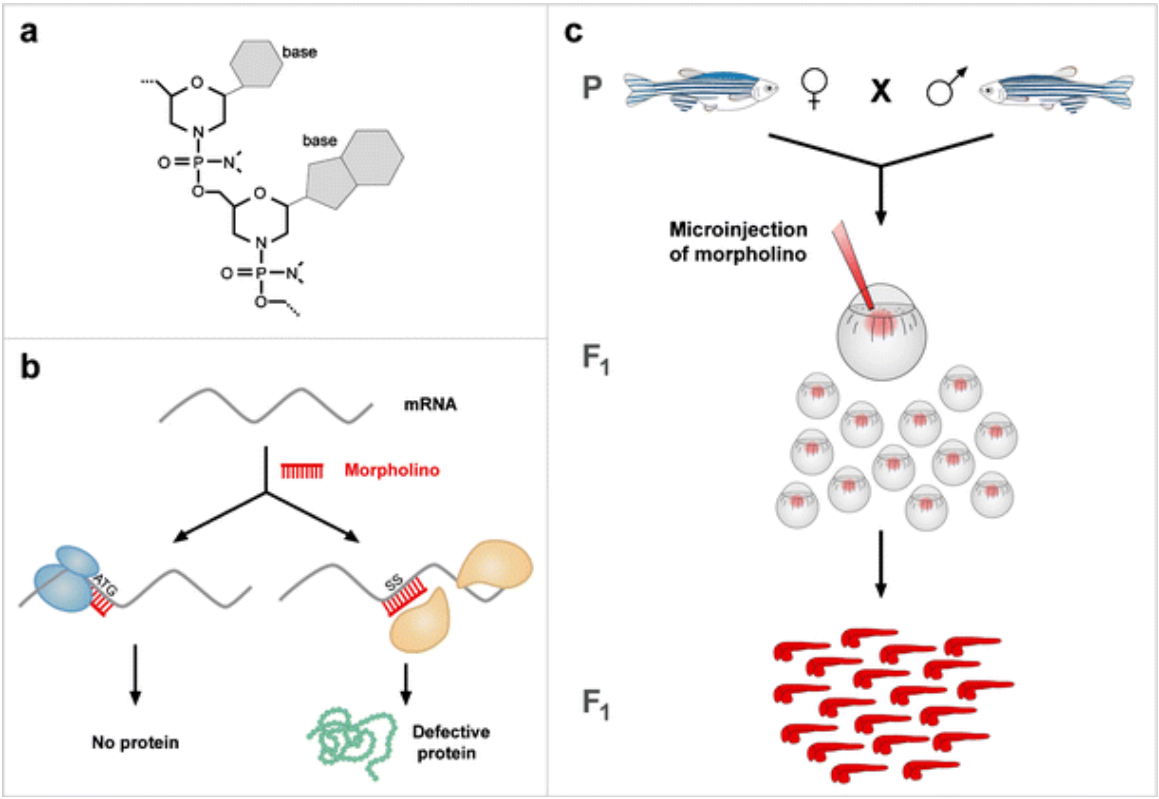

Figure 1.12 Gene knockdown by antisense morpholino oligonucleotide technology.

Morpholinos are targeted to the genome via complementary base pairing to the specific mRNAs of interest. They knock down protein function through blocking translation or inhibiting splice-site binding, resulting in inactivation of production of the protein from the mRNA transcript or the production of a defective protein, respectively. Morpholinos are typically injected in 1-8 cell-stage embryos, with morpholino effects persisting for up to 5 days. Reprinted from (Renninger, Schonthaler, Neuhauss, & Dahm, 2011) with permission from Springer Nature. Copyright © Springer-Verlag 2011.

The reliability and reproducibility of results obtained through the use of morpholinos have been under scrutiny, along with concerns about off-target effects. However, studies have also shown that provided that doses do not induce p53 expression (which cause off-target effects), and accounting for genetic compensation seen in mutants compared to morphants, morpholinos can be highly informative and reliable (Rossi et al., 2015). Furthermore, morpholinos can be used in a titratable manner to examine the effect of altering gene dosage on disease phenotypes.

There have been a variety of glaucoma studies have conducted on the zebrafish model. A mutational screen for adult ocular defects has resulted in the identification of a complex zebrafish mutant referred to as bugeye, linked to non-sense mutations in low-density lipoprotein receptor-related protein 2 (Lrp2) (Veth et al., 2011). They present with adult onset-phenotypes including myopia and elevated IOP, both of which are glaucoma risk factors. Techniques have also been developed to measure IOP in zebrafish, along with the identification of zebrafish *brass* mutants, which present with hypopigmentation, elevated IOP, and iris hypoplasia (Link, Gray, Smith, & John, 2004). The gene underlying the brass phenotype has been linked to chr. 13 (Link et al., 2004), and is yet to be identified.

Given the gap in the literature pertaining to the mechanism underlying *FOXC1*-associated glaucoma pathogenesis, the high amount of structural and biological similarity between the human eye and the zebrafish eye, and the advantages and ease that come with using the zebrafish as an animal model, we sought to investigate how mutations in *FOXC1* cause glaucomatous RGC neuropathy using the zebrafish model.

1.5 Hypothesis and Research Objectives

1.5.1 Hypotheses

FOXC1 mutations cause glaucomatous RGC loss through disruption of RGC differentiation downstream.

In addition, *FOXC1* mutations may also cause glaucomatous RGC loss through increased susceptibility of RGCs to oxidative damage.

1.5.2 Research Objectives:

Zebrafish are an ideal model for genetic ocular disorders due to the high degree of conservation of the retinal laminar structure with humans, and the conservation of genes involved in eye development such as *foxc1* and *atoh7*. Therefore, we sought to use the zebrafish as a model for *FOXC1*-associated glaucoma.

1. Map out *foxc1a* and *foxc1b* expression in wild-type zebrafish embryo.
2. Investigate the effects of the reduction of *foxc1* dosage/complete loss of *foxc1* function on the number of cells in the ganglion cell layer and optic nerve width in the zebrafish embryonic eye compared to a control.
3. Examine the effects of *foxc1* loss of function on the expression of genes involved in RGC differentiation and early eye development.
4. Examine the effects of *foxc1* loss of function on the expression of genes involved in the oxidative stress response.
5. Investigate whether *foxc1a* expression is upregulated when *foxc1b* function is lost in the zebrafish embryo

2 Materials and Methods

2.1 Zebrafish care and husbandry

All zebrafish strains used were reared under standard conditions – water temperature of 28˚C, pH 7.2-8.0, water conductivity of 600-750 µS, and a 14h:10h light-dark cycle (Kimmel, Ballard, Kimmel, Ullmann, & Schilling, 1995). Fish were fed with dry feed (Lot No.: 7145357; Skretting France, Le Pont de Pierre, Fontaine-lès-Vervins, France) in the mornings and live brine shrimp (Lot No.: 071332) Brine Shrimp Direct, Ogden, UT, USA) in the afternoons. All experiments were performed in compliance with the standards set by Memorial University of Newfoundland Animal Care facility and by the Canadian Council on Animal Care. The strains of zebrafish used in this thesis were the AB strain (Bermann Lab, Dalhousie Zebrafish Core Facility) and the *foxc1b*^{ua1018} strain (Lehmann lab, University of Alberta).

Individual zebrafish obtained from a heterozygous outcross with a *foxc1b* 40 base-pair deletion were exposed to a 4.2% ethyl-3-aminobenzoate methanosulfate anesthetic (Ref #: E10521-10G; Sigma-Aldrich, St. Louis, MO, USA) (Umali et al., 2019). Once equilibrium was lost (as displayed by the fish's inability to swim upright) and gill beats slowed down, small clippings of the fish's caudal fins were obtained and placed in individual labelled 0.2 mL tubes, with each respective fish undergoing recovery separately, and isolated in individually-labelled tanks.

2.2 Genotyping

DNA was isolated from each fin clipping by incubating each sample in 50ul of 50mM sodium hydroxide (NaOH; Cat. #: S-3700; ACP Chemicals Inc., Montreal, QC) at 95˚C

for 20 min., after which 5 µl of 1M Tris(hydroxymethyl)aminomethane Hydrochloride (Tris-HCl) (pH 8.0; see Appendix D) was added.

Isolated DNA from each fin clipping was then amplified by Polymerase Chain Reaction (PCR) using the outlined primers (**Table 2.1**). For each PCR reaction, 2.5 µL of DNA template isolated from each fin clip was added to 22.5 µL of a prepared master mix. This master mix was pre-mixed with 2.5 µl of 10X ThermoPol® Reaction Buffer (Cat. #.: B9004S, New England Biolabs, Ipswitch, MA, USA) , 1 µl of deoxynucleoside triphosphate (dNTP; Lot No.:081, FroggaBio, Toronto, Canada), 1 µl of a 1/20 dilution of the forward primer, 1 µl of a 1/20 dilution of the reverse primer, 16.25 µl of nuclease-free water, 0.25 µl of Magnesium chloride ($MgCl_2$, Cat. #: B9021S, New England Biolabs, Ipswitch, MA, USA) and 0.5 µl of Taq (Lot No.: 050, FroggaBio, Toronto, Canada) for each PCR reaction. The PCR program temperatures cycles are outlined in **Table 2.2.**

Table 2.1 *foxc1b* Forward and Reverse primers used for genotyping via PCR amplification

Gene Primer	Sequence	Tm	Size (bases)
foxc1b Forward Primer (Integrated DNA Technologies, Coralville, Iowa, USA)	5'-GTTGGATGACCGTTTTGAGACA-3'	55.5˚C	22
foxc1b Reverse Primer (Integrated DNA Technologies, Coralville, Iowa, USA)	5'-CATCTCTTGGCACCTTCACAAAG-3'	56.3˚C	23

Table 2.2 PCR program cycle for genotyping foxc1b homozygotes and heterozygotes

Procedure	Temperature	Time	
Initialization	94°C	2 min.	
Denaturation	94°C	20 sec.	40x
Annealing	54.5°C	30 sec.	
Extension	72°C	40 sec	
Final elongation	72°C	5 min.	

PCR products were run on a 1.8% gel made from agarose (Cat. #: A87-500G; FroggaBio, Toronto, Canada) 1X TAE Buffer (see Appendix D), and RedSafe™ (Cat. #: O008-090401.51; Intron BioTechnology) to visualize bands that correspond to either wild type or heterozygous fish (See Appendix C). Bands were compared to a 1 Kb DNA Ladder (Cat. # DM010-R500F; FroggaBio, Toronto, Canada). Identified *foxc1b* heterozygotes were then bred incross to produce embryos to be used in *in situ* hybridization and RGC quantification studies.

2.3 Embryo Collection

Embryos bred from *foxc1b* heterozygote incross were raised on embryo media (see Appendix D), with embryos to be used for *in situ* hybridizations treated with 0.003% 1-phenyl 2-thiourea (PTU; Ref. #: P7629-10G; Sigma-Aldrich, St. Louis, MO) to prevent endogenous pigment formation.

Embryos were staged at various time points as needed by fixing in 4% paraformaldehyde (PFA; Cat. #: 158127-500G; Sigma-Aldrich, St. Louis, MO, USA) in Phosphate Buffered Saline with 20% Tween-20 (PBST; see Appendix D) either for 3 hours at room temperature or overnight at 4˚C (**Table 2.3**).

Table 2.3 Embryo collection time points for in situ hybridization studies

Gene	Time points (hpf)
foxc1a	24, 48
foxc1b	24, 48
atoh7	32, 48
fibroblast growth factor 19 (*fgf19*)	24
platelet-derived growth factor receptor alpha (*pdgfrα*)	24, 48
platelet-derived growth factor receptor beta (*pdgfrβ*)	24, 48
heat shock 70 kDa protein 5 (*hspa5*)	32
heat shock 70 kDa protein 9 (*hspa9*)	32
foxo1a	48
foxo1b	48

Embryos were washed five times in PBST. Following examination and photography of expression patterns revealed by *in situ* hybridizations, DNA from these embryos were isolated and amplified using PCR with the same method used to genotype fin clips. PCR products were run on a 2% agarose gel. Genotyping was performed after expression patterns were examined as a tool to blind the observer to the embryos' genotype, to minimize bias.

Embryos from *foxc1b* heterozygote incross breedings were also injected with *foxc1a* morpholino oligonucleotides to knock down *foxc1a* function and were raised and staged in a similar manner.

A portion of embryos was grown to adulthood for genotyping via the described fin clipping method. *foxc1b* homozygotes and wild-type fish were then separated and bred incross to produce *foxc1b-/-* and wild type embryos for *in situ* hybridizations and RGC quantification experiments.

2.4 Morpholino injections

Injection of translation-blocking morpholinos for *foxc1a* was performed to knock down *foxc1a* function in both *foxc1b* homozygous mutants and wild-type embryos at the one-cell stage. Capillary needles used for microinjection were pulled using a Sutter P-97 Micropipette Puller (Sutter Instrument Co.). Needles were pulled with the following settings: Heat=650, Pull = 150, Velocity = 75, Time = 150. Injections were done using the microINJECTOR™ Analog Pressure Injector (Tritech Research Inc., Los Angeles, CA, U.S.A).

Negative control morpholinos have no specific target in the zebrafish genome, while *p53* morpholinos show no overt phenotype in early embryos (Robu et al., 2007). Therefore, for control conditions, *foxc1b-/-* and wild type embryos from the same cohort/sibling group were injected with a negative control morpholino or morpholinos against p53 (**Table 2.4**). Embryos were raised on embryo media, with embryos to be used for *in situ* hybridizations treated with 0.003% PTU (Lot. No.: BCBR8967V; Sigma-Aldrich, St. Louis, MO, USA) to prevent pigment formation. This ensures clear visualization of gene expression patterns revealed by *in situ* hybridization.

Table 2.4 Morpholino oligonucleotides used for RGC quantification studies and in situ hybridization studies

Name	Oligo Sequence	Molecular Weight (Da)	Delivered concentration (ng/µl)
foxc1a ((Skarie & Link, 2009); Gene Tools, LLC. Philomath, OR, USA)	5'-CCTGCATGACTGCTCTCCAAAACGG-3'	8,389	1.6
Negative Control (Gene Tools, LLC. Philomath, OR, USA)	5'-CCTCTTACCTCAGTTACAATTTATA-3'	8,328	1.5
Zebrafish *p53* (Gene Tools, LLC. Philomath, OR, USA)	5'-GCGCCATTGCTTTGCAAGAATTG-3'	7,805	1.5

2.5 Whole-mount *in situ* hybridizations

2.5.1 Antisense probe synthesis

Complementary Deoxyribonucleic Acid (cDNA) synthesis

Anti-sense probe synthesis and *in situ* hybridization methods have been previously described (Thisse & Thisse, 2014), and was followed with a few modifications. The protocol with the modifications is described below.

cDNA fragments for anti-sense probe synthesis were obtained through two different methods. For the *atoh7* cDNA template, linearization of *atoh7* DNA was performed from circular pCR4-TOPO plasmids (Lot. #: 1809825; Invitrogen, ThermoFisher Scientific, Waltham, MA, USA) using the *Not1* restriction enzyme (Cat. #: RO189S; New England Biolabs, Ipswitch, MA, USA), with the presence of the linear DNA product confirmed by running the linear DNA alongside a sample of the original circular plasmid DNA on an 0.8% gel made from agarose (Cat. #: A87-500G; FroggaBio, Toronto, Canada), 1X TAE Buffer (see Appendix D) and RedSafe™ (Cat. #: O008-090401.51; Intron BioTechnology). Linearized *atoh7* cDNA was then stored at -20C until ready for probe synthesis.

For the other probes used in this thesis, 72hpf *foxc1b* +/- outcross mutant embryos were lysed in 500 µl of Trireagent® (Product #: T9424; Sigma, St. Louis, MO, USA) with about 50 embryos per tube. Each tube was then vortexed until embryos were dissociated, followed addition of another 500 µl of Trireagent®. Samples were then incubated for 5 minutes at room temperature, after which 200 µl of chloroform (Ref. #: C-3300; ACP Chemicals Inc., Montreal, QC) was added. Samples were shaken for 15 seconds,

incubated at room temperature for 5 minutes, and then spun for 15 minutes at 4°C. The upper aqueous phase of the reaction was removed and placed into a separate microcentrifuge tube. An addition of isopropanol to the aqueous phase in a 1:1 ratio was performed, and mixed by gently pipetting, followed by incubation at room temperature for a minimum of 10 minutes. The samples were then spun at 4°C for 15 minutes, after which the supernatant was removed. The pellet was then washed with 500 µl of 75% ethanol, spun for 5 minutes at 4°C, and air dried. Pellets were then re-suspended with 40 µl of RNAse-free water. The final products were then distributed in 2 aliquots: 35 µl for downstream work and 5 µl for testing for RNA concentration and integrity. RNA concentrations and purity were measured using nanodrop spectrophotometry (Nanodrop 1000 Sectrophotometer, ThermoFisher Scientific, Waltham, MA, USA). The nanodrop spectrophotometer was calibrated with 1.5 µL of sterile water prior to measuring the concentration of isolated RNA. Concentrations within the range of 50-250 ng/µL were the acceptable standard for quantity, while the standard used to assess the purity of the RNA sample was the ratio of absorbance at 260 nm and 280 nm (260/280), which should be between 1.7-2.2. Isolated RNA samples were stored at -80˚C.

The RNA isolated from *foxc1b* +/- outcross mutant embryos were used as template RNA to synthesize cDNA, which would then be used as a template for anti-sense mRNA probe synthesis. Reverse Transcription Polymerase Chain reaction (RT-PCR) was performed using the One-Step RT-PCR kit (Lot. #: 2010000; Invitrogen, ThermoFisher Scientific, Waltham, MA, USA) using the primers outlined in **Table 2.5**. Following the One-Step RT-PCR kit protocol, 1/20 dilutions of each primer were prepared from the 100 µM

primer stocks. In 0.2 mL nuclease-free PCR tubes, 2.5 µL of template RNA was added to 12.5 µL of 2X Reaction Mix (One-Step RT-PCR kit [Lot. #: 2010000; Invitrogen, ThermoFisher Scientific, Waltham, MA, USA]), 1 µL of sense primer, 1 µL of anti-sense primer, 7 µL autoclaved distilled water, and 1 µL of Taq SuperScript III (One-Step RT-PCR kit [Cat. #: 12574-018; Invitrogen, ThermoFisher Scientific, Waltham, MA, USA]), for a total of 25 µL. The tubes were then incubated in a thermocycler at 55°C for 30 minutes, 94°C for 2 minutes, [94°C for 15 seconds, 54.5°C for 30 seconds, and 60°C for 1 minute and 15 seconds] x 40, and 68°Cfor 5 minutes.

Table 2.5 Primer sequences for PCR-based antisense RNA Probes

Primer	Sequence	Tm	PCR Product Size (bases)
foxc1a Forward primer	5'-GTTTTGGAGAGCAGTCATGCAG-3'	56.6	1032
foxc1a Reverse primer	5'-TAATACGACTCACTATAGGGGCGTTGGAGGTAGTCGAGATAG-3'	64.9	
foxc1b Forward primer	5'-TGAAGCAAAGGGAGGAAGAGAC-3'	56.7	1139
foxc1b Reverse Primer	5'-TAATACGACTCACTATAGGGATAGAGGAGGCGTTTGTTGTGT-3'	64.4	
foxo1a Forward primer	5'-TAGTAGGTTCATCCGAGTGCAG-3'	56.0	1068
foxo1a Reverse primer	5'-TAATACGACTCACTATAGGGGGAGATTTACCACTTCCCAGGC-3'	65.5	
foxo1b Forward primer	5'-ACTAGAAGAGACCGAGGACTACC-3'	56.8	1056

foxo1b Reverse primer	5'-TAATACGACTCACTATAGGGGGATTTAGTCCACCCACTCCAC-3'	65.4	
pdgfrα Forward Primer	5'-ATCATCCTCCCTCTCACAGACA-3'	57.1	1179
pdgfrα Reverse Primer	5'-TAATACGACTCACTATAGGGTAGAGTCCTGCTCATTCCTCCA-3'	64.7	
pdgfrβ Forward Primer	5'-AGCCAGCATCAACATCAGTGTA-3'	56.5	1058
pdgfrβ Reverse primer	5'-TAATACGACTCACTATAGGGTGTTGATGTGAGGACCCAGATG-3'	64.5	
hspa5 Forward primer	5'-TGTTTGCCGAAGAGGACGATAA-3'	56.4	1070
hspa5 Reverse primer	5'-TAATACGACTCACTATAGGGCTGGATCTTCGGGATACGAGTG-3'	65.1	
hspa9 Forward primer	5'-ATATGTTGTCTGTGTCGAGAACGG-3'	56.8	929

hspa9 Reverse primer	5'-TAATACGACTCACTATAGGGCTGCAGTGCCATGTTGTCTTTC-3'	65.4	
fgf19 Forward primer	5'-CACTGTTTGTGGAAGTATCGGC-3'	65.2	699
fgf19 Reverse primer	5'-TAATACGACTCACTATAGGGATCGTGGCAGGACTGATTTTCT-3'	64.4	

The presence of synthesized cDNA sequences was confirmed by running RT-PCR products on a 0.8% gel made from agarose ((Cat. #: A87-500G; FroggaBio, Toronto, Canada) and 1X TAE Buffer (see Appendix D), with each cDNA fragment being extracted via gel purification. The DNA fragment was excised from the gel using a scalpel and transferred into a 1.5 mL microcentrifuge tube.

Gel purification was done using the Zymoclean™ Gel DNA Recovery Kit (Cat. #: D4007; Zymo Research, Irvine, CA, U.S.A). A buffer was prepared by adding 24 mL of 100% ethanol to the 6 mL of DNA Wash Buffer concentrate provided in the kit. Add 96 mL 100% ethanol to the 24 mL DNA Wash Buffer concentrate. These buffers were then centrifuged at 10,000 x g. 3 volumes of agarose dissolving buffer provided in the kit were added to the excised DNA from the gel in their respective tubes. These were then incubated at 55°C for 10 minutes until the gel slice is completely dissolved. The melted agarose solution was transferred to the Zymo-Spin™ column in a collection tube, and the tubes were then centrifuged for 30-60 seconds, and the flow-through was discarded. 200 µL of DNA Wash Buffer to the column and centrifuged for 30 seconds. Discard the flow-through and repeat the wash step. Add 12 µL of water directly to the column matrix, after which the column was placed into a 1.5 mL tube and centrifuged for 30-60 seconds to elute DNA. DNA concentration and purity were measured using nanodrop spectrophotometry.

PCR of cDNA fragments was performed to increase purity and concentration as necessary. This was done by combining 1 µl of cDNA, 2 µl of each gene's respective forward primer, 2 µl of each gene's respective reverse primer, and 45 µl of a prepared

master mix. For each reaction, pre-mix 5 µl of 10X ThermoPol® Reaction Buffer [Cat. #.: B9004S, New England Biolabs, Ipswitch, MA, USA], 2 µl of dNTP [Lot No.:081, FroggaBio, Toronto, Canada], 24 µl of 20% glycerol, 2.5 µl formamide, 10.5 µl of nuclease-free water, and 1 µl of Taq [Lot No.: 050, FroggaBio, Toronto, Canada]). The PCR program was: 94°C for 5 mins., 40 x [94°C for 30 sec., 56°C for 30 sec., 72°C for 70 sec.], and 72°C for 5 min.

PCR Cleanup was performed as necessary using the GenepHlow PCR Cleanup Kit (Cat. # : DFC100; Geneaid, New Taipei City, Taiwan). Following the protocol, absolute ethanol was added to the wash buffer at the beginning of the procedure. Sample preparation involved adding 1 mL of the kit's PB Buffer and 4 µl pH indicator to a new 1.5 mL microcentrifuge tube, and shaking the tube gently to mix the solutions until the solution turns yellow. The PCR products were then added to separate, individually labelled 1.5 mL microcentrifuge tubes. The volume of the PCR products were multiplied by five, and this amount was the volume of pH/PB Buffer solution that was added to each PCR Product. In the event that the solutions turned purple, 10 µl of 3 M sodium acetate (provided in the kit) was added to the tubes.

For the DNA Binding phase of the PCR cleanup, each mixture was transferred to separate 2 mL DFH Column/collection tubes (provided in the kit), and centrifuged at 16,000g for 30 seconds. The flow-through was discarded, after which 600 µl of wash buffer was added to the column. The mixtures were incubated at room temperature for 1 minute, and were then centrifuged at 16,000g for 30 seconds. Flow-through was discarded, and columns were once again centrifuged at 16,000 g for 3 minutes. For the elution phase, the

dried DFH columns were transferred to new 1.5 mL microcentrifuge tubes. 40 µl of elution buffer (provided in the kit) were pipetted in the center of the column matrix, and the columns were incubated at room temperature for 2 minutes. The columns were centrifuged at 16, 000g for 2 minutes, and the eluted DNA product was stored at -20˚C.

Probe synthesis

Anti-sense probes werethen synthesized using either a T3 (Ref. #: M0378S; RNAP; New England Biolabs, Ipswitch, MA, USA) or T7 ribonucleic acid polymerase (Ref. #: M0251S; New England Biolabs, Ipswitch, MA, USA), with the following components mixed into sterile microcentrifuge tubes (**Table 2.6** and **Table 2.7**).

Table 2.6 Reagents used to synthesize PCR-based antisense RNA probes

Reagent	Volume per reaction
Template DNA	10 µl (2 µg)
RNA Polymerase Reaction Buffer (10X) (Ref. #: B9012S; New England Biolabs, Ipswitch, MA, USA)	2 µl
DIG RNA Labeling Mix (10X) (Ref. #: 11277073910; Roche, Mannheim, Germany)	2 µl
T7 RNAP (Lot. #: 10054654; New England Biolabs, Ipswitch, MA, USA)	1 µl
RNAse Out (Ref. #: 10777-019; Invitrogen, ThermoFisher Scientific, Waltham, MA, USA)	1 µl
DEPC Water (See Appendix D)	4 µl
Total volume per reaction	20 µl

Table 2.7 Reagents used to synthesize vector-based antisense RNA probes

Reagent	Volume per reaction
Linearized template DNA	5 µl (2 µg)
RNA Polymerase Reaction Buffer (10X) (Ref. #: B9012S; New England Biolabs, Ipswitch, MA, USA)	2 µl
DIG RNA Labeling Mix (10X) (Ref. #: 11277073910; Roche, Mannheim, Germany)	2 µl
T3 RNAP (Ref. #: M0378S; New England Biolabs, Ipswitch, MA, USA)	1 µl
RNAse Out (Ref. #: 10777-019; Invitrogen, ThermoFisher Scientific, Waltham, MA, USA)	1 µl
DEPC Water (see Appendix D)	9 µl
Total volume per reaction	20 µl

The reactions were incubated for 1 hour at 37˚C, after which 1 µl RNAP was added to each reaction, followed by re-incubation for 1 hour at 37C. An incubation period of 5 minutes at 37˚C was done after the addition of 1 µl Turbo DNAse (Cat. #: AM2238; Invitrogen, ThermoFisher Scientific, Waltham, MA, USA) was for digestion and removal of the DNA template. The transcription reaction was stopped by adding 2 µl of 0.25M ethylenediaminetetraacetic acid (EDTA) pH 8.0 (see Appendix D).

Sigma post-reaction purification columns (Cat. #: S5059-70EA; Sigma-Aldrich, St. Louis, MO, USA; Lot #: SLBW6340) were used as previously described (Thisse & Thisse, 2014) to purify the transcribed RNA. Each column was spun in a collection tube for 15 seconds at 750g, followed by breaking the base of the column and loosening of the lid prior to another spin for 2 minutes at 750g. Each column was placed in a new collection tube. Each RNA sample was then pipetted into separate columns, and were spun for 4 minutes at 750g. 2 µl of 0.25M EDTA pH 8.0, 2 µl of RNase Out (Ref. #: 10777-019; Invitrogen, ThermoFisher Scientific, Waltham, MA, USA), 15 µl of DEPC water, and 10 µl of RNAlater (Ref. #: R0901; Sigma-Aldrich, St. Louis, MO, USA) were added to the final product in the collection tube. Probes were stored at -80˚C, with the synthesis of the probe being confirmed by visualization of 4 µl of the aliquoted probe on a 1% agarose gel (See Appendix B).

2.5.2 Embryo permeabilization and Hybridization

Thisse and Thisse's protocol was adopted with a few modifications as described below (Thisse & Thisse, 2014). Permeabilization of embryos was performed by treatment with Proteinase K (10µg/ml; Sigma-Aldrich, St. Louis, MO, USA) at room temperature. The

permeabilization times of embryos at various time points were as follows: 5 minutes for 24 hpf, 15 minutes for 32 hpf, and 25 minutes for 48 hpf.

Embryos were re-fixed in 4% PFA for 20 minutes, and were washed 5 x 5 minutes in PBST, followed by prehybridization in 500 µl of hybridization solution **(**see Appendix D) for at least 1 hour at 65˚C. Embryos were distributed among separate, individually-labelled tubes for each gene being assessed. Each RNA probe was diluted in hybridization solution to produce a 1/200 probe dilution and then added to their respective tubes of embryos for incubation at 65˚C for 48 hours.

2.5.3 Washes and Incubation with the Alkaline Phosphatase Anti-DIG Antibody

Embryos underwent a succession of 5-minute washes in pre-warmed 66% hybridization solution / 33% 2X saline sodium citrate (SSC; see Appendix D), 33% hybridization solution / 66% 2X SSC, and 2X SSC at 65˚C. This was followed by one 20-minute wash in 0.2X SSC + 0.1% Tween-20, and two 20-minute washes in 0.1X SSC + 0.1% Tween-20, all of which were done at 65˚C. The embryos were then washed at room temperature for 5 minutes each in 66% 0.2X SSC/33% PBST, followed by 33% 0.2X SSC/66% PBST, and PBST.

Embryos were incubated in blocking solution (PBST [see appendix D], 2% Sheep serum [Ref. #: S3772; Sigma-Aldrich, St. Louis, MO, USA], 2 mg/mL bovine serum albumin [Ref. #: A2153-50G; Sigma-Aldrich, St. Louis, MO, USA]) on a horizontal shaker for at least 1 hour at room temperature. The blocking solution was replaced, and embryos were incubated in a 1/5000 dilution of anti-digoxigenin-alkaline phosphatase antibody (Ref. #: 11093274910; Roche, Mannheim, Germany) in blocking solution overnight at 4˚C.

After a 5 x 15-minute wash in PBST, colouration reactions were done using a solution of 45 µl of 4-Nitro blue tetrazolium chloride (Ref. #: 11383213001;NBT; Roche, Mannheim, Germany) and 5-Bromo-4-chloro-3-indolyl-phosphate (Ref. #: 11383221001; BCIP; Roche, Mannheim, Germany) in Colouration Buffer (see Appendix D). Colouration was stopped by washing the embryos two to five times in stop solution (see Appendix D) and were then immersed in the stop solution for two, 15-minute periods at room temperature after which embryos were stored in PBST. Embryos were then viewed using a Nikon SMZ18 stereomicroscope and were photographed using a Nikon DS-Ri2 camera**.**

2.6 Eye Sections:

Wild-type and *foxc1b-/-* embryos born from *foxc1b+/-* incross were grown to 5 dpf, then fixed in 4% PFA on a horizontal shaker either for 3 hours at room temperature or overnight at 4˚C. Fixed embryos were washed in 3 x 5-minute PBST washes, and embryo heads were severed from their respective tails, with the latter being used for genotyping. Embryos obtained from wild-type and *foxc1b-/-* homozygous crosses were injected with either a *foxc1a* morpholino or a negative control and were similarly fixed in 4% PFA, followed by embedding for sectioning as outlined below. Photographs of all sections, both cryosection and resin, were blinded prior to performing counts. Genotypes were cross-indexed with photographs of each section after counts were completed.

2.6.1 Cryosections

Embryo heads were embedded as per Uribe and Gross's previously described protocol (Uribe & Gross, 2007). Embryo heads were soaked in a 25% sucrose (dissolved in 1X

PBST) solution at room temperature until the embryos were saturated and sank to the bottom of the tube. This was followed by a 35% sucrose solution soak at room temperature until the specimens sank to the bottom of the tube. Embryos were soaked in a solution of 50% (35% sucrose)/ 50% Tissue-Tek Optimal Cutting Temperature (Ref. #: 4583; OCT; Sakura Finetek, Torrance, CA, USA) compound for 5 minutes and were transferred to a solution of pure OCT to soak for 5 minutes. The specimens were then transferred into an OCT-filled cryomold (Cat. #: 62534-10; Sakura Finetek, Torrance, CA, USA) and were submerged and positioned to line up with their heads against the wall of the mold. Specimens were then frozen at -80˚C.

A cryostat was used to cut 14um thick sections, which were adhered to charged slides Millenia 2.0™ Adhesion Slides, Cat. #: 318; StatLab, McKinney, TX, USA) on a heating plate set to 37˚C. Slides were then stained by Memorial University of Newfoundland's Histology department with a haematoxylin and eosin general structure stain to visualize retinal layers. The methods of Mayer's Haematoxylin and Eosin General Structure Stain were followed with modifications. Slides were immersed in Mayer's haematoxylin (Surgipath, Leica Biosystems, Wetzlar, Germany) for 5 minutes, rinsed with water, and placed in Scotts Tap Water Substitute (Histology Department, Faculty of Medicine, Memorial University of Newfoundland, St. John's, NL) for 3 minutes until sections turn blue. Sections were then rinsed in water for 5 minutes, followed by staining in eosin for 15 seconds. This was followed by dehydration by dipping the slides 10-15 times in 95% alcohol, followed by 10-15 dips in absolute alcohol.

2.6.2 Resin Sections

Resin sections were prepared by Memorial University of Newfoundland's Histology department. Fixed embryos were dehydrated through a series of ethanol washes, followed by a wash in 50% Ethanol/50% Methacrylate, and finally polymerized in Methacrylate for at least 12 hours. Using a Leica RM2165 automated microtome, 3 μm sections were cut and were processed for staining.

Resin sections were stained with a Celestine-Blue (Matheson Coleman & Bell Manufacturing Chemists, Norwood, OH, USA) and Eosin-Phloxine (Surgipath, Leica Biosystems, Wetzlar, Germany; GURR's, George T. Gurr Ltd.) Stain. Sections were then viewed using Zeiss AxioImager Z1 Compound microscope and were photographed using a Carl Zeiss AxioCam Mrm camera.

2.7 RGC and Optic Nerve Quantifications and Statistical Analysis

For the cryosections, RGC quantification and optic nerve measurements were obtained using ImageJ software (Schneider, Rasband, & Eliceiri, 2012). RGC counts were performed within the central retina. This area was defined and standardized by drawing two lines tangential to the lens. The optic nerve width was measured at the point where the inner plexiform and photoreceptor layers meet.

Means and standard errors for RGC counts were obtained for 5-day old wild type embryos injected with a control morpholino (N=29), wild type embryos injected with a *foxc1a* morpholino (N=28), *foxc1b-/-* embryos injected with control morpholino (N=16), and *foxc1b-/-* embryos injected with a *foxc1a* morpholino (N=29).

Means and standard errors for optic nerve width measurements were obtained for 5-day old wild type embryos injected with a control morpholino (N=6), wild type embryos injected with a *foxc1a* morpholino (N=5), *foxc1b-/-* embryos injected with control morpholino (N=5), and *foxc1b-/-* embryos injected with a *foxc1a* morpholino (N=12).

For the resin sections, ganglion cell quantification was performed by counting ganglion cells spanning the whole RGC layer of one section from each eye for 5-day old wild type embryos injected with a control morpholino (N=13), wild type embryos injected with a *foxc1a* morpholino (N=8), *foxc1b-/-* embryos injected with control morpholino (N=12), and *foxc1b-/-* embryos injected with a *foxc1a* morpholino (N=14).

A similar point of measurement for optic nerve width was used when quantifying the optic nerve in the resin sections, located at the point where inner plexiform and photoreceptor layers meet for 5-day old wild type embryos injected with a control morpholino (N=8), wild type embryos injected with a *foxc1a* morpholino (N=5), *foxc1b-/-* embryos injected with control morpholino (N=5), and *foxc1b-/-* embryos injected with a *foxc1a* morpholino (N=8).

All statistical analyses were performed using GraphPad Prism version 5.0b for MAC OS (GraphPad Software, San Diego, California, USA, www.graphpad.com). Significance testing was done by performing a one-way ANOVA with a post-hoc Tukey test, with the assigned level of significance set at $p < 0.05$.

3 Results

3.1 *foxc1a* and *foxc1b* are expressed in the cells of the periocular mesenchyme and neural crest

Using the zebrafish to understand *FOXC1*-associated glaucoma, we sought to map out the expression patterns of *foxc1a* and *foxc1b* in the wild-type zebrafish embryo. At 24 hpf, *foxc1a* and *foxc1b* expression overlap in the periocular mesenchyme and neural crest cells. Although *foxc1b* expression is concentrated in the posterior domain of the periocular mesenchyme, it is also present in a small number of cells in the eye (**Figure 3.1**) (Umali et al., 2019). At 48 hpf, both *foxc1a* and *foxc1b* are expressed in the pharyngeal arches, with *foxc1a* being expressed in the front-most pharyngeal arches, and *foxc1b* expression being confined to the more dorsal pharyngeal arches.

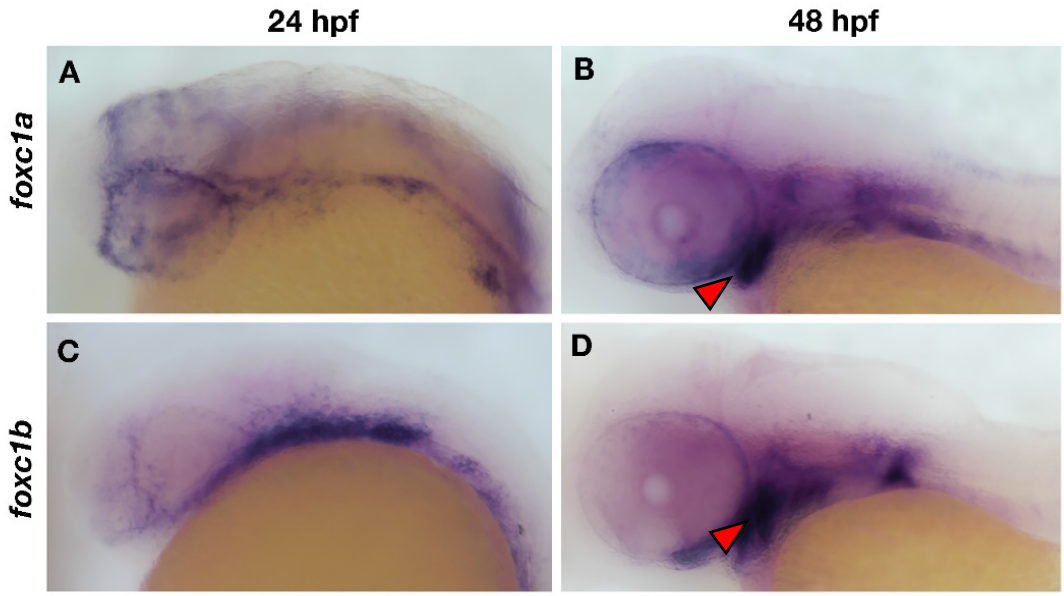

Figure 3.1 Expression of the zebrafish *FOXC1* paralogs, *foxc1a* and *foxc1b*.

foxc1a and *foxc1b* expression overlap in the neural crest and periocular mesenchyme at 24 hpf. By 48 hpf, both genes are expressed in the pharyngeal arches (as indicated by arrows) (Umali et al., 2019).

3.2 Loss of *foxc1b* alone does not result in significant RGC loss or optic nerve thinning in embryos borne from a heterozygous incross

To investigate the effects of the reduction of *foxc1* dosage on RGC number and optic nerve size, a comparison of RGC numbers and optic nerve measurements between *foxc1b*$^{-/-}$ and *foxc1b*$^{+/+}$ siblings from a *foxc1b* heterozygous incross were performed. No significant differences in RGC number nor optic nerve width were observed at 5- and 7-dpf (**Figure 3.2**).

3.3 Zebrafish loss of *foxc1* function models present with significant RGC loss and thinning of the optic nerve

Given the lack of significant findings in *foxc1b*$^{-/-}$ mutants, we suspected that loss of *foxc1b* alone is insufficient to result in significant RGC loss. We proceeded to produce loss of *foxc1* function models by injecting *foxc1a* morpholino into *foxc1b*$^{-/-}$ embryos. *foxc1b* homozygous mutants borne from a *foxc1b*$^{-/-}$ homozygous incross are viable and were produced in line with Mendelian ratios. RGCs were then quantified in a standardized area in the central retina, which was defined by drawing two lines tangential to the lens.

At 5dpf, no significant effect was seen in the RGC numbers of *foxc1a* morphants compared to their wild type siblings in cryosections (**Figure 3.3**). *foxc1b* mutants injected with a control morpholino presented with a significant loss of RGCs in the region directly tangential to the lens compared to their wild type siblings in sections obtained by cryosectioning. In addition, a pronounced reduction in the number of RGCs was

quantified in *foxc1b* mutants injected with a *foxc1a* morpholino in sections obtained by cryosectioning (**Figure 3.3**).

Given that we have confirmed an RGC loss phenotype in loss of *foxc1* function cryosectioned embryos, we proceeded to investigate whether a similar phenotype would be observed in finer sections of embryonic eyes embedded in resin (**Figure 3.5**). In terms of RGC number, no significant effect was seen in *foxc1a* morphants compared to their wild type siblings in resin sections. Though *foxc1b* mutants injected with a control morpholino presented with a significant loss of RGCs in the central retina in the cryosections, this effect was not seen in their resin section counterparts. Similar to the cryosectioned embryos, a significant decrease in RGCs was also quantified in resin sections of 5 dpf *foxc1b* mutants injected with *foxc1a* morpholino. Therefore, a significant reduction in RGCs is only observed in these embryos when total *foxc1* function is lost.

In humans, glaucoma diagnosis is based on the degeneration of the optic nerve head as indicated by an increasing optic cup-to disc ratio (Quigley, 2011). We sought to investigate whether a reduction in optic nerve size occurs in the zebrafish loss of *foxc1* model. Our data shows that knockdown of *foxc1a* via injection of morpholinos into a *foxc1b* mutant background resulted in a significant reduction in the width of the optic nerve in both cryosections and resin sections (Umali et al., 2019) **(Figure 3.4 and 3.6)**. Though *foxc1a* morphants presented with a significant reduction in optic nerve width in the cryosections, this effect was not seen in their resin section counterparts. No significant differences in optic nerve size were seen between wild type embryos and *foxc1b* mutants injected with a control morpholino regardless of sectioning method.

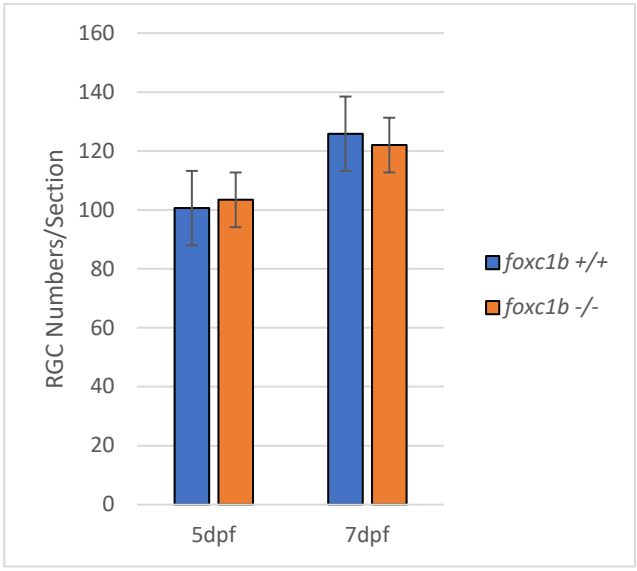

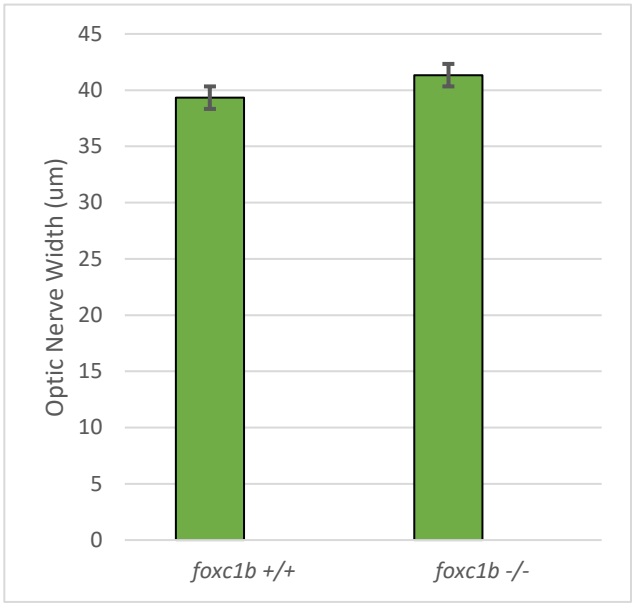

Figure 3.2 Loss of *foxc1b* alone does not result in any changes in the number of cells in the ganglion cell layer nor optic nerve width.

No significant differences in the number of cells in the RGC layer are observed in *foxc1b*-/- embryos bred from a heterozygous in-cross (N=7) compared to *foxc1b*+/+ embryos(N=8) at 5 dpf (p=0.80) (top). No significant difference is also seen in cell

numbers in *foxc1b*-/- embryos (N=3) compared to *foxc1b*+/+ embryos (N=7) at 7 dpf (p=0.86) (top). No significant alterations in the width of the optic nerve were also seen in a small number of 5 dpf foxc1b-/- embryos (N=3) compared to their wildtype counterparts (N=3) (bottom). Significance testing was done by performing a student's T-test. Data are presented as mean ±SEM.

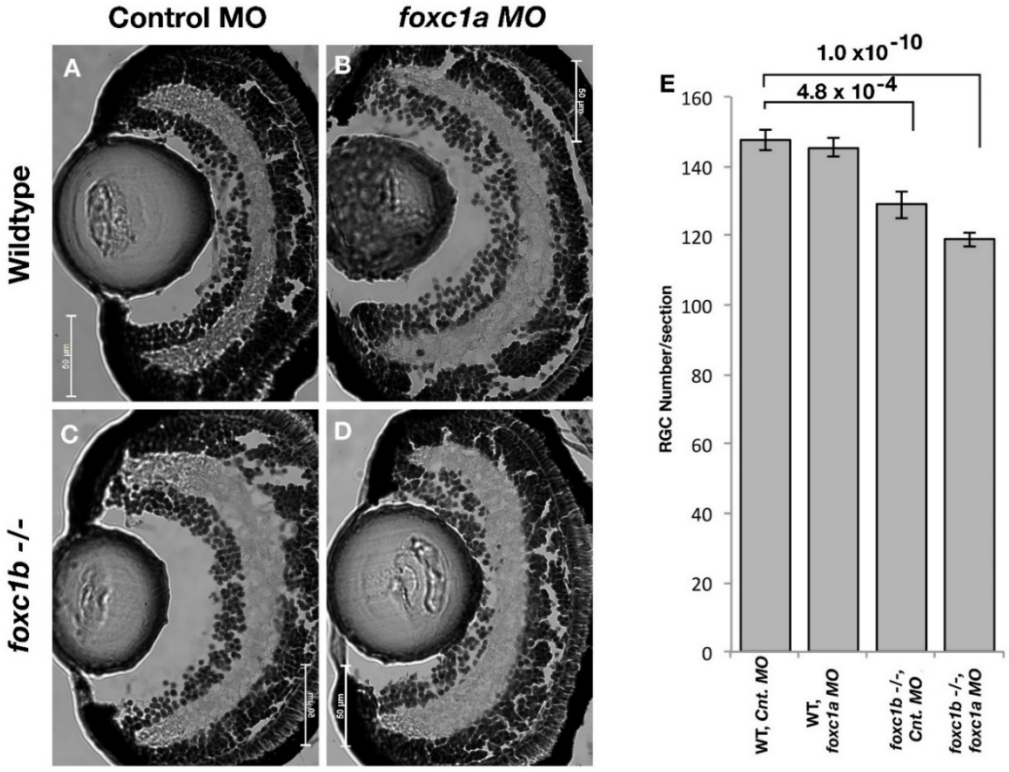

Figure 3.3 Loss of *foxc1* function in the zebrafish model results in a significant reduction of RGCs, as seen in cryosectioned embryos.

A reduction in the number of RGC is seen in cryosections of *foxc1b-/-* embryos injected with *foxc1a* morpholino (N=29) (D) compared to wild type embryos injected with a control morpholino (N=29) (A). Morpholino inhibition of *foxc1a* alone (N=28) has no significant effect on the ganglion cell numbers in wild type embryos (B). *foxc1b-/-* mutants injected with a control morpholino (N=16) present with a significant reduction of RGCs as well, although not as pronounced as embryos with a complete loss of *foxc1* function. Quantification of RGC was performed on 14 µm-thick cryosections of 5 dpf embryos in a standardized area directly tangential to the lens. Significance testing was done by performing a one-way ANOVA with a post-hoc Tukey test (E).

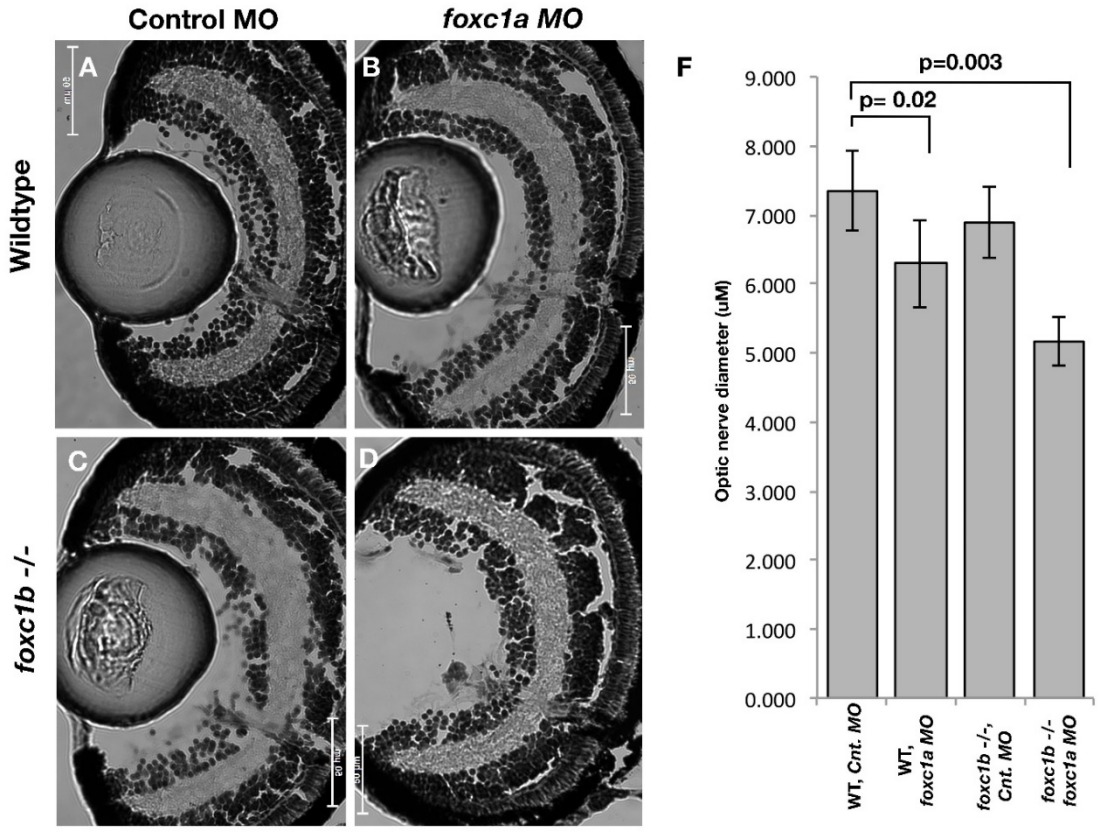

Figure 3.4: Loss of *foxc1* function in the zebrafish model results in thinning of the optic nerve, as seen in cryosectioned embryos.

A reduction in optic nerve width is seen in cryosections of *foxc1b-/-* embryos injected with *foxc1a* morpholino (N=12) (D) compared to wild type embryos injected with a control morpholino (N=6) (A). Morpholino inhibition of *foxc1a* alone (N=5) results in a significant reduction in optic nerve width (B). No significant change in optic nerve width was observed in *foxc1b-/-* mutants injected with a control morpholino (N=5). Optic nerve measurements were performed on 14 µm-thick cryosections of 5 dpf embryos. Significance testing was done by performing a one-way ANOVA with a post-hoc Tukey test (F).

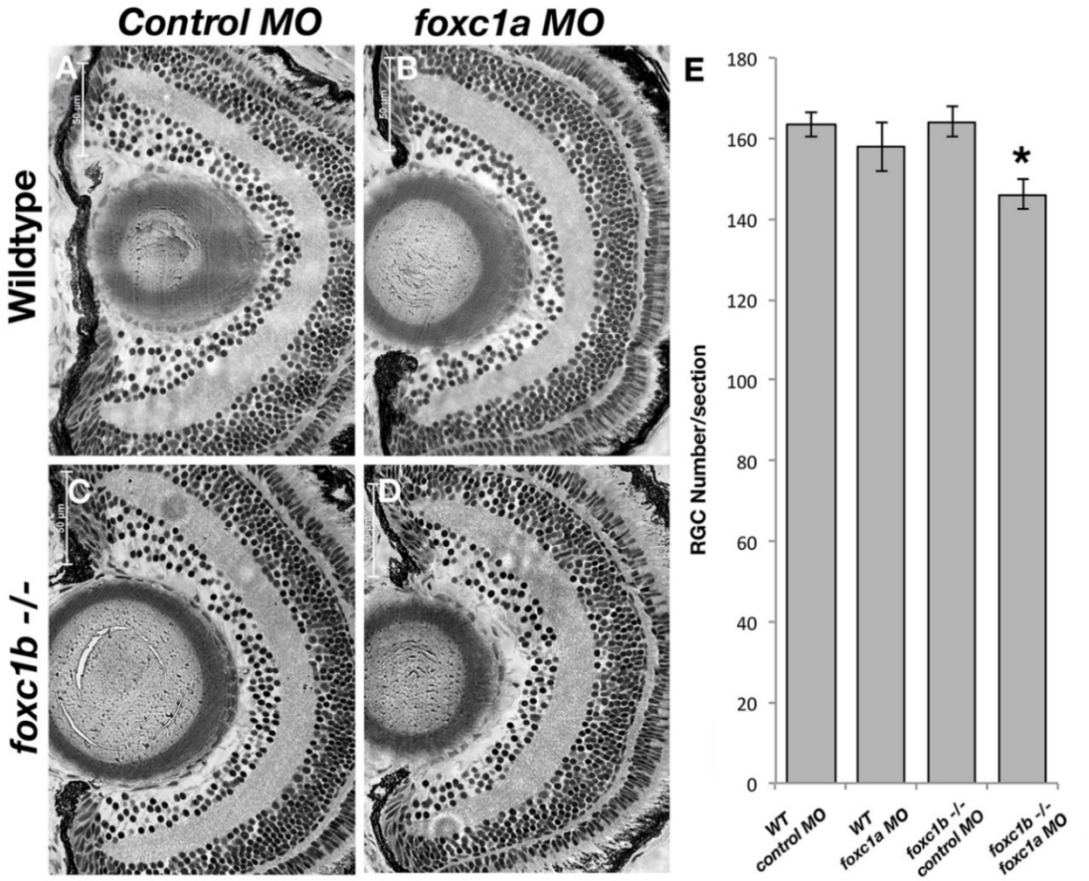

Figure 3.5 *foxc1a* morpholino inhibition in a *foxc1b-/-* background results in a reduced number of cells in the RGC layer, as seen in resin sections of 5 dpf zebrafish embryos.

A significant reduction of cells in the RGC layer is seen in the zebrafish loss of *foxc1* function model (N=14) (D) compared to wild type embryos injected with a control morpholino (N=13) (A). Neither morpholino inhibition of *foxc1a* alone (N=8) (B), nor injection of a control morpholino into *foxc1b-/-* mutants (N=12) (C) have a significant effect on cell number in the ganglion cell layer compared to wild type embryos. Significance testing was done by performing a one-way ANOVA with a post-hoc Tukey test, resulting in a p=0.038 (E). Data are presented as mean ±SEM (Umali et al., 2019).

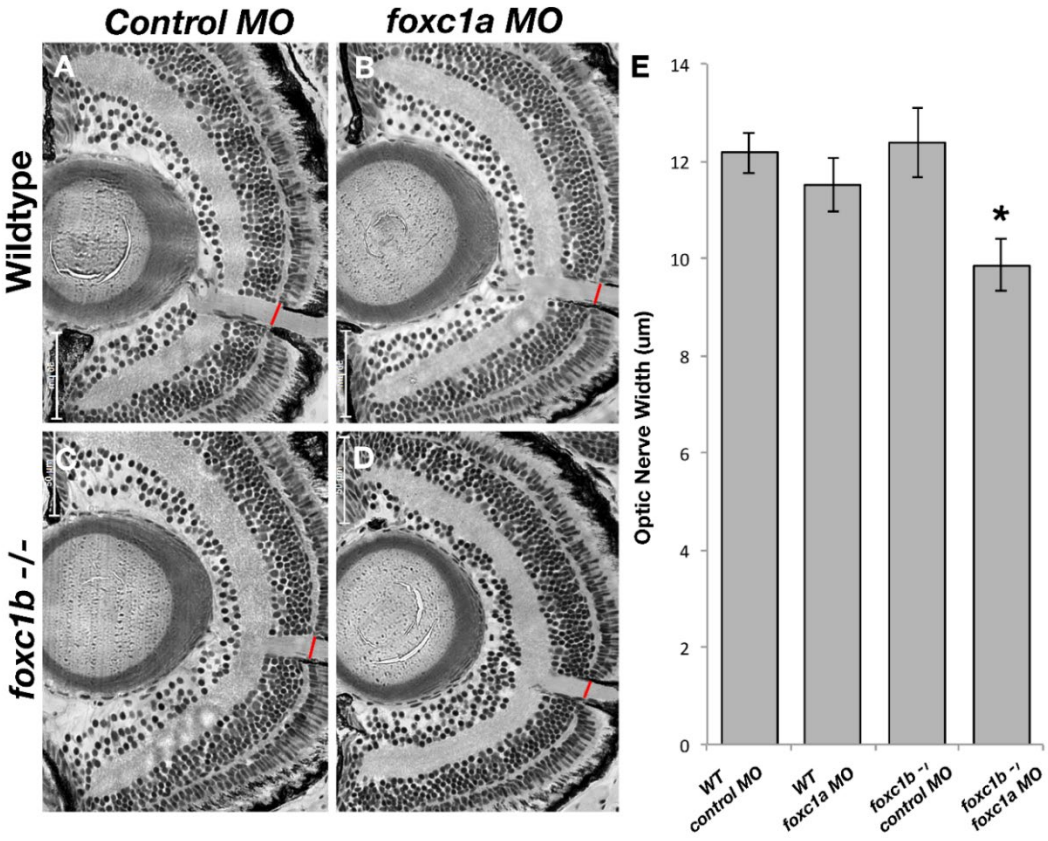

Figure 3.6 Loss of *foxc1* function in the zebrafish model results in a reduction of optic nerve thickness, as seen in resin sections of 5 dpf embryos.

A reduction in optic nerve width is seen in *foxc1b-/-* embryos injected with *foxc1a* morpholino (N=8) (D) compared to wild type embryos injected with a control morpholino (N=8) (A). No significant change in optic nerve width is observed in wild type embryos injected with foxc1a morpholino (N=5) (B), or *foxc1b-/-* mutants injected with a control morpholino (N=5) (C). This is statistically significant at p=0.018, with significance testing performed through a one-way ANOVA with a post-hoc Tukey test (E). Data are presented as mean ±SEM. Measurement of optic nerve width was done at the point where the IPL and the photoreceptor layers meet, as indicated by the red line (Umali et al., 2019).

3.4 Zebrafish loss of *foxc1* function models present with significant downregulation of *atoh7*

To investigate how loss of *foxc1* function causes a reduction in RGCs and thinning of the optic nerve, we examined the effects of *loss* of *foxc1* on the expression pattern of *atoh7,* a gene involved in RGC differentiation and early eye development. Expression of *atoh7* is initiated in the ventro-nasal domain of the zebrafish wild type eye at 32 hpf (N=3/3) (**Figure 3.7A**). This expression is significantly delayed or absent in *foxc1b*$^{-/-}$ embryos injected with *foxc1a* morpholinos (N=20/34) (**3.7D**), while the rest display either a subtle reduction or normal *atoh7* expression. Expression appears to be unaffected in over half of *foxc1a* morphants (N=5/9) (**3.7B**), with the minority displaying delayed or reduced expression. *foxc1b*$^{-/-}$ embryos injected with a control morpholino present with similar expression patterns to the wild-type (N=21/21) (**3.7C**).

By 48 hpf, *atoh7* is expressed in a fan-like pattern throughout the eye of wild type embryos (N= 14/15) (**Figure 3.7E**) (Umali et al., 2019). Loss of *foxc1a* and *foxc1b* zebrafish embryos mostly present with reduced *atoh7* expression, with a disruption of its fan-like pattern of expression being observed (N = 40/56) (**3.7H)**, while the minority display normal expression. Similar to observations at 32 hpf, both *foxc1a* morphants (N=10/20) (**3.7F**) and *foxc1b* mutants injected with a control morpholino (N=12/23) (**3.7G**) mostly presented with a normal pattern of expression at 48 hpf, not unlike that of wild type embryos. The minority of *foxc1a* morphants and *foxc1b* mutants injected with a control morpholino displayed a subtle reduction in *atoh7* expression.

Haploinsufficiency of *FOXC1* has been hypothesized to cause glaucoma as stringent *FOXC1* dosage is crucial to the development of anterior eye structures (Nishimura et al., 2001). To examine the effects of *foxc1b* dosage on *atoh7* expression, we compared *atoh7* expression in a small number of 32 hpf wild type, *foxc1b+/-,* and *foxc1b-/-* siblings borne from a *foxc1b* heterozygous incross. At 32 hpf, *atoh7* expression is initiated in the ventro-nasal domain of the eye in wild type embryos (N=3/3) (**Figure 3.8A**). A slight delay or reduction in *atoh7* expression is observed in half of *foxc1b* heterozygotes injected with a control morpholino (N= 2/4) (**Figure 3.8B**), with a more pronounced reduction in *foxc1b*$^{+/-}$ embryos with *foxc1a* morpholino inhibition (N=14/16) (**Figure 3.8C)** (Umali et al., 2019)**.**

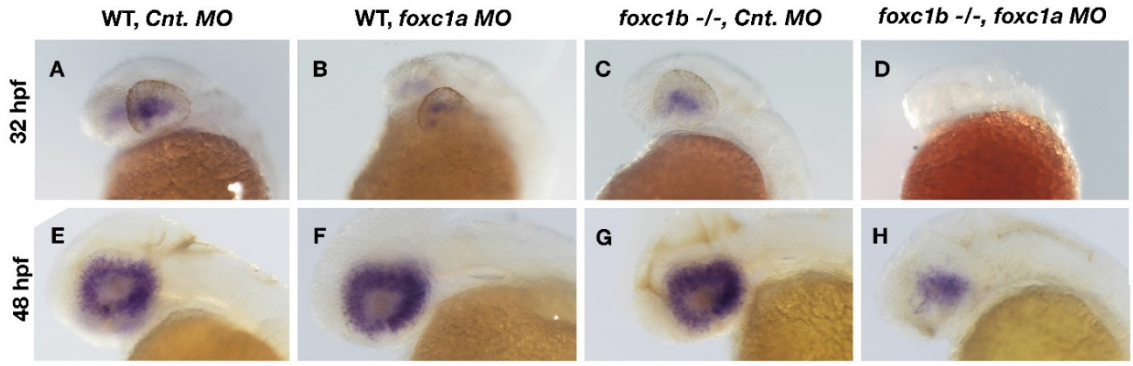

Figure 3.7 Loss of *foxc1* embryos have reduced and disrupted *atoh7* expression.

In the wildtype embryo injected with control morpholino, *atoh7* expression is initiated in the ventral domain of the retina at 32 hpf (A) and is dynamically expressed in a fan-like manner throughout the entire retina by 48 hpf (E). Embryos with loss of *foxc1a* alone through morpholino inhibition at 32 and 48 hpf (B and F), or in *foxc1b-/-* embryos injected with a control morpholino (C and G) at both time points mostly presented with *atoh7* expression similar to that of their wild-type siblings. Absent or delayed initiation of *atoh7* expression was observed in *foxc1b-/-* embryos injected with a *foxc1a* morpholino at 32 hpf (D), with a reduction and disruption of *atoh7* expression seen in the retina of the loss of *foxc1* models at 48 hpf (H) (Umali et al., 2019).

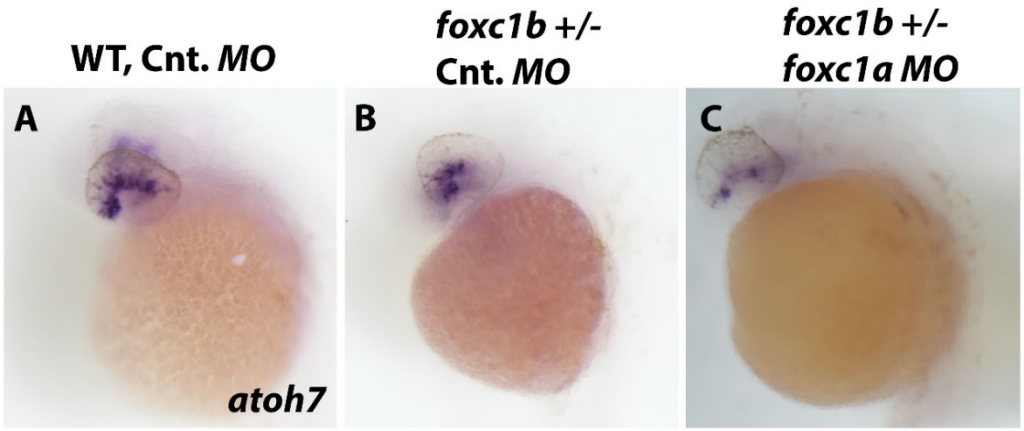

Figure 3.8 *foxc1b* heterozygotes appear to have a mild reduction of *atoh7* signalling in 50% of a small number of embryos.

At 32 hpf, wild-type embryos injected with control morpholino present with *atoh7* expression that has been initiated in the ventronasal domain and moves around the eye in a clockwise, fan-like pattern (A). A slight delay and reduction of expression are observed in 2 out of 4 (50%) *foxc1b* heterozygotes injected with a control morpholino (B), with the reduction in signalling being more pronounced in *foxc1b*+/- embryos with inhibition of *foxc1a* function through injection of a *foxc1a* morpholino (C).

3.5 Loss of *foxc1* function results in a downregulation in *fgf19* expression

In humans, *FGF19* is directly regulated by *FOXC1* in the eye, while *fgf19* signalling is required for the development of the zebrafish retina and the lens (Nakayama et al., 2008; Tamimi et al., 2006). Given *fgf19's* role in early eye development, we examined the impact of loss of *foxc1* on *fgf19* expression. At 24 hpf, *fgf19* is expressed in the eye, neural tube, and pectoral fin bud in wildtype embryos injected with a control morpholino (N=14/17) (**Figure 3.9A**) (Umali et al., 2019). *fgf19* expression is subtly reduced in 24 hpf loss of *foxc1* zebrafish embryos, which were obtained through injection of *foxc1a* morpholino into embryos of a *foxc1b*$^{-/-}$ mutant background (N=23/23) (**3.9B**).

3.6 Loss of *foxc1 function* results in a mild downregulation of *pdgfrα* but does not appear to reduce *hspa5,* and *hspa9* signalling

Susceptibility to oxidative damage has been hypothesized to underlie glaucoma pathogenesis, with several *FOXC1* targets involved in the oxidative stress response being previously identified (Berry et al., 2008). We examined the expression of a few *FOXC1* targets that are known to be expressed in the eye and are involved in the response to oxidative stress: *pdgfrα, hspa5,* and *hspa9.*

pdgfrα is expressed in the lens, head mesenchyme, and pharyngeal arches at 24 hpf in wildtype embryos injected with a control morpholino (N=22/26) (**Figure 3.9C**), with signalling being concentrated in the pharyngeal arches in the wildtype embryos injected with a control morpholino at 48 hpf (N=30/30) (**3.9E**) (Umali et al., 2019). A mild reduction in *pdgfrα* signalling is observed in *foxc1b*$^{-/-}$ embryos injected with *foxc1a* morpholino (N=18/21) (**3.9D**), with the effect being more pronounced at 48 hpf in the

majority of the loss of *foxc1* embryos (N=13/25) (**3.9F**). Meanwhile, minority of loss of *foxc1*embryos displayed a subtle reduction to normal expression of *pdgfra* at 48 hpf.

In wild type embryos injected with a control morpholino, *hspa5* signalling is ubiquitous at 32hpf, including the lens and the choroidal fissure (N=25/25) (**3.9G**) (Umali et al., 2019). No significant alterations in *hspa5* expression is observed in *foxc1b*$^{-/-}$ embryos injected with *foxc1a* morpholino (N=15/15) (**3.9H**). At 32 hpf, *hspa9* is expressed in the eye and the tectum in wildtype embryos injected with a control morpholino (N=17/17) (**3.9I**). No change is observed in the expression of *hspa9* in the majority of loss of *foxc1* embryos (**3.9J**) (N=18/27), while the minority of the embryos displayed seemingly increased expression (N=6/27) or no in situ staining (N=3/27).

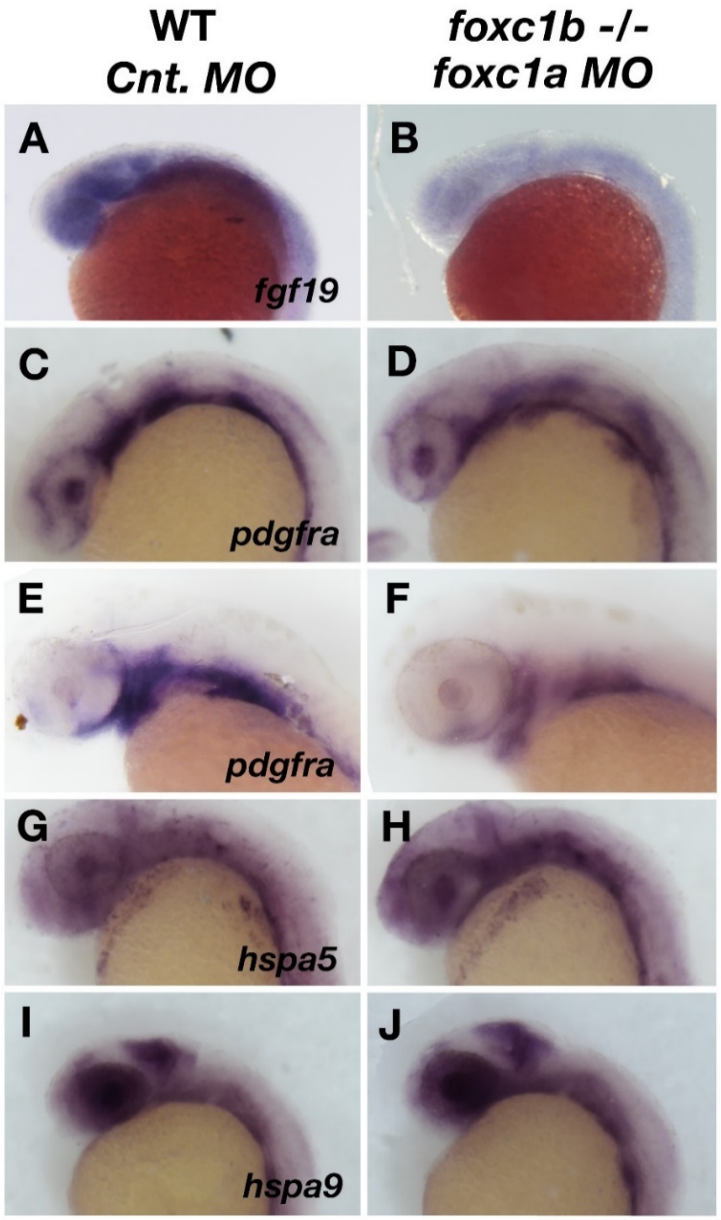

Figure 3.9 Loss of *foxc1* embryos have reduced *fgf19* expression, but minimal changes are observed in the signalling of oxidative stress genes.

At 24 hpf, *fgf19* is expressed ubiquitously in the head of the wild-type/control embryo (A), and signalling is reduced in *foxc1b-/-* embryos injected with foxc1a morpholino (B). At 24 hpf, a mild reduction is observed in the expression of *pdgfrα*, an oxidative response gene, in *foxc1a*

morphants of a *foxc1b-/-* background compared to their wild-type/control counterparts (C and D), with the reduction being more pronounced at 48 hpf (E and F). No changes in the expression of *hspa5* and *hspa9*, two heat shock proteins, are observed upon loss of *foxc1* function (I and J) (Umali et al., 2019).

3.7 Loss of *foxc1 function* results in a mild downregulation of *foxo1a and foxo1b* in a small number of embryos

FOXC1 has been previously shown to directly regulate *FOXO1A*, a gene required for cell survival and resistance to oxidative stress in trabecular meshwork cells (Berry et al., 2008). The loss of *FOXC1* expression has been shown to result in the reduction of *FOXO1A* expression in human trabecular meshwork cells, while *in situ* hybridization studies in the zebrafish injected with morpholinos against both *foxc1* orthologues have found a similar effect in terms of the downregulation of *foxo1a* and *foxo1b* (Berry et al., 2008). We sought to examine whether we could replicate previous findings by *in situ* analysis of *foxo1a* and *foxo1b* signalling in zebrafish loss of *foxc1* function models obtained via injection of *foxc1a* morpholino into embryos of *foxc1b*$^{-/-}$ genetic background.

At 48 hpf, *foxo1a* has been reported to be expressed in the periocular mesenchyme, pharyngeal arches, and pancreatic bud in the wild type embryo (Berry et al., 2008). Our findings concur with this expression pattern in wild type embryos (N=21/25) (Figure **3.10A).** *foxo1b* expression overlaps with *foxo1a* in the wild type embryo at 48 hours as well, although *foxo1b* signalling is more concentrated in the nasal epithelium and the pharyngeal arches (N=22/30) **(3.10C)**. In *foxc1b*$^{-/-}$ embryos injected with *foxc1a* morpholino, 48 hpf embryos present with reduced expression of both *foxo1a* (N=15/26) (10B) and *foxo1b* (N=16/29) **(3.10D).** The minority of loss of *foxc1* embryos presented with either subtle reductions to normal expression of both *foxo1a* and *foxo1b.*

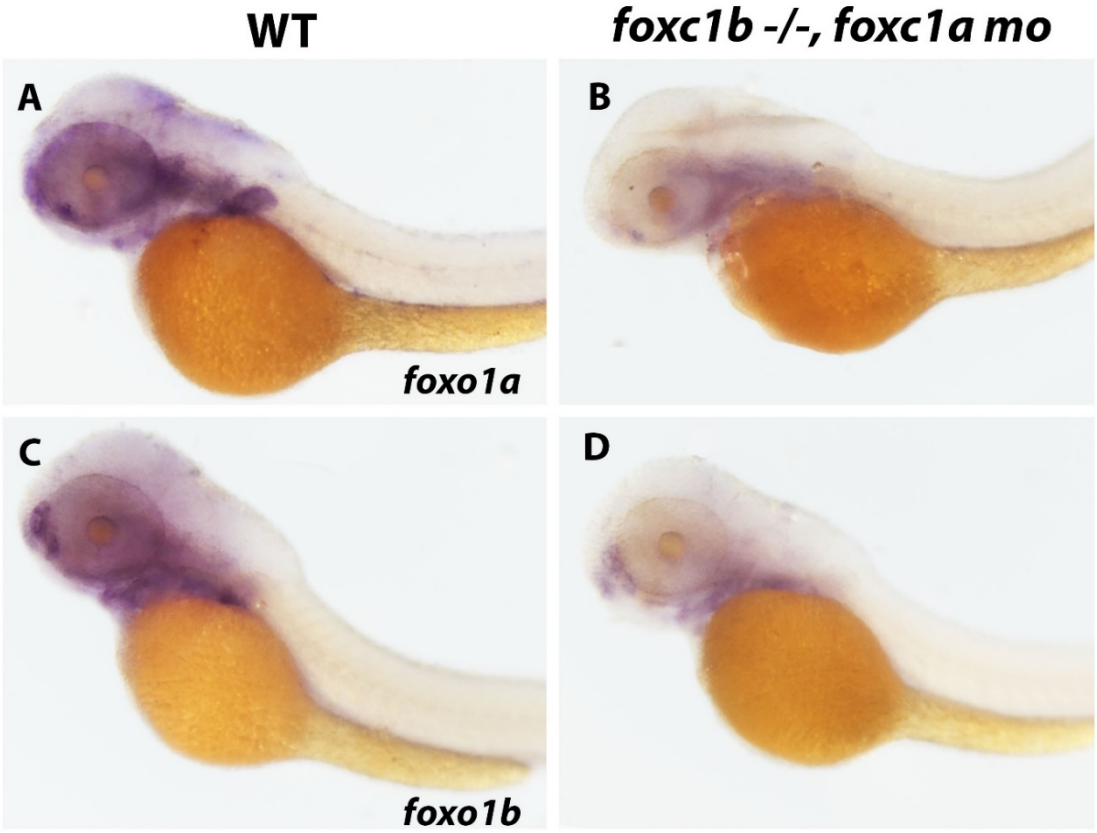

Figure 3.10 Loss of *foxc1* function results in a reduction in *foxo1a* and *foxo1b* signalling in a small number of embryos.

In the wildtype embryo injected with control morpholino, *foxo1a* is expressed in the periocular mesenchyme and the pharyngeal arches at 48 hpf (A). *foxo1a* expression appears to be decreased when *foxc1* function is lost, as seen in 15 out of 26 *foxc1b-/-* embryos injected with *foxc1a* morpholinos (B). At 48 hpf, *foxo1b* expression overlaps with *foxo1a*, with concentration in the nasal epithelium and pharyngeal arches (C), with reduction in signalling also being observed in loss of *foxc1* function embryos (N=16/29) (D).

3.8 *foxc1b*$^{-/-}$ embryos present with a subtle upregulation of *foxc1a* expression

Given the lack of significant RGC loss and optic nerve thinning in *foxc1b*$^{-/-}$ embryos, we explored the possibility that *foxc1a* compensates for the loss of *foxc1b* in the zebrafish embryo. At 48 hpf, *foxc1a* is expressed in the anterior pharyngeal arches and head mesenchyme (N=18/19) (**Figure 3.11A and C**). To investigate whether *foxc1a* plays a compensatory role during loss of *foxc1b* function, we examined *foxc1a* signalling in 48 hpf *foxc1b-/-* embryos. A mild increase of *foxc1a* expression in the pharyngeal arches is observed in *foxc1b-/-* embryos, along with a subtle decrease of expression in the head mesenchyme (N=8/8) (**3.11B and D**).

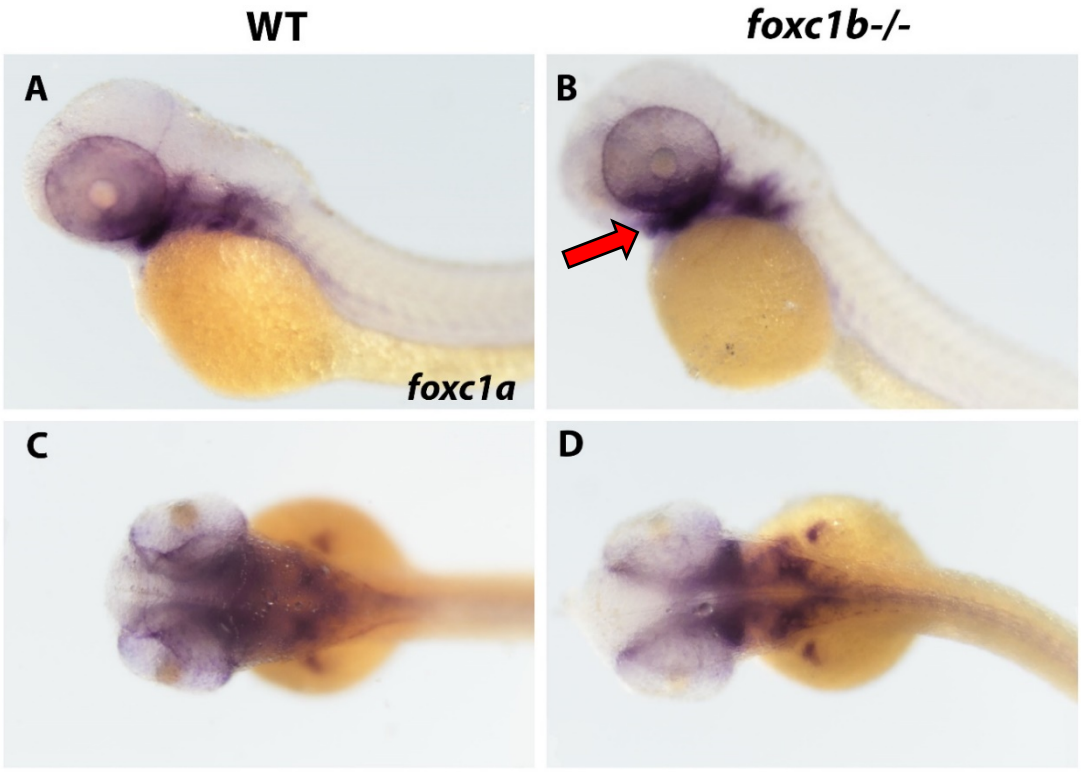

Figure 3.11 Loss of *foxc1b* function results in subtle upregulation of *foxc1a*.

In the wild-type embryo, *foxc1a* is expressed in the anterior pharyngeal arches and head mesenchyme at 48 hpf (**A** and **C**). A subtle upregulation of *foxc1a* expression in the pharyngeal arches (arrow) is observed when *foxc1b* function is lost, as seen in *foxc1b-/-* embryos (**B** and **D**).

4 Discussion

Overview

RGC differentiation and survival are essential for the maintenance of vision, as their axons form the optic nerve, which carries information from the eye to the visual processing centres of the brain. Damage to RGCs and damage to the optic nerve are characteristic of glaucoma, a leading cause of irreversible blindness worldwide predicted to affect 79.6 million people by the year 2020 (Quigley & Broman, 2006). Glaucoma is understood to have a hereditary component, with congenital and early-onset forms typically presenting in a Mendelian pattern of inheritance, and late-onset forms presenting in a multifactorial fashion, with the latter being a result of interaction between genetic risk factors that contribute to the development of certain glaucoma endophenotypes and environmental risk factors (Liu & Allingham, 2017). Elevated IOP is the leading risk factor for glaucoma, however, about 30% of patients present with IOPs within the reference range (Kim & Park, 2016). This suggests other underlying mechanisms that contribute to glaucomatous cell death. Studies have shown that non-IOP-related genetic risk factors may play an important role in glaucoma pathogenesis regardless of IOP phenotype (Mabuchi et al., 2015), highlighting the importance of learning about these risk factors and their developmental etiology.

Loss of function mutations or copy number variations in the forkhead box transcription factor *FOXC1* have been linked to early-onset and congenital glaucoma, frequently presenting with ASD disorders such as ARS (Lehmann et al., 2000; Micheal et al., 2016; Nishimura et al., 1998). Recently, *FOXC1* has also been found to be associated with a

late-onset POAG in a genome-wide associated study (Bailey et al., 2016). This SNP alters a *Barh1* transcription factor binding site, which is a gene target of *Atoh7* in zebrafish and is expressed in distinct retinal cell lineages (Schuhmacher, Albadri, Ramialison, & Poggi, 2011).

Given the many roles of *FOXC1* in early development, and its well-documented causative relationship with glaucoma, the objective of this thesis was to examine whether the zebrafish, *Danio rerio,* may be used as a viable genetic model for *FOXC1*-associated glaucoma. To achieve this, the expression patterns of *foxc1a* and *foxc1b* were mapped in the developing zebrafish embryo, followed by investigations on whether loss of *foxc1* or complete loss of function would result in the reduction of cells in the RGC layer and thinning of the optic nerve in the developing zebrafish eye at 5 dpf. The effects of loss of *foxc1* function on the expression of genes involved in RGC differentiation, early eye development, and the oxidative stress response were studied to identify underlying mechanism through which RGCs are lost early in development. In addition, an investigation on whether genetic compensation may be taking place was conducted through expression studies of *foxc1a* when *foxc1b* is lost, thus accounting for the lack of significant reduction in cell numbers and optic nerve width when only one zebrafish *foxc1* paralog is lost.

4.1 *foxc1a* and *foxc1b* have overlapping functions in the development of the zebrafish eye

FOXC1 exists in duplicate in zebrafish, with a homology of 83% for *foxc1a* (located on Ch2), and 84% for *foxc1b* (Zerbino et al., 2017). While previous studies have reported *foxc1a* to be the homolog for human *FOXC1* and *foxc1b* to be the homolog of *FOXC2* (Skarie & Link, 2009; Topczewska et al., 2001), both copies of zebrafish *foxc1* are syntenic with human Chr. 6p25 where *FOXC1* is mapped. This may point to possible redundancies in function and genetic compensation between *foxc1a* and *foxc1b*, though other possibilities such as each duplicate having separate and/or overlapping functions, or one duplicate having no role in retinal development, also need to be considered.

Our expression studies show that *foxc1a* and *foxc1b* have overlapping expression in the cells of the neural crest and periocular mesenchyme at 24 hpf and continue to overlap at 48 hpf with concentration of *foxc1a* in the anterior pharyngeal arches and *foxc1b* being confined to the more dorsal pharyngeal arches (Umali et al., 2019). This thesis also shows that loss of *foxc1b* alone in embryos borne from a heterozygous incross, or the loss of *foxc1b* alone in embryos borne from a homozygous incross do not result in significant loss of cells in the ganglion cell layer or thinning of the optic nerve. Significant loss of cells in the ganglion cell layer and thinning of the optic nerve present in *foxc1a* morphants, or when complete loss of *foxc1* function occurs, as demonstrated through antisense morpholino inhibition of *foxc1a* in *foxc1b-/-* mutants. Similarly, dysregulation of *atoh7* is observed in loss of *foxc1* function embryos (Umali et al., 2019). This effect is not seen in *foxc1a* morphants or in *foxc1b*$^{-/-}$ embryos. Altogether, our data suggests at

least partial redundancy and overlap in the functions of the two paralogs in zebrafish eye development given that a drastic phenotype is observed upon loss of both *foxc1a* and *foxc1b*. These results indirectly highlight the specificity of the *foxc1a* morpholino. Given that the phenotype is observed mostly upon injection of *foxc1a* morpholino into *foxc1b* mutants, this favours a model where reductions RGC number and optic nerve width are due to the combined mutation/knockdown of *foxc1b/foxc1a*, as opposed to off target effects of morpholino inhibition (Umali et al., 2019).

Our findings show a subtle upregulation of *foxc1a* in the pharyngeal arches and a subtle decrease in *foxc1a* expression in the head mesenchyme of 48 hpf *foxc1b* mutant embryos (Umali et al., 2019). Based on this, we hypothesize that *foxc1a* and *foxc1b* may have a compensatory genetic relationship, in which upregulation of one ortholog occurs to compensate for the loss of function of the other. We have not, however, directly tested for changes in *foxc1b* expression when *foxc1a* is lost, which may provide conclusive data to understand the relationship between the two *FOXC1* paralogs further.

4.2 Normal RGC differentiation in the developing eye requires *foxc1* function

In this thesis, we demonstrate reduced cell numbers in the ganglion cell layer and thinning of the optic nerve as early as 5 dpf when *foxc1* function is lost in zebrafish embryos (Umali et al., 2019). RGC loss and optic nerve neuropathy is characteristic of glaucoma as seen in humans (Quigley, 2011), and a similar phenotype is observed in zebrafish. However, in the resin sections, these phenomena do not present when only one copy of zebrafish *foxc1* is lost, and thus, the duplicity and genetic compensation of certain orthologs of human genes in the zebrafish must be kept in mind for future studies.

RGC loss and optic nerve thinning were initially observed in eye cryosections, after which resin sections were performed to confirm the phenotype in thinner sections. Cryosections are beneficial as this histological technique provides an opportunity for inexpensive, rapid generation of large numbers of eye sections, with zebrafish embryos being processed right after fixation (Von Bartheld, 2002). However, cryosections may yield thick sections of relatively poor quality, given that sections may curl, and the melting process may result in displacement and distortion of cells (Xu & Xu, 2001). These were evident in our cryosections, and we opted to count within a standardized area tangential to the lens to account for artefacts cellular distortion at the edges of the cryosections.

Light-microscopic paraffin sections have been previously used to examine optic nerve degeneration and RGC loss in murine models for spontaneous glaucoma (Fujikawa et al., 2010; Li, Fang, & Jiang, 2010). Embedding in resin (methacrylate), though requiring more complex equipment, time, and histological expertise, has been shown to result in production of thinner sections, as seen in human tissue, murine, and fish specimen (Barthel & Raymond, 1990; Blythe et al., 1997; Helander, 1983; Xu & Xu, 2001). The fixation and dehydration involved in the sectioning process may result in changes to cellular structure, impact tissue reactivity, and specimen size (Newman & Hobot, 1999). In our research, sections were processed the same way and at the same time in an effort to minimize individual error. Overall sizes of the embryonic eyes were unchanged, and sections obtained through this histological technique were of superior quality compared to cryosections and allowed us to visualize and quantify the cells in the entire ganglion cell

layer for each section. For increased accuracy in the quantification of optic nerve degeneration and RGC loss, ultrastructural examination of cross-sections of the optic nerve through electron microscopy could be performed for future studies (Li et al., 2010; Lidster et al., 2013).

Our data also demonstrates that complete loss of *foxc1* function results in dysregulation of *atoh7,* a gene implicated in RGC differentiation. This suggests that aberrant RGC differentiation contributes to the reduction of cells in the ganglion cell layer and thinning of the optic nerve. Once again, this only presents upon loss of both *foxc1* orthologs in the zebrafish and is not seen in *foxc1b*$^{-/-}$ mutants borne from a heterozygous incross, or when either *foxc1a* or *foxc1b* alone is lost in embryos borne from a homozygous incross. In our assessment of the effects of *foxc1b* dosage on *atoh7* expression, a slight delay or reduction in *atoh7* expression appears to occur in half of *foxc1b* heterozygotes injected with a control morpholino. This may indicate that *foxc1b* mutations may have a potential dominant negative effect. The more pronounced reduction of *atoh7* expression observed in *foxc1b*$^{+/-}$ embryos with *foxc1a* morpholino inhibition is more consistent with the expected effect of the reduction of *foxc1* dosage, although given the small number of embryos, repetition of this experiment with a larger sample size in future studies may provide conclusive data on the impacts of *foxc1b* dosage on *atoh7* expression.

Furthermore, subsequent studies done in our laboratory were performed to understand the underlying cause of reduction in cells in the ganglion cell layer. No increased cell death is observed in zebrafish loss of *foxc1* function embryos, suggesting that increased ganglion cell death does not contribute to the reduction of cells we see in the ganglion cell layer

nor the thinning of the optic nerve (Umali et al., 2019). Previous studies have shown that loss of RGC fate has been observed to occur with an increased disposition of cells to amacrine cell fate (Brown et al., 2001; Cherry, Trimarchi, Stadler, & Cepko, 2009; Kay et al., 2001). However, expression studies to look at *scrt1a,* a marker for amacrine cell fate, show no difference in the expression of these genes compared to wildtype embryos injected with a control morpholino (Umali et al., 2019). This suggests no increased amacrine cells in conjunction with a reduction in the number of cells in the ganglion cell layer.

4.3 *foxc1* is required for the expression of *atoh7,* a regulator for RGC differentiation

bHLH transcription factors are crucial to the regulation and development of the vertebrate retina (Vetter & Brown, 2001). Structurally, most of the proteins in this family possess basic DNA-binding and helix-loop-helix protein dimerization domains. bHLH genes coordinate neurogenesis through proneural and antagonistic functions, with antagonistic bHLH genes forming inactivating heterodimers or through inhibition of transcription (Vetter & Brown, 2001).

The *Drosophila* bHLH gene *atonal,* a vertebrate proneural bHLH gene, expressed in the neural progenitor cells of the fruit fly, has been initially identified to be essential for photoreceptor development (Jarman et al., 1995). Various *atonal* homologs have been identified in different vertebrates, from the murine *Atoh7* to the Xenopus *Xath5* and the zebrafish *atoh7* (Brown et al., 1998; Kanekar et al., 1997; Masai et al., 2000). These genes have all been identified to play a role in retinoneurogenesis, being expressed by

retinal progenitor cells during the early stages of eye development (Brown et al., 2001; Kanekar et al., 1997; Kay et al., 2001). In the mouse model, *Atoh7* is specifically expressed by retinal progenitor cells, with expression being detected at E11 prior to any other proneural gene (Brown et al., 1998). *Atoh7*'s spatial and temporal patterns of expression correlate with the appearance of RGCs, preceding the appearance of RGCs by a full day and is subsequently downregulated in the adult retina. In the zebrafish, *atoh7* is exclusively expressed in the developing retina, with initial expression being observed at the ventronasal domain at around 25 hpf, and dynamically spreads throughout the remainder of the neural retina, after which it is downregulated at around 72 hpf (Masai et al., 2000). The pattern of *atoh7* expression coincides with neuronal differentiation, which is also initiated in the ventronasal retina. Based on the well-described and dynamic expression pattern of *atoh7,* we aimed to determine whether aberrant neuronal differentiation underlies the loss of RGC in zebrafish loss of *foxc1* function embryos. This was performed by investigating these embryos for disruptions in *atoh7* expression compared to their wild-type siblings.

Our data demonstrates that loss of *foxc1* function leads to dysregulation of *atoh7,* a gene that has been demonstrated to be expressed by retinal progenitor cells as they differentiate into RGCs in various vertebrate models (Brown et al., 2001; Kay et al., 2001). Complete loss of *Atoh7* has been shown to result in complete absence of ganglion cells, optic nerves, and chiasmata in mice, whereas *atoh7* zebrafish mutants present with loss of visual function and a significant loss of cells in the ganglion cell layer and a barely visible optic nerve (Brown et al., 2001; Kay et al., 2001). These animal models presented with

displaced amacrine cells in the ganglion cell layer and an increased number of cells in the inner nuclear layer. No increase in expression of the amacrine cell marker *scrt1a* is observed in loss of *foxc1* function embryos (Umali et al., 2019). However, analysis of cells in the inner nuclear layer such as bipolar and glial cells was not conducted given that glaucoma primarily involves RGC loss.

Studies on mice show that as a transcription factor, *Atoh7* initiates and controls retinal neurogenesis as part of a gene network and controls RGC specification and differentiation through a variety of downstream targets. One of these networks involve the *Atoh7* target *Pou4f2,* a class IV POU-domain transcription factor required for differentiation, axon outgrowth and pathfinding, and survival (Wang, S. W. et al., 2000; Wang, S. W. et al., 2001). Further studies of *atoh7* downstream targets show that a decrease in *pou4f2* is observed when *foxc1* function is lost (Umali et al., 2019), confirming our hypothesis that mutations in *foxc1* result in disruption of RGC differentiation, leading to cellular loss in the ganglion cell layer and thinning of the optic nerve. However, many RGC genes are not affected by the absence of *pou4f2* (Wang, S. W. et al., 2000; Wang, S. W. et al., 2001), indicating that other regulatory genetic pathways under transcriptional control of *Atoh7* contribute to retinal neurogenesis in parallel. In mice, a huge number of downstream targets of *Atoh7* have been identified, with *Atoh7* targets having diverse functional roles including transcriptional regulation, cell adhesion, and cell signalling (Mu & Klein, 2004). These studies all highlight the importance of gene interactions in the development of the vertebrate neural retina, and how elucidation of genetic pathways

would improve knowledge of the underlying pathways that may be disrupted in glaucomatous eyes.

Foxc1 has been shown to play a role in the development of the anterior segment in mice (Smith et al., 2000), and has also been shown to be important in the development and maintenance of ocular and cerebral vasculature (French et al., 2014; Skarie & Link, 2009). As shown in this thesis, zebrafish *foxc1* homologs are expressed in the neural crest and periocular mesenchyme, yet neither homologs are expressed in the retinal progenitor cells at 24 hpf, nor at 48 hpf, when *atoh7* is shown to have completed its dynamic, clockwise expression around the zebrafish retina. This shows that despite *foxc1* not being expressed in the retina, it may still regulate signalling of genes involved in RGC differentiation, as demonstrated in this dissertation, and highlights the cell non-autonomous effects of loss of *foxc1* function with regards to other biological mechanisms as well.

In humans, *ATOH7* is mapped to Chr. 10q21-q22 and has been identified as a major determinant for optic disc area and VCDR, risk factors for glaucoma (Macgregor et al., 2010; Ramdas et al., 2010). *ATOH7* has also been found to be significantly associated with glaucoma, particularly as a non-IOP related genetic risk factor for normal-tension glaucoma (Mabuchi et al., 2012; Ramdas et al., 2011). In addition, *ATOH7* has been linked to defects in ocular vasculature, particularly with regards to persistence and proliferation of fetal blood vessels in the eye (Khan et al., 2011; Prasov et al., 2012), which often leads to glaucoma. A disruption of the retinal vasculature, particularly the persistence of fetal vasculature, has also been observed in *Atoh7* mice mutants (Edwards

et al., 2012). Researchers have speculated on interactions between neurons, astrocytes, and endothelial cells in retinal development (Fruttiger et al., 1996), and studies on *ATOH7* confirm the importance of normal retinal neurogenesis to ocular vascular development. Furthermore, mutations in *foxc1* have also been shown to cause ocular vascular defects in zebrafish (Skarie & Link, 2009), as well as in mice (Seo et al., 2012; Smith et al., 2000). Given that vascular factors have been speculated to play a role in glaucoma pathogenesis (Yanagi et al., 2011), aberrant RGC differentiation may coincide with vasculature defects, which then leads to glaucoma.

4.4 Loss of *foxc1* may influence retinal neurogenesis through the downregulation of *fgf19*

The fibroblast growth factor *(FGF*) family consists of evolutionarily conserved polypeptide growth factors, most of which function by binding and interacting with tyrosine kinase FGF receptors (*Fgfr*). While these genes have been identified in a multitude of multicellular organisms, in humans and mice, 22 *Fgf* and 4 *Fgfr* genes have been identified (Itoh & Ornitz, 2004). Most *FGFs* in this category have N-terminal signal peptides and are secreted from cells (Itoh & Ornitz, 2004). These include human FGF19 and its mouse ortholog FGF15. In humans, FGFs have been implicated in various biological functions, such as mitogenesis, cellular differentiation, and embryonic development.

Human *FGF19,* located on Chr. 11q13.3, and its zebrafish orthologue *fgf19* (mapped to Chr. 7) (Katoh & Katoh, 2003; Xie et al., 1999), have been shown to be direct targets of *FOXC1* in the eye in human cell culture and in the zebrafish model respectively,

particularly in the cornea (Tamimi et al., 2006). In concurrence with previous studies (Tamimi et al., 2006), we demonstrate that *fgf19* and *foxc1* transcripts have overlapping expression in the periocular mesenchyme at 24 hpf. *foxc1* morphant zebrafish have been found to present with a 2.5-fold decrease in *fgf19* expression, small eye phenotype, reduced cellular differentiation in the periocular mesenchyme, and delayed retinal delamination compared to wild-type embryos (Tamimi et al., 2006). Our data demonstrates a reduction of *fgf* expression in *foxc1b*$^{-/-}$ mutant embryos injected with *foxc1a* morpholino, although analysis of other phenotypes was not performed.

fgf19 was first identified to be expressed in the forebrain, midbrain, and hindbrain (Miyake, Nakayama, Konishi, & Itoh, 2005). Regulated by *Hedgehog* signalling, it plays an essential role in cell proliferation and survival in the development of the forebrain. In the developing chick eye, it is expressed in the optic vesicle and in a subset of progenitor cells of the neural retina (Kurose et al., 2005), and has been shown to play a role in eye development in the zebrafish model, particularly with regards to the lens and the retina (Nakayama et al., 2008). *fgf19* is required for nasal-temporal patterning in the zebrafish retina, guiding RGC axons that form the optic nerve between the eye and the tectum (Hernandez-Bejarano et al., 2015; Nakayama et al., 2008). Retinal cell fate determination involves contributions from intrinsic and extrinsic cues, with bHLH genes such as *atonal genes,* determining intrinsic properties such as competence to respond to extrinsic cues (Cepko, 1999). Studies have demonstrated the possibility of *FGFs* and their receptors, *FGFR*s, as extrinsic cues to ganglion cell differentiation through downstream targets that interact with *atoh7* (Cepko, 1999; Willardsen, Minde, Hutcheson, Moore, & Vetter, 2014;

Willardsen, Minde I. et al., 2009). Therefore, a network between *foxc1, fgf19,* and *atoh7* may be underlying normal RGC generation, and loss of *foxc1* may result in a disruption of this genetic pathway, leading to loss of ganglion cells and thinning of the optic nerve. However, we did not directly investigate this gene network in this thesis to provide conclusive data for this hypothesis.

An additional possible implication for loss of *foxc1* and subsequent downregulation of *fgf19* may be aberrant development and maintenance of the anterior segment. *Fgf19* is a key element of the *FGF19-FGFR4-MAPK* pathway, which regulates tight junction formation and maintenance of corneal cells in the human eye (Tamimi et al., 2006). As *FOXC1* directly regulates *FGF19*, a disruption of *Fgf19* may be behind abnormalities seen in *Foxc1* mutant mice that displayed corneal abnormalities, such as the failure for separation to occur between the cornea and the lens, disorganized corneal stroma, and a thicker epithelium (Smith et al., 2000). These abnormalities were not immediately evident in the eyes of our loss of *foxc1* zebrafish model. Corneal abnormalities may be the underlying mechanism responsible for increased central corneal thickness and cellular hyperplasia in humans, which are risk factors for glaucoma. Future directions for this research may involve addressing this hypothesis through direct investigation for corneal abnormalities in the eye sections of our zebrafish *loss* of *foxc1* model.

4.5 Response to oxidative stress is not a key factor in the regulation of RGC numbers in the 5 dpf zebrafish embryo

In mammals, the trabecular meshwork is constantly exposed to aqueous humour, which is a significant source of oxidative stress (Green, 2001; Richer & Rose, 1998). Oxidative

damage has been speculated to contribute to glaucoma pathogenesis, with direct exposure to reactive oxygen species being shown to trigger apoptosis and degeneration in RGCs which, due to their non-proliferative nature, further emphasize the impact of apoptosis and degeneration (Chrysostomou, Rezania, Trounce, & Crowston, 2013; Ster, Popp, Petrisor, Stan, & Pop, 2014). Genetic downregulation of *FOXC1* in human trabecular meshwork cells and the zebrafish model have been shown to lead to increased rates of apoptosis in trabecular meshwork cells through a decrease in *FOXO1A* expression (Berry et al., 2008). Another *FOXC1* target speculated to have a protective role in human trabecular meshwork cells is *HSPA6,* a heat-shock protein, that has been shown to be reduced when *FOXC1* is knocked down (Berry et al., 2008; Ito et al., 2014). *FOXC1* itself seems to have an anti-apoptotic role against oxidative damage as well (Ito et al., 2014).

We examined the expression of a few *FOXC1* targets known to be expressed in the eye and are known to be involved in response to oxidative stress. *pdgfrα* has been detected in the RGC layer in mice, and has been shown to play a role in the response to oxidative stress and may have a protective effect on RGCs (Johnson et al., 2013; Kanamoto, Rimayanti, & Kiuchi, 2011). Our data shows that in earlier stages of zebrafish development (24 hpf), a subtle downregulation of *pdgfrα* in the lens and periocular mesenchyme is observed in loss of *foxc1* function embryos. This decrease in *pdgfrα* in the pharyngeal arches is pronounced at later stages (48 hpf). This may contribute to craniofacial defects observed in patients with ARS, but given the later stage at which significant *pdgfrα* downregulation occurs, this may have little effect on eye development (Umali et al., 2019). At 32 hpf, no significant changes in the expression of *hspa5* and

hspa9, heat shock proteins implicated in the oxidative stress response, were observed upon loss of *foxc1* function compared to wild type embryos injected with a negative control morpholino. Thus, we do not attribute the loss of cells in the ganglion cell layer and thinning of the optic nerve phenotypes we see in our zebrafish model to susceptibility to oxidative damage. However, we have not directly tested the response of the loss of *foxc1* embryos to oxidative stress challenge, nor looked at ganglion cell loss or optic nerve width in adult zebrafish to provide conclusive data for this hypothesis. A large number of *FOXC1*-regulated genes involved in the oxidative stress response also remain to be tested and understood.

Our expression studies show that in the wildtype zebrafish embryo, *foxo1* and *foxo1b* have overlapping expression in the periocular mesenchyme and pharyngeal arches at 48 hpf, with *foxc1b* being more concentrated in the nasal epithelium and pharyngeal arches. *FOXO1A* is a direct target of *FOXC1,* with previous studies demonstrating inhibition of *FOXC1* to result in downregulation of *FOXO1A* in human trabecular meshwork cells and zebrafish injected with morpholinos against both *foxc1* orthologues (Berry et al., 2008). We replicated these findings in over half of our zebrafish loss of *foxc1* embryos, which was obtained through injection of *foxc1a* morpholino into *foxc1b* mutants. We did not, however, directly test for *foxo1a* and *foxo1b* expression in response to oxidative stress challenges to have a more in-depth understanding of this interaction.

4.6 Morpholino knockdown efficiency in the loss of *foxc1* zebrafish model

Morpholino antisense oligonucleotides are popular tools used to inhibit gene function, particularly in the zebrafish model. They offer significant advantages in that they are

stable due to their resistance to nucleases, are less likely to interact non-specifically as they do not carry a negatively charged backbone, and are titratable to a level that is not lethal to the embryo in cases when a gene is required for development (Bill et al., 2009; Eisen & Smith, 2008; Timme-Laragy, Karchner, & Hahn, 2012). Summerton reports that about 80% of the morpholinos designed and produced by Gene Tools, the exclusive commercial source for research quantities of morpholinos, typically achieve about 70-98% knockdown of the expression of their intended targets due to the extended length and the inherent high affinity of morpholinos for complementary RNA sequences (Summerton, 2007). A quantitative assessment of the knockdown efficiency of morpholinos by Kamachi and colleagues show that the most efficient morpholinos cause >80% inhibition of translation and significant knockdown effects in zebrafish embryos when used singularly at 1-2 ng/embryo, while modestly effective morpholinos may need injection at higher doses to achieve similar knockdown effects (Kamachi, Okuda, & Kondoh, 2008). In most of our experiments, the penetrance of morpholino phenotypes appear to fall within the range of 50-75%. This may indicate the need to increase morpholino dosage in future studies. Furthermore, the simultaneous use of two morpholinos have been shown to result in a synergistic effect, with >90% knockdown efficiency that produces a nearly null phenotype (Kamachi et al., 2008). This may also be kept in mind for future studies. The use of *foxc1a*$^{-/-}$/*foxc1b*$^{-/-}$ mutants may be the next step in confirming phenotypes observed with regards to the effects of loss of *foxc1* on the number of cells in the RGC layer and optic nerve size, and on the expression of *atoh7* and oxidative stress genes. Given that mutants may not show obvious phenotypes compared to morphants as a result of the activation of a compensatory genes (Rossi et al., 2015),

morpholino technologies still prove to be useful in revealing the full effects of the loss of function of genes involved in glaucoma pathogenesis.

4.7 Summary

We demonstrate that loss of *foxc1* function causes reduction of cells in the ganglion cell layer and thinning of the optic nerve in the zebrafish eye. These phenotypes are characteristic of glaucoma in humans. This occurs through disruption of *atoh7,* a key regulator of RGC differentiation. This suggests that aberrant RGC differentiation is a contributing factor to the pathogenesis of early-onset and congenital glaucoma. We also show that loss of *foxc1* function results in downregulation of *fgf19*, a gene involved in retinal neurogenesis, in early eye development. At later stages, loss of *foxc1* results in a decrease in *pdgfrα* and *foxo1a* expression, two genes implicated in the response to oxidative stress, however, given the temporality of this effect, we do not attribute the early-onset phenotypes observed to susceptibility to oxidative damage.

4.8 Future directions

Our findings show a subtle upregulation of *foxc1a* in the pharyngeal arches and a subtle decrease in *foxc1a* expression in the head mesenchyme of 48 hpf *foxc1b* mutant embryos. To provide conclusive data to understand the relationship between the two *FOXC1* paralogs in the zebrafish model, future studies may involve assessing for changes in *foxc1b* expression when *foxc1a* is lost. An understanding of this relationship would be useful for future *FOXC1* studies in zebrafish.

Furthermore, investigation on the effects of *foxc1b* haploinsufficiency on *atoh7* expression may also be pursued, given that our findings show that a slight delay or reduction in *atoh7* expression appears to occur in half of *foxc1b* heterozygotes injected with a control morpholino. A more pronounced reduction is observed in *foxc1b*$^{+/-}$ embryos with *foxc1a* morpholino inhibition, which indicate that *foxc1b* mutations may have a potential dominant negative effect. Given the small number of embryos, repetition of this experiment with a larger sample size in future studies may provide conclusive data on the impacts of *foxc1b* dosage on *atoh7* expression.

In humans, glaucoma is mostly asymptomatic, with vision loss slowly occurring in a peripheral to central manner over a long period of time. Health surveys show that glaucoma may be undetected, and that significant ganglion cell degeneration may progress before defects in visual function are reported by the individuals (Anraku et al., 2011). Our findings show that a reduction in the number of cells in the RGC layer and a thinner optic nerve is observed in the loss of *foxc1* zebrafish embryo. It would be interesting to observe optic nerve morphology and the number of cells in the RGC layer

in the adult loss of *foxc1* zebrafish, before and after exposure to oxidative stress challenges. Furthermore, the impact of the loss of cells in the RGC layer and optic nerve thinning on the visual function of the loss of *foxc1* model would also be interesting to assess, potentially through the use of a variety of assays. Electroretinograms (ERG) measure electrical signals produced by the retina in response to light stimulation and can be used with both zebrafish larvae and adults (Angueyra & Kindt, 2018). This provides a readout on retinal activity. Behavioural assays such as the optokinetic and optomotor responses may also be performed, in which visual stimuli are tracked by eye movements, a behaviour present and reliable as early as 5 dpf (Angueyra & Kindt, 2018). In the case of the optomotor response, swimming in the same direction as the moving stimulus is also monitored.

Finally, given that our findings show a downregulation of *atoh7* when *foxc1* is lost, and possibility of *FGFs* and *FGFR*s, acting as extrinsic cues to ganglion cell differentiation through downstream targets that interact with *atoh7*, the potential network between *foxc1, fgf19,* and *atoh7* in regulating normal RGC differentiation would be worthy to investigate in future studies. Investigating this gene network may also reveal other genes implicated in ganglion cell differentiation and retinal neurogenesis, which may also be implicated in glaucoma.

5 References

Abu-Amero, K. K., & Edward, D. P. (2017). Primary congenital glaucoma. In M. P. Adam, H. H. Ardinger, R. A. Pagon, S. E. Wallace, L. J. H. Bean, K. Stephens & A. Amemiya (Eds.), *GeneReviews((R))* (). Seattle (WA): University of Washington, Seattle. doi:NBK1135 [bookaccession]

Ali, M., McKibbin, M., Booth, A., Parry, D. A., Jain, P., Riazuddin, S. A., Hetjmancik, J. F., Khan, S. N., Firasat, S., Shires, M. (2009). Null mutations in LTBP2 cause primary congenital glaucoma. *The American Journal of Human Genetics, 84*(5), 664-671.

Altshuler, D., Lo Turco, J. J., Rush, J., & Cepko, C. L. (1993). Taurine promotes the differentiation of a vertebrate retinal cell type in vitro. *Development (Cambridge, England), 119*(4), 1317-1328.

Angueyra, J. M., & Kindt, K. S. (2018). Leveraging zebrafish to study retinal degenerations. *Frontiers in Cell and Developmental Biology, 6*

Anraku, A., Jin, Y. P., Butty, Z., Jinapriya, D., Alasbali, T., Mammo, Z., Flanagan, J. G., Trope, G. E. (2011). The Toronto epidemiology glaucoma survey: A pilot study. *Canadian Journal of Ophthalmology.Journal Canadien D'Ophtalmologie, 46*(4), 352-357. doi:10.1016/j.jcjo.2011.06.013 [doi]

Asefa, N. G., Neustaeter, A., Jansonius, N. M., & Snieder, H. (2018). Heritability of glaucoma and glaucoma-related endophenotypes: Systematic review and meta-analysis protocol. *The BMJ, 8*(2), e019049-2017-019049. doi:10.1136/bmjopen-2017-019049 [doi]

Avanesov, A., & Malicki, J. (2010). Analysis of the retina in the zebrafish model. *Methods in cell biology* (pp. 153-204) Elsevier.

Bailey, J. N. C., Loomis, S. J., Kang, J. H., Allingham, R. R., Gharahkhani, P., Khor, C. C., Burdon, K. P., Aschard, H., Chasman, D. I., Igo Jr, R. P. (2016). Genome-wide association analysis identifies TXNRD2, ATXN2 and FOXC1 as susceptibility loci for primary open-angle glaucoma. *Nature Genetics, 48*(2), 189.

Barthel, L. K., & Raymond, P. A. (1990). Improved method for obtaining 3-microns cryosections for immunocytochemistry. *The Journal of Histochemistry and Cytochemistry : Official Journal of the Histochemistry Society, 38*(9), 1383-1388. doi:10.1177/38.9.2201738 [doi]

Berry, F. B., Saleem, R. A., & Walter, M. A. (2002). FOXC1 transcriptional regulation is mediated by N- and C-terminal activation domains and contains a phosphorylated transcriptional inhibitory domain. *The Journal of Biological Chemistry, 277*(12), 10292-10297. doi:10.1074/jbc.M110266200 [doi]

Berry, F. B., Skarie, J. M., Mirzayans, F., Fortin, Y., Hudson, T. J., Raymond, V., Link, B. A., Walter, M. A. (2008). FOXC1 is required for cell viability and resistance to

oxidative stress in the eye through the transcriptional regulation of FOXO1A. *Human Molecular Genetics, 17*(4), 490-505. doi:ddm326 [pii]

Bill, B. R., Petzold, A. M., Clark, K. J., Schimmenti, L. A., & Ekker, S. C. (2009). A primer for morpholino use in zebrafish. *Zebrafish, 6*(1), 69-77.

Blythe, D., Hand, N. M., Jackson, P., Barrans, S. L., Bradbury, R. D., & Jack, A. S. (1997). Use of methyl methacrylate resin for embedding bone marrow trephine biopsy specimens. *Journal of Clinical Pathology, 50*(1), 45-49. doi:10.1136/jcp.50.1.45 [doi]

Boije, H., MacDonald, R. B., & Harris, W. A. (2014). Reconciling competence and transcriptional hierarchies with stochasticity in retinal lineages. *Current Opinion in Neurobiology, 27*, 68-74.

Branchek, T., & Bremiller, R. (1984). The development of photoreceptors in the zebrafish, brachydanio rerio. I. structure. *Journal of Comparative Neurology, 224*(1), 107-115.

Brown, N. L., Kanekar, S., Vetter, M. L., Tucker, P. K., Gemza, D. L., & Glaser, T. (1998). Math5 encodes a murine basic helix-loop-helix transcription factor expressed during early stages of retinal neurogenesis. *Development (Cambridge, England), 125*(23), 4821-4833.

Brown, N. L., Patel, S., Brzezinski, J., & Glaser, T. (2001). Math5 is required for retinal ganglion cell and optic nerve formation. *Development (Cambridge, England), 128*(13), 2497-2508.

Burgoyne, C. F., Downs, J. C., Bellezza, A. J., Suh, J. F., & Hart, R. T. (2005). The optic nerve head as a biomechanical structure: A new paradigm for understanding the role of IOP-related stress and strain in the pathophysiology of glaucomatous optic nerve head damage. *Progress in Retinal and Eye Research, 24*(1), 39-73.

Buys, Y. M. (2011). The need for "made in canada" glaucoma epidemiology data. *Canadian Journal of Ophthalmology.Journal Canadien D'Ophtalmologie, 46*(4), 300-302. doi:10.1016/j.jcjo.2011.06.003 [doi]

Buys, Y. M. (2013). Glaucoma in canada: Challenges and changing paradigms. *Glaucoma Today,*

Carnes, M. U., Liu, Y. P., Allingham, R. R., Whigham, B. T., Havens, S., Garrett, M. E., Qiao, C., Katsanis, N., Wiggs, J. L., Pasquale, L. R. (2014). Discovery and functional annotation of SIX6 variants in primary open-angle glaucoma. *PLoS Genetics, 10*(5), e1004372.

Cascella, R., Strafella, C., Germani, C., Novelli, G., Ricci, F., Zampatti, S., & Giardina, E. (2015). The genetics and the genomics of primary congenital glaucoma. *BioMed Research International, 2015*

Cepko, C. L. (1999). The roles of intrinsic and extrinsic cues and bHLH genes in the determination of retinal cell fates. *Current Opinion in Neurobiology, 9*(1), 37-46.

Cepko, C. L., Austin, C. P., Yang, X., Alexiades, M., & Ezzeddine, D. (1996). Cell fate determination in the vertebrate retina. *Proceedings of the National Academy of Sciences of the United States of America, 93*(2), 589-595.

Chang, D. F. (2011). Ophthalmologic examination. In P. Riordan-Eva, & E. T. Cunningham (Eds.), *Vaughan & asbury's general ophthalmology* (18th ed.. ed., pp. 27). New York, N.Y.; New York; Toronto: New York, N.Y. : McGraw-Hill Education LLC.

Cherry, T. J., Trimarchi, J. M., Stadler, M. B., & Cepko, C. L. (2009). Development and diversification of retinal amacrine interneurons at single cell resolution. *Proceedings of the National Academy of Sciences of the United States of America, 106*(23), 9495-9500. doi:10.1073/pnas.0903264106 [doi]

Chi, Z., Yasumoto, F., Sergeev, Y., Minami, M., Obazawa, M., Kimura, I., Takada, Y., Iwata, T. (2010). Mutant WDR36 directly affects axon growth of retinal ganglion cells leading to progressive retinal degeneration in mice. *Human Molecular Genetics, 19*(19), 3806-3815.

Choosing Wisely NL. (2017). Community care: The diagnosis of spondyloarthritis using HLA-B27. *Practice points, volume 3* (pp. 20). Memorial University of Newfoundland, St. John's, NL, Canada: Quality Care NL/Choosing Wisely NL.

Chou, T., Tomarev, S., & Porciatti, V. (2014). Transgenic mice expressing mutated Tyr437His human myocilin develop progressive loss of retinal ganglion cell electrical responsiveness and axonopathy with normal iop. *Investigative Ophthalmology & Visual Science, 55*(9), 5602-5609.

Choudhary, D., Jansson, I., Rezaul, K., Han, D. K. M., Sarfarazi, M., & Schenkman, J. B. (2007). Cyp1b1 protein in the mouse eye during development: An immunohistochemical study. *Drug Metabolism and Disposition: The Biological Fate of Chemicals, 35*(6), 987. doi:10.1124/dmd.106.014282

Chrysostomou, V., Rezania, F., Trounce, I. A., & Crowston, J. G. (2013). Oxidative stress and mitochondrial dysfunction in glaucoma. *Current Opinion in Pharmacology, 13*(1), 12-15.

Conte, I., Carrella, S., Avellino, R., Karali, M., Marco-Ferreres, R., Bovolenta, P., & Banfi, S. (2010). miR-204 is required for lens and retinal development via Meis2 targeting. *Proceedings of the National Academy of Sciences of the United States of America, 107*(35), 15491-15496. doi:10.1073/pnas.0914785107 [doi]

Cruess, A. F., Gordon, K. D., Bellan, L., Mitchell, S., & Pezzullo, M. L. (2011). The cost of vision loss in canada. 2. results. *Canadian Journal of Ophthalmology, 46*(4), 315-318.

Ding, S., Kumar, S., & Mok, P. (2017). Cellular reparative mechanisms of mesenchymal stem cells for retinal diseases. *International Journal of Molecular Sciences, 18*(8), 1406.

Downs, J. C., Roberts, M. D., & Sigal, I. A. (2011). Glaucomatous cupping of the lamina cribrosa: A review of the evidence for active progressive remodeling as a mechanism. *Experimental Eye Research, 93*(2), 133-140.

Du, R., Huang, H., Fan, L., Li, X., Xia, K., & Xiang, R. (2016). A novel mutation of FOXC1 (R127L) in an Axenfeld–Rieger syndrome family with glaucoma and multiple congenital heart diseases. *Ophthalmic Genetics, 37*(1), 111-115.

Edwards, M. M., McLeod, D. S., Li, R., Grebe, R., Bhutto, I., Mu, X., & Lutty, G. A. (2012). The deletion of Math5 disrupts retinal blood vessel and glial development in mice. *Experimental Eye Research, 96*(1), 147-156.

Eisen, J. S., & Smith, J. C. (2008). Controlling morpholino experiments: Don't stop making antisense. *Development (Cambridge, England), 135*(10), 1735-1743. doi:10.1242/dev.001115 [doi]

Ezzeddine, Z. D., Yang, X., DeChiara, T., Yancopoulos, G., & Cepko, C. L. (1997). Postmitotic cells fated to become rod photoreceptors can be respecified by CNTF treatment of the retina. *Development (Cambridge, England), 124*(5), 1055-1067.

Fadool, J. M., & Dowling, J. E. (2008). Zebrafish: A model system for the study of eye genetics. *Progress in Retinal and Eye Research, 27*(1), 89-110.

Faiq, M., Sharma, R., Dada, R., Mohanty, K., Saluja, D., & Dada, T. (2013). Genetic, biochemical and clinical insights into primary congenital glaucoma. *Journal of Current Glaucoma Practice, 7*(2), 66-84. doi:10.5005/jp-journals-10008-1140 [doi]

Fletcher, E. C., Chong, N. V., Augsburger, J. J., & Correa, Z. M. (2011). Retina. In P. Riordan-Eva, & E. T. Cunningham (Eds.), *Vaughan & asbury's general ophthalmology* (18th ed.. ed., pp. 190). New York, N.Y.; New York; Toronto: New York, N.Y. : McGraw-Hill Education LLC.

French, C. R., Seshadri, S., Destefano, A. L., Fornage, M., Arnold, C. R., Gage, P. J., Skarie, J. M., Dobyns, W. B., Millen, K. J., Liu, T. (2014). Mutation of FOXC1 and PITX2 induces cerebral small-vessel disease. *The Journal of Clinical Investigation, 124*(11), 4877-4881.

Friedman, J. S., & Walter, M. A. (1999). Glaucoma genetics, present and future. *Clinical Genetics, 55*(2), 71-79.

Fruttiger, M., Calver, A. R., Krüger, W. H., Mudhar, H. S., Michalovich, D., Takakura, N., Nishikawa, S. I., Richardson, W. D. (1996). PDGF mediates a neuron–astrocyte interaction in the developing retina. *Neuron, 17*(6), 1117-1131.

Fuhrmann, S., Levine, E. M., & Reh, T. A. (2000). Extraocular mesenchyme patterns the optic vesicle during early eye development in the embryonic chick. *Development (Cambridge, England), 127*(21), 4599-4609.

Fujikawa, K., Iwata, T., Inoue, K., Akahori, M., Kadotani, H., Fukaya, M., Watanabe, M., Chang, Q., Barnett, E. M., Swat, W. (2010). VAV2 and VAV3 as candidate disease genes for spontaneous glaucoma in mice and humans. *PloS One, 5*(2), e9050. doi:10.1371/journal.pone.0009050 [doi]

Fujitani, Y., Fujitani, S., Luo, H., Qiu, F., Burlison, J., Long, Q., Kawaguchi, Y., Edlund, H., MacDonald, R. J., Furukawa, T., Fujikado, T., Magnuson, M. A., Xiang, M., Wright, C. V. (2006). Ptf1a determines horizontal and amacrine cell fates during mouse retinal development. *Development (Cambridge, England), 133*(22), 4439-4450. doi:133/22/4439 [pii]

Gage, P. J., Rhoades, W., Prucka, S. K., & Hjalt, T. (2005). Fate maps of neural crest and mesoderm in the mammalian eye. *Investigative Ophthalmology & Visual Science, 46*(11), 4200-4208.

Gage, P. J., Suh, H., & Camper, S. A. (1999). Dosage requirement of Pitx2 for development of multiple organs. *Development (Cambridge, England), 126*(20), 4643-4651.

Gallenberger, M., Meinel, D. M., Kroeber, M., Wegner, M., Milkereit, P., Bösl, M. R., & Tamm, E. R. (2010). Lack of WDR36 leads to preimplantation embryonic lethality in

mice and delays the formation of small subunit ribosomal RNA in human cells in vitro. *Human Molecular Genetics, 20*(3), 422-435.

Gao, S., & Jakobs, T. C. (2016). Mice homozygous for a deletion in the glaucoma susceptibility locus INK4 show increased vulnerability of retinal ganglion cells to elevated intraocular pressure. *The American Journal of Pathology, 186*(4), 985-1005.

Gharahkhani, P., Burdon, K. P., Fogarty, R., Sharma, S., Hewitt, A. W., Martin, S., Law, M. H., Cremin, K., Bailey, J. N. C., Loomis, S. J. (2014). Common variants near ABCA1, AFAP1 and GMDS confer risk of primary open-angle glaucoma. *Nature Genetics, 46*(10), 1120.

Glass, A. S., & Dahm, R. (2004). The zebrafish as a model organism for eye development. *Ophthalmic Research, 36*(1), 4-24. doi:10.1159/000076105 [doi]

Goel, M., Picciani, R. G., Lee, R. K., & Bhattacharya, S. K. (2010). Aqueous humor dynamics: A review. *The Open Ophthalmology Journal, 4*, 52-59. doi:10.2174/1874364101004010052 [doi]

Gould, D. B., & John, S. W. M. (2002). Anterior segment dysgenesis and the developmental glaucomas are complex traits. *Human Molecular Genetics, 11*(10), 1185-1193.

Gould, D. B., Mears, A. J., Pearce, W. G., & Walter, M. A. (1997). Autosomal dominant axenfeld-rieger anomaly maps to 6p25. *American Journal of Human Genetics, 61*(3), 765-768. doi:S0002-9297(07)64340-7 [pii]

Gould, D. B., Smith, R. S., & John, S. W. M. (2004). Anterior segment development relevant to glaucoma. *The International Journal of Developmental Biology, 48*(8-9), 1015-1029. doi:041865dg [pii]

Govindarajan, V., Ito, M., Makarenkova, H. P., Lang, R. A., & Overbeek, P. A. (2000). Endogenous and ectopic gland induction by FGF-10. *Developmental Biology, 225*(1), 188-200.

Gray, M. P., Smith, R. S., Soules, K. A., John, S. W., & Link, B. A. (2009). The aqueous humor outflow pathway of zebrafish. *Investigative Ophthalmology & Visual Science, 50*(4), 1515-1521.

Green, K. (2001). In Green K. (Ed.), *Free radicals and aging of anterior segment tissues of the eye*

Haleem, M. S., Han, L., Van Hemert, J., & Li, B. (2013). Automatic extraction of retinal features from colour retinal images for glaucoma diagnosis: A review. *Computerized Medical Imaging and Graphics, 37*(7-8), 581-596.

Harwerth, R., Wheat, J., Fredette, M., & Anderson, D. (2010). Linking structure and function in glaucoma. *Progress in Retinal and Eye Research, 29*(4), 249-271.

Hay, E. D. (1980). Development of the vertebrate cornea. *International review of cytology* (pp. 263-322) Elsevier.

Helander, K. (1983). Thickness variations within individual paraffin and glycol methacrylate sections. *Journal of Microscopy, 132*(2), 223-227.

Hernandez-Bejarano, M., Gestri, G., Spawls, L., Nieto-Lopez, F., Picker, A., Tada, M., Brand, M., Bovolenta, P., Wilson, S. W., Cavodeassi, F. (2015). Opposing shh and fgf signals initiate nasotemporal patterning of the zebrafish retina. *Development (Cambridge, England), 142*(22), 3933-3942. doi:10.1242/dev.125120 [doi]

Howe, K., Clark, M. D., Torroja, C. F., Torrance, J., Berthelot, C., Muffato, M., Collins, J. E., Humphray, S., McLaren, K., Matthews, L. (2013). The zebrafish reference genome sequence and its relationship to the human genome. *Nature, 496*(7446), 498-503.

Hu, M., & Easter Jr, S. S. (1999). Retinal neurogenesis: The formation of the initial central patch of postmitotic cells. *Developmental Biology, 207*(2), 309-321.

Iglesias, A. I., Springelkamp, H., van der Linde, H., Severijnen, L., Amin, N., Oostra, B., Kockx, C. E. M., van den Hout, M. C. G. N., van Ijcken, W. F. J., Hofman, A. (2013). Exome sequencing and functional analyses suggest that SIX6 is a gene involved in an altered proliferation–differentiation balance early in life and optic nerve degeneration at old age. *Human Molecular Genetics, 23*(5), 1320-1332.

Ito, Y., Goping, I., Berry, F., & Walter, M. (2014). Dysfunction of the stress-responsive FOXC1 transcription factor contributes to the earlier-onset glaucoma observed in axenfeld-rieger syndrome patients. *Cell Death & Disease, 5*(2), e1069.

Itoh, N., & Ornitz, D. M. (2004). Evolution of the fgf and fgfr gene families. *TRENDS in Genetics, 20*(11), 563-569.

Jarman, A. P., Sun, Y., Jan, L. Y., & Jan, Y. N. (1995). Role of the proneural gene, atonal, in formation of drosophila chordotonal organs and photoreceptors. *Development (Cambridge, England), 121*(7), 2019-2030.

Johnson, T. V., DeKorver, N. W., Levasseur, V. A., Osborne, A., Tassoni, A., Lorber, B., Heller, J. P., Villasmil, R., Bull, N. D., Martin, K. R. (2013). Identification of retinal ganglion cell neuroprotection conferred by platelet-derived growth factor through analysis of the mesenchymal stem cell secretome. *Brain, 137*(2), 503-519.

Kachaner, D., Genin, P., Laplantine, E., & Weil, R. (2012). Toward an integrative view of optineurin functions. *Cell Cycle, 11*(15), 2808-2818.

Kamachi, Y., Okuda, Y., & Kondoh, H. (2008). Quantitative assessment of the knockdown efficiency of morpholino antisense oligonucleotides in zebrafish embryos using a luciferase assay. *Genesis, 46*(1), 1-7.

Kanamoto, T., Rimayanti, U., & Kiuchi, Y. (2011). Platelet-derived growth factor receptor alpha is associated with oxidative stress-induced retinal cell death. *Current Eye Research, 36*(4), 336-340.

Kanekar, S., Perron, M., Dorsky, R., Harris, W. A., Jan, L. Y., Jan, Y. N., & Vetter, M. L. (1997). Xath5 participates in a network of bHLH genes in the developing xenopus retina. *Neuron, 19*(5), 981-994.

Katoh, M., & Katoh, M. (2003). Evolutionary conservation of CCND1-ORAOV1-FGF19-FGF4 locus from zebrafish to human. *International Journal of Molecular Medicine, 12*(1), 45-50.

Kaur, K., Reddy, A., Mukhopadhyay, A., Mandal, A., Hasnain, S., Ray, K., Thomas, R., Balasubramanian, D., Chakrabarti, S. (2005). Myocilin gene implicated in primary congenital glaucoma. *Clinical Genetics, 67*(4), 335-340.

Kay, J. N., Finger-Baier, K. C., Roeser, T., Staub, W., & Baier, H. (2001). Retinal ganglion cell genesis requires lakritz, a zebrafish atonal homolog. *Neuron, 30*(3), 725-736.

Khan, K., Logan, C. V., McKibbin, M., Sheridan, E., Elcioglu, N. H., Yenice, O., Parry, D. A., Fernandez-Fuentes, N., Abdelhamed, Z. I. A., Al-Maskari, A. (2011). Next generation sequencing identifies mutations in atonal homolog 7 (ATOH7) in families with global eye developmental defects. *Human Molecular Genetics, 21*(4), 776-783.

Khor, C. C., Do, T., Jia, H., Nakano, M., George, R., Abu-Amero, K., Duvesh, R., Chen, L. J., Li, Z., Nongpiur, M. E. (2016). Genome-wide association study identifies five new susceptibility loci for primary angle closure glaucoma. *Nature Genetics, 48*(5), 556.

Kidson, S. H., Kume, T., Deng, K., Winfrey, V., & Hogan, B. L. (1999). The forkhead/winged-helix gene, Mf1, is necessary for the normal development of the cornea and formation of the anterior chamber in the mouse eye. *Developmental Biology, 211*(2), 306-322.

Kim, K. E., & Park, K. (2016). Update on the prevalence, etiology, diagnosis, and monitoring of normal-tension glaucoma. *The Asia-Pacific Journal of Ophthalmology, 5*(1), 23-31.

Kimmel, C. B., Ballard, W. W., Kimmel, S. R., Ullmann, B., & Schilling, T. F. (1995). Stages of embryonic development of the zebrafish. *Developmental Dynamics, 203*(3), 253-310.

Kolb, H. (1995). Simple anatomy of the retina. In H. Kolb, E. Fernandez & R. Nelson (Eds.), *Webvision: The organization of the retina and visual system* (). Salt Lake City (UT): Webvision. doi:NBK11534 [bookaccession]

Kume, T., Deng, K., Winfrey, V., Gould, D. B., Walter, M. A., & Hogan, B. L. (1998). The forkhead/winged helix gene Mf1 is disrupted in the pleiotropic mouse mutation congenital hydrocephalus. *Cell, 93*(6), 985-996.

Kurose, H., Okamoto, M., Shimizu, M., Bito, T., Marcelle, C., Noji, S., & Ohuchi, H. (2005). FGF19-FGFR4 signaling elaborates lens induction with the FGF8-L-Maf cascade in the chick embryo. *Development, Growth & Differentiation, 47*(4), 213-223.

Lehmann, O. J., Ebenezer, N. D., Ekong, R., Ocaka, L., Mungall, A. J., Fraser, S., McGill, J. I., Hitchings, R. A., Khaw, P. T., Sowden, J. C. (2002). Ocular developmental abnormalities and glaucoma associated with interstitial 6p25 duplications and deletions. *Investigative Ophthalmology & Visual Science, 43*(6), 1843-1849.

Lehmann, O. J., Ebenezer, N. D., Jordan, T., Fox, M., Ocaka, L., Payne, A., Leroy, B. P., Clark, B. J., Hitchings, R. A., Povey, S. (2000). Chromosomal duplication involving the forkhead transcription factor gene FOXC1 causes iris hypoplasia and glaucoma. *The American Journal of Human Genetics, 67*(5), 1129-1135.

Lelievre, E., Lek, M., Boije, H., Houille-Vernes, L., Brajeul, V., Slembrouck, A., Roger, J. E., Sahel, J., Matter, J., Sennlaub, F. (2011). Ptf1a/rbpj complex inhibits ganglion cell fate and drives the specification of all horizontal cell subtypes in the chick retina. *Developmental Biology, 358*(2), 296-308.

Leske, M. C., Connell, A., Wu, S., Hyman, L. G., & Schachat, A. P. (1995). Risk factors for open-angle glaucoma: The barbados eye study. *Archives of Ophthalmology, 113*(7), 918-924.

Levene, R. Z., Workman, P. L., Broder, S. W., & Hirschhorn, K. (1970). Heritability of ocular pressure. *Archives of Ophthalmology, 84*(6), 730-734.

Li, S., Fang, J. H., & Jiang, F. G. (2010). Histological observation of RGCs and optic nerve injury in acute ocular hypertension rats. *International Journal of Ophthalmology, 3*(4), 311-315. doi:10.3980/j.issn.2222-3959.2010.04.08 [doi]

Lidster, K., Jackson, S. J., Ahmed, Z., Munro, P., Coffey, P., Giovannoni, G., Baker, M. D., Baker, D. (2013). Neuroprotection in a novel mouse model of multiple sclerosis. *PloS One, 8*(11), e79188. doi:10.1371/journal.pone.0079188 [doi]

Link, B. A., Gray, M. P., Smith, R. S., & John, S. W. (2004). Intraocular pressure in zebrafish: Comparison of inbred strains and identification of a reduced melanin mutant with raised IOP. *Investigative Ophthalmology & Visual Science, 45*(12), 4415-4422.

Liu, Y., & Allingham, R. R. (2017). Major review: Molecular genetics of primary open-angle glaucoma. *Experimental Eye Research, 160*, 62-84.

Mabuchi, F., Sakurada, Y., Kashiwagi, K., Yamagata, Z., Iijima, H., & Tsukahara, S. (2012). Association between genetic variants associated with vertical cup-to-disc ratio and phenotypic features of primary open-angle glaucoma. *Ophthalmology, 119*(9), 1819-1825.

Mabuchi, F., Sakurada, Y., Kashiwagi, K., Yamagata, Z., Iijima, H., & Tsukahara, S. (2015). Involvement of genetic variants associated with primary open-angle glaucoma in pathogenic mechanisms and family history of glaucoma. *American Journal of Ophthalmology, 159*(3), 437-444. e2.

Macgregor, S., Hewitt, A. W., Hysi, P. G., Ruddle, J. B., Medland, S. E., Henders, A. K., Gordon, S. D., Andrew, T., McEvoy, B., Sanfilippo, P. G. (2010). Genome-wide association identifies ATOH7 as a major gene determining human optic disc size. *Human Molecular Genetics, 19*(13), 2716-2724.

Masai, I., Stemple, D. L., Okamoto, H., & Wilson, S. W. (2000). Midline signals regulate retinal neurogenesis in zebrafish. *Neuron, 27*(2), 251-263.

McCabe, K. L., Gunther, E. C., & Reh, T. A. (1999). The development of the pattern of retinal ganglion cells in the chick retina: Mechanisms that control differentiation. *Development (Cambridge, England), 126*(24), 5713-5724.

McMahon, C., Semina, E., & Link, B. (2004). Using zebrafish to study the complex genetics of glaucoma. *Comparative Biochemistry and Physiology Part C: Toxicology & Pharmacology, 138*(3), 343-350.

Mears, A. J., Jordan, T., Mirzayans, F., Dubois, S., Kume, T., Parlee, M., Ritch, R., Koop, B., Kuo, W., Collins, C. (1998). Mutations of the forkhead/winged-helix gene, FKHL7, in patients with axenfeld-rieger anomaly. *The American Journal of Human Genetics, 63*(5), 1316-1328.

Micheal, S., Siddiqui, S. N., Zafar, S. N., Villanueva-Mendoza, C., Cortés-González, V., Khan, M. I., & den Hollander, A. I. (2016). A novel homozygous mutation in FOXC1 causes axenfeld rieger syndrome with congenital glaucoma. *PloS One, 11*(7), e0160016.

Mirzayans, F., Gould, D. B., Heon, E., Billingsley, G. D., Cheung, J. C., Mears, A. J., & Walter, M. A. (2000). Axenfeld-rieger syndrome resulting from mutation of the FKHL7 gene on chromosome 6p25. *European Journal of Human Genetics: EJHG, 8*(1), 71.

Miyake, A., Nakayama, Y., Konishi, M., & Itoh, N. (2005). Fgf19 regulated by hh signaling is required for zebrafish forebrain development. *Developmental Biology, 288*(1), 259-275.

Monemi, S., Spaeth, G., DaSilva, A., Popinchalk, S., Ilitchev, E., Liebmann, J., Ritch, R., Héon, E., Crick, R. P., Child, A. (2005). Identification of a novel adult-onset primary open-angle glaucoma (POAG) gene on 5q22. 1. *Human Molecular Genetics, 14*(6), 725-733.

Mu, X., & Klein, W. H. (2004). A gene regulatory hierarchy for retinal ganglion cell specification and differentiation. Paper presented at the *Seminars in Cell & Developmental Biology, , 15*(1) 115-123.

Nakayama, Y., Miyake, A., Nakagawa, Y., Mido, T., Yoshikawa, M., Konishi, M., & Itoh, N. (2008). Fgf19 is required for zebrafish lens and retina development. *Developmental Biology, 313*(2), 752-766.

Newman, G. R., & Hobot, J. A. (1999). Resins for combined light and electron microscopy: A half century of development. *The Histochemical Journal, 31*(8), 495-505.

Nishimura, D. Y., Searby, C. C., Alward, W. L., Walton, D., Craig, J. E., Mackey, D. A., Kawase, K., Kanis, A. B., Patil, S. R., Stone, E. M. (2001). A spectrum of FOXC1 mutations suggests gene dosage as a mechanism for developmental defects of the anterior chamber of the eye. *The American Journal of Human Genetics, 68*(2), 364-372.

Nishimura, D. Y., Swiderski, R. E., Alward, W. L., Searby, C. C., Patil, S. R., Bennet, S. R., Kanis, A. B., Gastier, J. M., Stone, E. M., Sheffield, V. C. (1998). The forkhead transcription factor gene FKHL7 is responsible for glaucoma phenotypes which map to 6p25. *Nature Genetics, 19*(2), 140-147.

OMIM®. (2019). *Online mendelian inheritance in man*. Baltimore, MD: McKusick-Nathans Institute of Genetic Medicine, Johns Hopkins University.

Paylakhi, S. H., Moazzeni, H., Yazdani, S., Rassouli, P., Arefian, E., Jaberi, E., Arash, E. H., Gilani, A. S., Fan, J., April, C. (2013). FOXC1 in human trabecular meshwork

cells is involved in regulatory pathway that includes miR-204, MEIS2, and ITGβ1. *Experimental Eye Research, 111*, 112-121.

Perruccio, A. V., Badley, E. M., & Trope, G. E. (2007). Self-reported glaucoma in canada: Findings from population-based surveys, 1994-2003. *Canadian Journal of Ophthalmology.Journal Canadien D'Ophtalmologie, 42*(2), 219-226. doi:S0008-4182(07)80076-7 [pii]

Philomenadin, F. S., Asokan, R., Viswanathan, N., George, R., Lingam, V., & Sarangapani, S. (2015). Genetic association of SNPs near ATOH7, CARD10, CDKN2B, CDC7 and SIX1/SIX6 with the endophenotypes of primary open angle glaucoma in indian population. *PloS One, 10*(3), e0119703.

Prasov, L., Masud, T., Khaliq, S., Mehdi, S. Q., Abid, A., Oliver, E. R., Silva, E. D., Lewanda, A., Brodsky, M. C., Borchert, M. (2012). ATOH7 mutations cause autosomal recessive persistent hyperplasia of the primary vitreous. *Human Molecular Genetics, 21*(16), 3681-3694.

Quigley, H. A. (2011). Glaucoma. *The Lancet, 377*(9774), 1367-1377. doi:10.1016/S0140-6736(10)61423-7

Quigley, H. A., & Broman, A. T. (2006). The number of people with glaucoma worldwide in 2010 and 2020. *The British Journal of Ophthalmology, 90*(3), 262-267. doi:90/3/262 [pii]

Ramachandran, S., Morris, S. M., Devamanoharan, P., Henein, M., & Varma, S. D. (1991). Radio-isotopic determination of hydrogen peroxide in aqueous humor and urine. *Experimental Eye Research, 53*(4), 503-506.

Ramdas, W. D., Van Koolwijk, L. M., Ikram, M. K., Jansonius, N. M., de Jong, P. T., Bergen, A. A. B., Isaacs, A., Amin, N., Aulchenko, Y. S., Wolfs, R. C. W. (2010). A genome-wide association study of optic disc parameters. *PLoS Genetics, 6*(6), e1000978.

Ramdas, W. D., van Koolwijk, L. M., Lemij, H. G., Pasutto, F., Cree, A. J., Thorleifsson, G., Janssen, S. F., Jacoline, T. B., Amin, N., Rivadeneira, F. (2011). Common genetic variants associated with open-angle glaucoma. *Human Molecular Genetics, 20*(12), 2464-2471.

Renninger, S., Schonthaler, H., Neuhauss, S., & Dahm, R. (2011). Investigating the genetics of visual processing, function and behaviour in zebrafish. *Neurogenetics, 12*(2), 97-116. doi:10.1007/s10048-011-0273-x

Rezaie, T., Child, A., Hitchings, R., Brice, G., Miller, L., Coca-Prados, M., Heon, E., Krupin, T., Ritch, R., Kreutzer, D., Crick, R. P., Sarfarazi, M. (2002). Adult-onset primary open-angle glaucoma caused by mutations in optineurin. *Science (New York, N.Y.), 295*(5557), 1077-1079. doi:10.1126/science.1066901 [doi]

Richardson, R., Tracey-White, D., Webster, A., & Moosajee, M. (2017). The zebrafish eye—a paradigm for investigating human ocular genetics. *Eye, 31*(1), 68-86.

Richer, S. P., & Rose, R. (1998). Water soluble antioxidants in mammalian aqueous humor: Interaction with UV B and hydrogen peroxide. *Vision Research, 38*(19), 2881-2888.

Riordan-Eva, P. (2011). Anatomy and embryology of the eye. In P. Riordan-Eva, & E. T. Cunningham (Eds.), *Vaughan & asbury's general ophthalmology* (18th ed.. ed., pp. 1). New York, N.Y.; New York; Toronto: New York, N.Y. : McGraw-Hill Education LLC.

Robu, M. E., Larson, J. D., Nasevicius, A., Beiraghi, S., Brenner, C., Farber, S. A., & Ekker, S. C. (2007). P53 activation by knockdown technologies. *PLoS Genetics, 3*(5), e78.

Rossi, A., Kontarakis, Z., Gerri, C., Nolte, H., Hölper, S., Krüger, M., & Stainier, D. Y. (2015). Genetic compensation induced by deleterious mutations but not gene knockdowns. *Nature, 524*(7564), 230-233.

Saleem, R. A., Banerjee-Basu, S., Berry, F. B., Baxevanis, A. D., & Walter, M. A. (2001). Analyses of the effects that disease-causing missense mutations have on the structure and function of the winged-helix protein FOXC1. *The American Journal of Human Genetics, 68*(3), 627-641.

Saleem, R. A., Banerjee-Basu, S., Murphy, T. C., Baxevanis, A., & Walter, M. A. (2004). Essential structural and functional determinants within the forkhead domain of FOXC1. *Nucleic Acids Research, 32*(14), 4182-4193.

Sanfilippo, P. G., Hewitt, A. W., Hammond, C. J., & Mackey, D. A. (2010). The heritability of ocular traits. *Survey of Ophthalmology, 55*(6), 561-583.

Schmitt, E. A., & Dowling, J. E. (1994). Early- eye morphogenesis in the zebrafish, brachydanio rerio. *Journal of Comparative Neurology, 344*(4), 532-542. doi:10.1002/cne.903440404

Schneider, C. A., Rasband, W. S., & Eliceiri, K. W. (2012). NIH image to ImageJ: 25 years of image analysis. *Nature Methods, 9*(7), 671.

Schuhmacher, L., Albadri, S., Ramialison, M., & Poggi, L. (2011). Evolutionary relationships and diversification of barhl genes within retinal cell lineages. *BMC Evolutionary Biology, 11*(1), 340.

Seo, S., Singh, H. P., Lacal, P. M., Sasman, A., Fatima, A., Liu, T., Schultz, K. M., Losordo, D. W., Lehmann, O. J., Kume, T. (2012). Forkhead box transcription factor FoxC1 preserves corneal transparency by regulating vascular growth. *Proceedings of the National Academy of Sciences of the United States of America, 109*(6), 2015-2020. doi:10.1073/pnas.1109540109 [doi]

Skarie, J. M., & Link, B. A. (2008). The primary open-angle glaucoma gene WDR36 functions in ribosomal RNA processing and interacts with the p53 stress–response pathway. *Human Molecular Genetics, 17*(16), 2474-2485.

Skarie, J. M., & Link, B. A. (2009). FoxC1 is essential for vascular basement membrane integrity and hyaloid vessel morphogenesis. *Investigative Ophthalmology & Visual Science, 50*(11), 5026-5034.

Slowicka, K., & van Loo, G. (2018). Optineurin functions for optimal immunity. *Frontiers in Immunology, 9*, 769.

Slowicka, K., Vereecke, L., & van Loo, G. (2016). Cellular functions of optineurin in health and disease. *Trends in Immunology, 37*(9), 621-633.

Smith, R. S., Zabaleta, A., Kume, T., Savinova, O. V., Kidson, S. H., Martin, J. E., Nishimura, D. Y., Alward, W. L. M., Hogan, B. L. M., John, S. W. M. (2000). Haploinsufficiency of the transcription factors FOXC1 and FOXC2 results in aberrant ocular development. *Human Molecular Genetics, 9*(7), 1021-1032.

Soules, K. A., & Link, B. A. (2005). Morphogenesis of the anterior segment in the zebrafish eye. *BMC Developmental Biology, 5*(1), 12.

Stamper, R. L. (2009). In Lieberman M. F., Drake M. V. and Becker B. (Eds.), *Becker-shaffer's diagnosis and therapy of the glaucomas* (8th ed. / Robert L. Stamper, Marc F. Lieberman, Michael V. Drake.. ed.). Edinburgh]: Edinburgh : Mosby/Elsevier.

Ster, A. M., Popp, R. A., Petrisor, F. M., Stan, C., & Pop, V. I. (2014). The role of oxidative stress and vascular insufficiency in primary open angle glaucoma. *Clujul Medical, 87*(3), 143.

Stone, E. M., Fingert, J. H., Alward, W. L., Nguyen, T. D., Polansky, J. R., Sunden, S. L., Nishimura, D. Y., Clark, A. F., Nystuen, A., Nichols, B. E., Mackey, D. A., Ritch, R., Kalenak, J. W., Craven, E. R., Sheffield, V. C. (1997). Identification of a gene that causes primary open angle glaucoma. *Science (New York, N.Y.), 275*(5300), 668-670. doi:10.1126/science.275.5300.668 [doi]

Straznicky, K., & Gaze, R. M. (1971). The growth of the retina in xenopus laevis: An autoradiographic study. *Journal of Embryology and Experimental Morphology, 26*(1), 67-79.

Summerton, J. E. (2007). Morpholino, siRNA, and S-DNA compared: Impact of structure and mechanism of action on off-target effects and sequence specificity. *Current Topics in Medicinal Chemistry, 7*(7), 651-660.

Surgucheva, I., & Surguchov, A. (2011). Expression of caveolin in trabecular meshwork cells and its possible implication in pathogenesis of primary open angle glaucoma. *Molecular Vision, 17*, 2878-2888. doi:312 [pii]

Tamimi, Y., Lines, M., Coca-Prados, M., & Walter, M. A. (2004). Identification of target genes regulated by FOXC1 using nickel agarose–based chromatin enrichment. *Investigative Ophthalmology & Visual Science, 45*(11), 3904-3913.

Tamimi, Y., Skarie, J. M., Footz, T., Berry, F. B., Link, B. A., & Walter, M. A. (2006). FGF19 is a target for FOXC1 regulation in ciliary body-derived cells. *Human Molecular Genetics, 15*(21), 3229-3240.

Tham, Y., Li, X., Wong, T. Y., Quigley, H. A., Aung, T., & Cheng, C. (2014). Global prevalence of glaucoma and projections of glaucoma burden through 2040: A systematic review and meta-analysis. *Ophthalmology, 121*(11), 2081-2090.

Thisse, B., & Thisse, C. (2014). In situ hybridization on whole-mount zebrafish embryos and young larvae. In B. Nielsen (Ed.), *In situ hybridization protocols. methods in molecular biology (methods and protocols)* (pp. 53-67). New York, NY: Humana Press.

Timme-Laragy, A. R., Karchner, S. I., & Hahn, M. E. (2012). Gene knockdown by morpholino-modified oligonucleotides in the zebrafish (danio rerio) model: Applications for developmental toxicology. *Developmental toxicology* (pp. 51-71) Springer.

Topczewska, J. M., Topczewski, J., Solnica-Krezel, L., & Hogan, B. L. M. (2001). Sequence and expression of zebrafish foxc1a and foxc1b, encoding conserved forkhead/winged helix transcription factors. *Mechanisms of Development, 100*(2), 343-347.

Topczewska, J. M., Topczewski, J., Shostak, A., Kume, T., Solnica-Krezel, L., & Hogan, B. L. (2001). The winged helix transcription factor Foxc1a is essential for somitogenesis in zebrafish. *Genes & Development, 15*(18), 2483-2493. doi:10.1101/gad.907401 [doi]

Tucker, B. A., Solivan-Timpe, F., Roos, B. R., Anfinson, K. R., Robin, A. L., Wiley, L. A., Mullins, R. F., Fingert, J. H. (2014). Duplication of TBK1 stimulates autophagy in iPSC-derived retinal cells from a patient with normal tension glaucoma. *Journal of Stem Cell Research & Therapy, 3*(5), 161-7633.1000161. doi:10.4172/2157-7633.1000161 [doi]

Umali, J., Hawkey-Noble, A., & French, C. R. (2019). Loss of foxc1 in zebrafish reduces optic nerve size and cell number in the retinal ganglion cell layer. *Vision Research, 156*, 66-72.

Uribe, R. A., & Gross, J. M. (2007). Immunohistochemistry on cryosections from embryonic and adult zebrafish eyes. *Cold Spring Harbor Protocols, 2007*, 4779.

van Koolwijk, L. M., Despriet, D. D., van Duijn, C. M., Cortes, L. M. P., Vingerling, J. R., Aulchenko, Y. S., Oostra, B. A., Klaver, C. C. W., Lemij, H. G. (2007). Genetic contributions to glaucoma: Heritability of intraocular pressure, retinal nerve fiber layer thickness, and optic disc morphology. *Investigative Ophthalmology & Visual Science, 48*(8), 3669-3676.

Veth, K. N., Willer, J. R., Collery, R. F., Gray, M. P., Willer, G. B., Wagner, D. S., Mullins, M. C., Udvadia, A. J., Smith, R. S., John, S. W. (2011). Mutations in zebrafish lrp2 result in adult-onset ocular pathogenesis that models myopia and other risk factors for glaucoma. *PLoS Genetics, 7*(2), e1001310.

Vetter, M. L., & Brown, N. L. (2001). The role of basic helix-loop-helix genes in vertebrate retinogenesis. Paper presented at the *Seminars in Cell & Developmental Biology, , 12*(6) 491-498.

Vincent, A. L., Billingsley, G., Buys, Y., Levin, A. V., Priston, M., Trope, G., Williams-Lyn, D., Héon, E. (2002). Digenic inheritance of early-onset glaucoma: CYP1B1, a potential modifier gene. *The American Journal of Human Genetics, 70*(2), 448-460.

Vitorino, M., Jusuf, P. R., Maurus, D., Kimura, Y., Higashijima, S., & Harris, W. A. (2009). Vsx2 in the zebrafish retina: Restricted lineages through derepression. *Neural Development, 4*(1), 14.

Von Bartheld, C. (2002). Counting particles in tissue sections: Choices of methods and importance of calibration to minimize biases. *Histology and Histopathology,*

Wang, R., & Wiggs, J. L. (2014). Common and rare genetic risk factors for glaucoma. *Cold Spring Harbor Perspectives in Medicine, 4*(12), a017244. doi:10.1101/cshperspect.a017244 [doi]

Wang, S. W., Gan, L., Martin, S. E., & Klein, W. H. (2000). Abnormal polarization and axon outgrowth in retinal ganglion cells lacking the POU-domain transcription factor brn-3b. *Molecular and Cellular Neuroscience, 16*(2), 141-156.

Wang, S. W., Kim, B. S., Ding, K., Wang, H., Sun, D., Johnson, R. L., Klein, W. H., Gan, L. (2001). Requirement for math5 in the development of retinal ganglion cells. *Genes & Development, 15*(1), 24-29.

Weinreb, R. N., Aung, T., & Medeiros, F. A. (2014). The pathophysiology and treatment of glaucoma: A review. *Journal of the American Medical Association, 311*(18), 1901-1911.

Wiggs, J. L., & Pasquale, L. R. (2017). Genetics of glaucoma. *Human Molecular Genetics, 26*(R1), R21-R27.

Willardsen, M. I., Suli, A., Pan, Y., Marsh-Armstrong, N., Chien, C., El-Hodiri, H., Brown, N. L., Moore, K. B., Vetter, M. L. (2009). Temporal regulation of Ath5 gene expression during eye development. *Developmental Biology, 326*(2), 471-481.

Willardsen, M., Hutcheson, D. A., Moore, K. B., & Vetter, M. L. (2014). The ETS transcription factor Etv1 mediates FGF signaling to initiate proneural gene expression during xenopus laevis retinal development. *Mechanisms of Development, 131*, 57-67.

Willoughby, C. E., Ponzin, D., Ferrari, S., Lobo, A., Landau, K., & Omidi, Y. (2010). Anatomy and physiology of the human eye: Effects of mucopolysaccharidoses disease on structure and function–a review. *Clinical & Experimental Ophthalmology, 38*, 2-11.

Wolfs, R. C., Klaver, C. C., Ramrattan, R. S., van Duijn, C. M., Hofman, A., & de Jong, P. T. (1998). Genetic risk of primary open-angle glaucoma: Population-based familial aggregation study. *Archives of Ophthalmology, 116*(12), 1640-1645.

Wray, N., & Visscher, P. (2008). Estimating trait heritability. *Nature Education, 1*(1), 29.

Xie, M., Holcomb, I., Deuel, B., Dowd, P., Huang, A., Vagts, A., Foster, J., Liang, J., Brush, J., Gu, Q., Hillan, K., Goddard, A., Gurney, A. L. (1999). Fgf- 19, a novel fibroblast growth factor with unique specificity for fgfr4. *Cytokine, 11*(10), 729-735. doi:10.1006/cyto.1999.0485

Xu, X., & Xu, P. (2001). A modified cryosection method for mouse testis tissue. *Tissue and Cell, 33*(2), 208-210.

Yanagi, M., Kawasaki, R., Wang, J. J., Wong, T. Y., Crowston, J., & Kiuchi, Y. (2011). Vascular risk factors in glaucoma: A review. *Clinical & Experimental Ophthalmology, 39*(3), 252-258.

Young, R. W. (1985). Cell differentiation in the retina of the mouse. *The Anatomical Record, 212*(2), 199-205.

Zerbino, D. R., Achuthan, P., Akanni, W., Amode, M. R., Barrell, D., Bhai, J., Billis, K., Cummins, C., Gall, A., Girón, C. G. (2017). Ensembl 2018. *Nucleic Acids Research, 46*(D1), D754-D761.

Zhao, Y., Sorenson, C. M., & Sheibani, N. (2015). Cytochrome P450 1B1 and primary congenital glaucoma. *Journal of Ophthalmic & Vision Research, 10*(1), 60-67. doi:10.4103/2008-322X.156116 [doi]

Zhao, Y., Wang, S., Sorenson, C. M., Teixeira, L., Dubielzig, R. R., Peters, D. M., Conway, S. J., Jefcoate, C. R., Sheibani, N. (2013). Cyp1b1 mediates periostin regulation of trabecular meshwork development by suppression of oxidative stress. *Molecular and Cellular Biology, 33*(21), 4225. doi:10.1128/MCB.00856-13

Zhou, Y., Grinchuk, O., Wawrousek, E., & Tomarev, S. (2007). Transgenic mice expressing the Tyr437his mutant human myocilin protein develop glaucoma. *Investigative Ophthalmology & Visual Science, 48*(13), 4033-4033.

6 Appendix A

Contributions

- Gerissa Fowler, an MSc. Candidate in the French laboratory, for masking all data before quantification.
- Alexia Hawkey-Noble, a PhD. Candidate in the French laboratory, for building on this work by performing apoptosis assays and *in situ* hybridization studies on *scrt1a* and *pou4f2*.
- Danielle French (Memorial University of Newfoundland) for technical support, guidance, and feedback.
- Iliana Dimitrova and the Histology Lab at the Faculty of Medicine, Memorial University of Newfoundland for histology services: resin embedding and sectioning, and staining of cryosections and resin sections.
- Dr. Jacqueline Vanderluit for the use of her microscope and camera.

7 Appendix B

Gel electrophoresis for synthesized probes

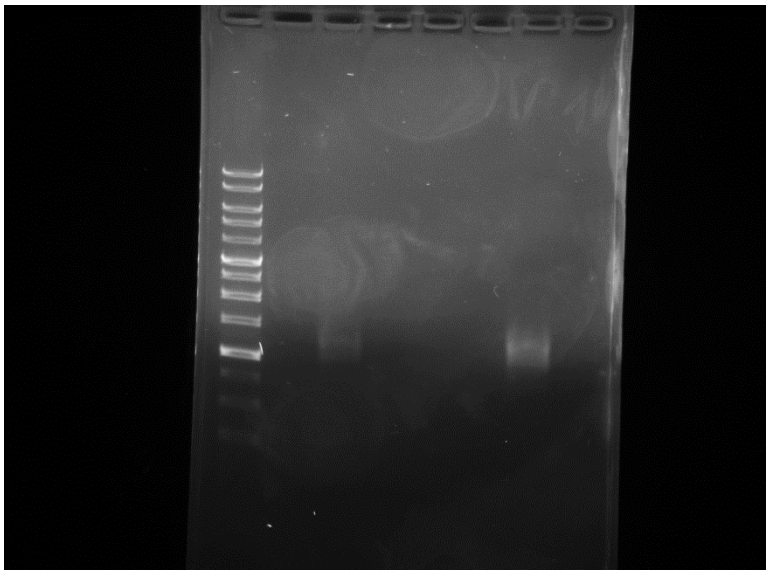

Left-Right: DNA ladder, *foxc1a* and *foxo1a* probes on a gel

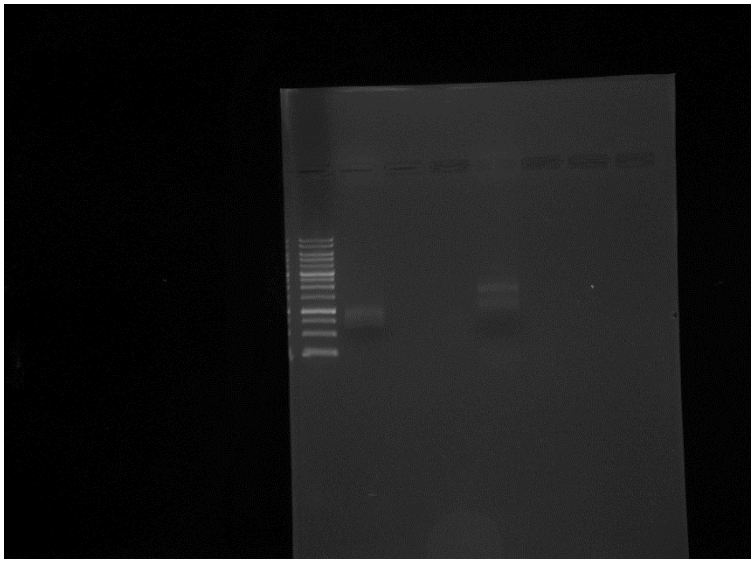

Left-Right: DNA ladder, *atoh7* and *fgf19* probes on a gel

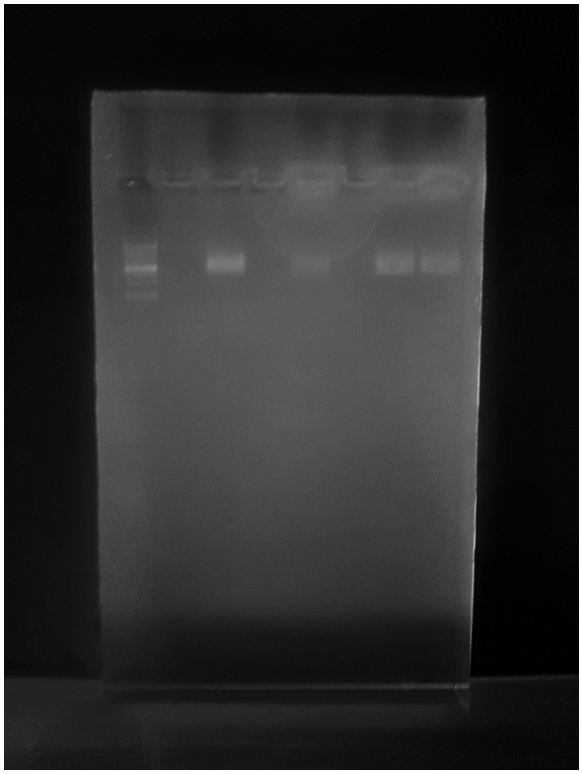

Left-Right: DNA ladder, *foxc1b, foxo1b, fgf19,* and *hspa9* probes on a gel

Left-Right: DNA ladder, *hspa5* and *pdgfrα* probes on a gel

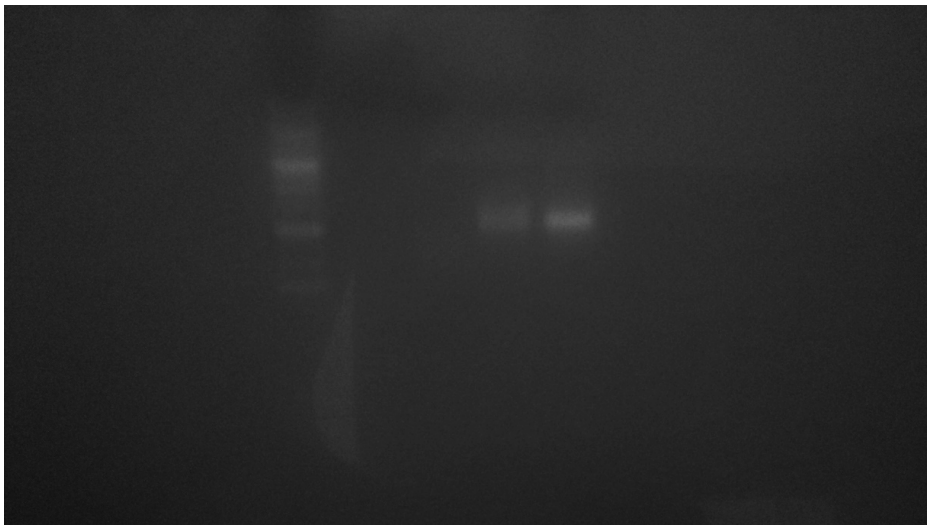

Left-Right: DNA ladder, *pfgfrβ* and *foxo1a* probes on a gel

8 Appendix C

Gel electrophoresis for Genotyping of *foxc1b* homozygous and heterozygous mutants with a 40 base-pair deletion

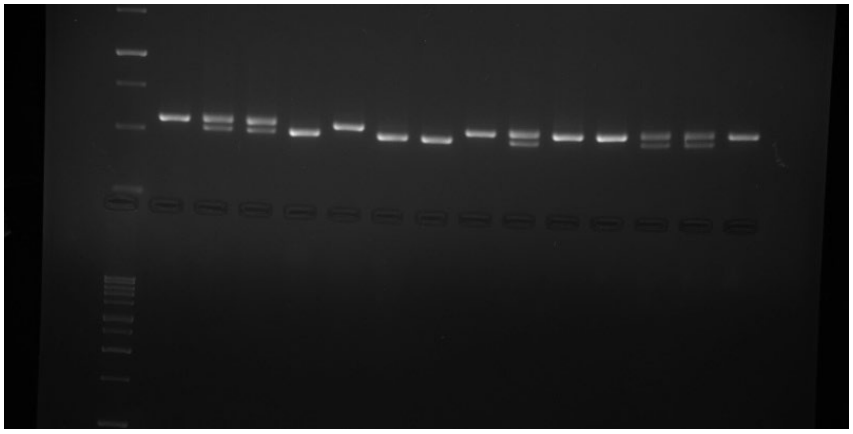

Left-Right: DNA ladder and PCR fragments of wild-type, *foxc1b*$^{+/-}$, *foxc1b*$^{+/-,}$ *foxc1b*$^{-/-,}$ wild-type, *foxc1b*$^{-/-,}$ *foxc1b*$^{-/-,}$ wild-type, *foxc1b*$^{+/-}$, wild-type, wild-type, *foxc1b*$^{+/-}$, *foxc1b*$^{+/-}$, and wild-type embryo.

9 Appendix D

Recipes

9.1 Zebrafish care

20X Embryo media

Per litre:

17.5 g NaCl [ThermoFisher Scientific, Waltham, MA, USA]

0.75 g KCl [Sigma-Aldrich, St. Louis, MO, USA]

2.9 g Calcium Chloride dihydrate ($CaCl\text{-}2H_2O$) [Ref. #: 223506-500G; Sigma-Aldrich, St. Louis, MO, USA]

Combine with sterile water to 800 mL.

Add:

0.41 g Potassium phosphate monobasic (KH_2PO4) [Sigma-Aldrich, St. Louis, MO, USA]

0.142 g NaH_2PO4 anhydrous [Sigma-Aldrich, St. Louis, MO, USA]

4.9 g Magnesium Sulfate heptahydrate ($MgSO_4\text{-}7H_2O$) [Ref. #: 230391-500G; Sigma-Aldrich, St. Louis, MO, USA]

Add sterile water up to 1 litre. Vacuum filter, store at 4°C.

500X Sodium Bicarbonate ($NaHCO_3$)

0.3 g Sodium Bicarbonate ($NaHCO_3$)

10 mL sterile water.

Embryo Media

Per litre:

50 mL 20X Embryo media

2 mL 500X $NaHCO_3$

Combine with sterile water in a graduated cylinder, topping it up to 1 L.

Make fresh each week and store at 25°C/room temperature.

9.2 Whole mount *in situ* hybridization reagents

4% PFA

In a 250 mL flask:

2 g PFA [Sigma-Aldrich, St. Louis, MO, USA]

5 mL 10X PBS

45 mL sterile water

1 NaOH pellet [ACP Chemicals Inc., Montreal, QC]

Stir overnight. Vacuum filter and store at 4° C. Make fresh every two weeks.

0.1% diethyl pryocarbonate in H2O (DEPC Water)

500 mL sterile water

500 µl DEPC [Sigma-Aldrich, St. Louis, MO, USA]

Shake at 37°C overnight. Autoclave.

0.25 M EDTA pH 8.0

Per litre:

93.05 g disodium Ethylenediaminetetraacetic acid disodium salt dihydrate (EDTA-2H_2O) [Ref. #: E5134-500G; Sigma-Aldrich, St. Louis, MO, USA]

800 mL DEPC water

Stir vigorously and heat or add NaOH pellet [ACP Chemicals Inc., Montreal, QC]. Adjust pH to 8.0 with NaOH pellets. Adjust final volume to 1 L. Autoclave.

50X Tris, Acetic Acid, EDTA (TAE) buffer

Per liter:

242 g Tris [Trizma® base, Ref. #: T1503-1KG; Sigma-Aldrich, St. Louis, MO, USA]

200 mL 0.25 M EDTA

57.1 mL acetic acid [ThermoFisher Scientific, Waltham, MA, USA]

Top up to 1 L with sterile water

For working solution, make 1X TAE buffer by adding 20 mLs of 50X TAE buffer to 980 mLs of sterile water.

10X PBS

Per 1000 mL:

80 g NaCl [ThermoFisher Scientific, Waltham, MA, USA]

2 g Potassium Chloride (KCl) [Ref. #: P9541-500G; Sigma-Aldrich, St. Louis,

MO, USA]

14.4 g Sodium Phosphate dibasic (anhydrous Na_2HPO_4) [Ref. #: S3264-250G; Sigma-Aldrich, St. Louis, MO, USA]

2.4 g Potassium Phosphate monobasic (anhydrous $KHPO_4$) [Ref. #: P9791-100G; Sigma-Aldrich, St. Louis, MO, USA]

800 mL sterile water

Adjust pH to 7.4 using NaOH pellets [ACP Chemicals, Inc., Montreal, QC].

PBST

Per 500 mL:

50 mL 10X PBS

2.5 mL 20% Tween®-20 [Ref. #: P1379-500ML; Sigma-Aldrich, St. Louis, MO, USA]

447.6 mL sterile water

Heparin

250 mg heparin sodium salt from porcine intestinal mucosa [Ref. #: H3393-50KU; Sigma-Aldrich, St. Louis, MO, USA]

5 mL DEPC water

Aliquot to 250 µL. Store at -20°C.

Hybridization solution

Make four 50 mL tubes at once. Put tRNA in only 1 of 4 tubes.

Per 50 mL:

25 mL 50% Formamide [Ambion Inc., ThermoFisher Scientific, Waltham, MA, USA]

12.5 mL 20X SSC

50 µL 50 mg/mL heparin

500 µL 50 mg/mL tRNA [Roche, Mannheim, Germany]

0.1% Tween-20 [Sigma-Aldrich, St. Louis, MO, USA]

Adjust pH to 6.0 using 0.092 M citric acid. Top up to 50 mL with sterile water.

Store at -20°C.

20X SSC

per 500 mL:

87.65 g Sodium Chloride (NaCl) [ThermoFisher Scientific, Waltham, MA, USA]

44.1 g Sodium citrate tribasic dihydrate [Ref. #: C8532-1KG; Sigma-Aldrich, St. Louis, MO, USA]

Add to 350 mL of sterile water. Stir, let sit and top up to 500 mL.

1 M Magnesium Chloride ($MgCl_2$)

Per litre:

203.3 g Magnesium Chloride hexahydrate ($MgCl2\text{-}6H_2O$) [Ref. #: M2393-100G; Sigma-Aldrich, St. Louis, MO, USA]

800 mL sterile water

Autoclave.

5 M NaCl

Per 500 mL:

146.1 g NaCl [ThermoFisher Scientific, Waltham, MA, USA]

450 mL sterile water

Heat and stir into solution. Autoclave.

1 M Tris

Per litre:

121.g Tris base [Trizma® base, Sigma-Aldrich, St. Louis, MO, USA]

800 mL sterile water

Adjust pH to desired level with concentrated hydrochloric acid (HCl). Autoclave.

Colour Buffer

Per 50 mL:

5 mL 1 M Tris-HCl pH 9.5

2.5 mL 1 M $MgCl_2$

1 mL 5 M NaCl

250 µL 20% Tween-20 [Sigma-Aldrich, St. Louis, MO, USA]

41.25 mL sterile water.

Make in plastic tube. Make fresh each time.

In situ Stop Solution

Per 500 mL:

50 mL 10X PBS

450 mL sterile water

2 mL 0.25 M EDTA pH 8.0

2.5 mL 0.1% Tween-20 [Sigma-Aldrich, St. Louis, MO, USA]

Adjust pH to 5.5 with concentrated HCl.